Contents

Lectures in Mathematical Neuroscience

Paul C. Bressloff

Lectures in Mathematical Neuroscience

Paul C. Bressloff

Neurons in the brain communicate with each other by transmitting electrical spikes known as action potentials (see Figure 1). An action potential propagates along the axon of a neuron until it reaches a terminal that forms the upstream or presynaptic component of the synaptic connection to a downstream or postsynaptic neuron. The arrival of the action potential induces the release of chemical transmitters into the synapse. These subsequently bind to receptors in the postsynaptic membrane resulting in the opening of various ion channels. This generates a synaptic current that flows along the dendritic tree of the postsynaptic neuron and combines with currents from other activated synapses. If the total synaptic current forces the membrane potential at a certain location within the cell body to cross some threshold, then the postsynaptic neuron fires an action potential and the process continues. One can thus view the brain as a vast collection of synaptically–coupled networks of spiking neurons. Each network is specialized for a particular range of tasks and receives inputs from other networks and possibly from external sources (eg. sensory stimuli). Some of the networks generate motor commands that control the movement of the organism in its environment. Many of the synaptic connections within and between networks are modifiable by experience (synaptic plasticity).
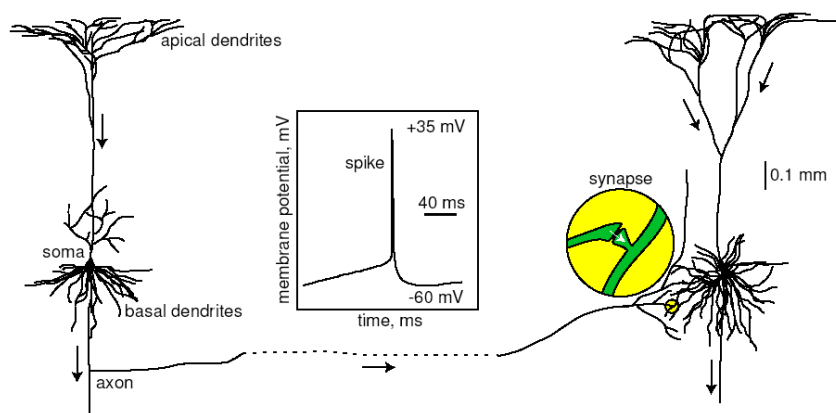

FIGURE 1. Communication with spikes. [Reprinted from [1], figure 1.1, by permission of the MIT Press.]

Department of Mathematics, Salt Lake City, Utah, USA 84112

E-mail address: bressloff@math.utah.edu

One of the ultimate challenges in neuroscience is to understand how networks of spiking neurons with modifiable connections allow an organism to carry out goal–directed behavior within a changing environment, based on current sensory input and previous experience? In addition to understanding computation and information processing during normal brain function, there is also the important clinical goal of finding the causes of dysfunctional brain states and behavior. In these lectures we will carry out the much more modest goal of unraveling some of the molecular, cellular and network mechanisms underlying the dynamics of synaptically–coupled spiking neurons. We will not focus on any particular specialized region of the brain, but consider some general principles of neuronal dynamics together with illustrative examples. The basic topics covered are single neuron models (Lecture 1), synaptic and dendritic processing (Lecture 2), firing rates, spike train statistics and the neural code (Lecture 3), network oscillations and synchrony (Lecture 4), and neural pattern formation (Lecture 5). In each lecture we describe in some detail a particular mathematical or modeling approach. For example, in Lecture 1 we consider phase reduction methods for analyzing single neural oscillators, which are extended to the case of synaptically coupled oscillators in Lecture 4. In Lecture 2 we emphasize the biophysical modeling of synapses at the molecular level, paying particular attention to the important topic of synaptic plasticity. In Lecture 3 we focus on the use of stochastic methods for studying noise in spiking neuron models. Finally, in Lecture 5 we consider the analysis of integrodifferential equations describing the large-scale dynamics of cortical tissue.

Single Neuron Models

We begin the first lecture by considering conductance–based models of a single neuron, in which the spatial structure of the neuron is neglected [**2, 3**]. Such models can reproduce electrophysiological measurements to a high degree of accuracy, but their intrinsic complexity makes them difficult to analyze, particularly at the network level. One way around this is to simplify the single neuron dynamics by carrying out some form of dimensional reduction. Reduction schemes typically exploit the presence of some small parameter in the system such as the strength of input, the degree of nonlinearity (as determined by distance from a bifurcation point, for example), or the rate of change of one or more slow variables. Regular or singular perturbation methods can then be combined with techniques from low–dimensional dynamical systems theory such as phase–plane analysis and bifurcation theory in order to analyze neural excitability, spiking and bursting [**4, 5, 1**]. Here we focus on the so–called phase reduction method [**6**], which is used to analyze the dynamics of a regular spiking neural oscillator under weak periodic forcing. One of the important applications of this method is analyzing conditions for synchrony in networks of synaptically coupled neural oscillators (see §4). We end the lecture by describing some formal threshold models of neuronal firing that are highly popular in studies of neural information processing, large–scale network dynamics, and memory [**7**].

1.1. Conductance–based models

The standard biophysical model for describing a neuron with spatially constant membrane potential u is based upon conservation of electric charge, so that

$$(1.1) \qquad C\frac{\mathrm{d}u}{\mathrm{d}t} = -F + I_{\mathrm{syn}} + I_{\mathrm{ext}},$$

where C is the cell capacitance, F the membrane current, I_{syn} the sum of synaptic currents entering the cell (see §2) and I_{ext} describes any externally injected currents. Ions can diffuse in and out of the cell through ion specific channels embedded in the cell membrane. Ion pumps within the cell membrane maintain concentration gradients, such that there is a higher concentration of Na^+ and Ca^{2+} outside the cell and a higher concentration of K^+ inside the cell. The membrane current through a specific channel varies approximately linearly with changes in the potential u relative to some equilibrium or reversal potential, which is the potential at which there is a balance between the opposing effects of diffusion and electrical forces. Summing over all channel types, the total membrane current (flow of positive ions) leaving the cell through the cell membrane is

$$(1.2) \qquad F = \sum_i g_i(u - u_i),$$

where g_i is the conductance due to channels of type i and u_i is the corresponding reversal potential. In the case of a channel selective to a single ion, u_i satisfies the Nernst equation

$$(1.3) \qquad u_i = \frac{k_B T}{q} \ln \left(\frac{[outside]_i}{[inside]_i} \right),$$

where q is the charge of the ion, k_B is the Boltzman constant, T is temperature (in degrees Kelvin) and $[outside]_i, [inside]_i$ denote the extracellular and intracellular concentrations of the given ion. Typical values for the common ion species are $u_K \approx -75mV$, $u_{Na} \approx 50mV$, $u_{Ca} \approx 150mV$ and $u_{Cl} \approx -60mV$ (which is close to the resting potential of the cell).

The generation and propagation of an action potential arises from nonlinearities associated with active membrane conductances. Recordings of the current flowing through single channels indicate that channels fluctuate rapidly between open and closed states in a stochastic fashion. Nevertheless, most models of a neuron use deterministic descriptions of conductance changes, under the assumption that there are a large number of approximately independent channels of each type. It then follows from the law of large numbers that the fraction of channels open at any given time is approximately equal to the probability that any one channel is in an open state. The conductance g_i for ion channels of type i is thus taken to be the product $g_i = \bar{g}_i P_i$ where $\bar{g}_i$ is equal to the density of channels in the membrane multiplied by the conductance of a single channel and P_i is the fraction of open channels. The voltage-dependence of the probabilities P_i in the case of a delayed-rectifier K^+ current and a fast Na^+ current were originally obtained by Hodgkin and Huxley [8] as part of their Nobel prize winning work on the generation of action potentials in the squid giant axon. The delayed-rectifier K^+ current is responsible for repolarizing a neuron after an action potential. One finds that opening of the K^+ channel requires structural changes in 4 identical and independent subunits so that $P_K = n^4$ where n is the probability that any one gate subunit has opened. In the case of the fast Na^+ current, which is responsible for the rapid depolarization of a cell leading to action potential generation, the probability of an open channel takes the form $P_{Na} = m^3 h$ where m^3 is the probability that an activating gate is open and h is the probability that an inactivating gate is open. Depolarization causes m to increase and h to decrease, whereas hyperpolarization has the opposite effect.

The dynamics of the gating variables m, n, h are usually formulated in terms of a simple kinetic scheme that describes voltage-dependent transitions of each gating subunit between open and closed states. More specifically, for each $X \in \{m, n, h\}$

$$(1.4) \qquad \frac{dX}{dt} = \alpha_X(u)(1 - X) - \beta_X(u)X,$$

where $\alpha_X(u)$ is the rate of the transition *closed* → *open* and $\beta_X(u)$ is the rate of the reverse transition *open* → *closed*. Equation (1.4) can be rewritten in the alternative form

$$(1.5) \qquad \tau_X(u)\frac{\mathrm{d}X}{\mathrm{d}t} = X_\infty(u) - X, \qquad \text{with } X \in \{m, n, h\},$$

where

$$\tau_X(u) = \frac{1}{\alpha_X(u) + \beta_X(u)}, \qquad X_\infty(u) = \alpha_X(u)\tau_X(u).$$

It follows that the conductance variables m, n and h approach the asymptotic values $m_\infty(u)$, $n_\infty(u)$ and $h_\infty(u)$ exponentially with time constants $\tau_m(u)$, $\tau_n(u)$ and $\tau_h(u)$ respectively. The following voltage-dependent rates $\alpha_X(u)$ and $\beta_X(u)$, $X \in \{m, n, h\}$ were obtained by Hodgkin and Huxley [**8**] using fits with experimental data:

$$\alpha_m = \frac{0.1(u + 40)}{1 - \exp[-0.1(u + 40)]} \qquad \alpha_h = 0.07 \exp[-0.05(u + 65)],$$

$$\alpha_n = \frac{0.01(u + 55)}{1 - \exp[-0.1(u + 55)]} \qquad \beta_m = 4.0 \exp[-0.556(u + 65)],$$

$$\beta_h = \frac{1}{1 + \exp[-0.1(u + 35)]} \qquad \beta_n = 0.125 \exp[-0.125(u + 65)].$$

All potentials are measured in mV, all times in ms and all currents in μA per cm^2. The corresponding asymptotic functions $X_\infty(u)$ and time constants $\tau_X(u)$ are plotted in Figure 1.
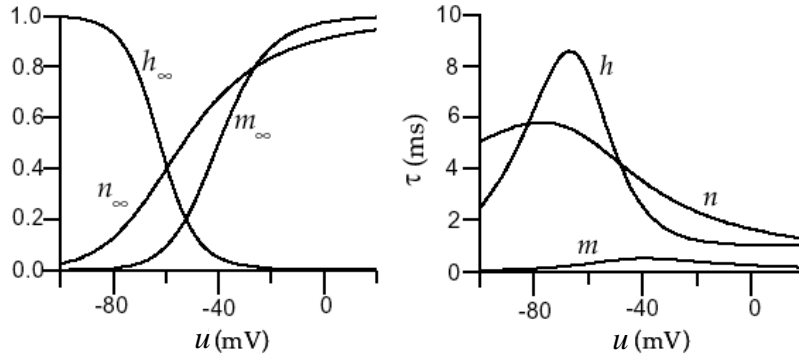
FIGURE 1. Voltage-dependent steady-state levels of activation and inactivation (left panel) and voltage-dependent time constants (right panel) for the Hodgkin-Huxley model.

We can now write down the Hodgkin-Huxley model for the generation of an action potential, which takes the membrane current to be the sum of a leakage current, a delayed-rectifier K$^+$ current and a fast Na$^+$ current,

$$(1.6) \qquad F(u, m, n, h) = g_L(u - u_L) + g_K n^4(u - u_K) + g_{Na} h m^3(u - u_{Na}).$$

The maximal conductances and reversal potentials used in the model are $g_L = 0.003 \ ms/mm^2$, $g_K = 0.36 \ mS/mm^2$, $g_{Na} = 1.2 \ mS/mm^2$, $u_L = -54.387 \ mV$, $u_K = -77 \ mV$ and $u_{Na} = 50 \ mV$. Note that the leakage current groups together various voltage-independent processes such as the currents carried by ion pumps that maintain the concentration gradients. The variables m, n, h evolve according to equation (1.4). The temporal evolution of the variables u, m, n, h during a single action potential is shown in Figure 2. Injection of a depolarizing current induces a rapid increase in the m variable describing activation of the Na$^+$ current. Since the slower h variable is initially around 0.6, there is a large influx of Na$^+$ ions, producing a sharp downward spike in the membrane current and a rapid depolarization through positive feedback. However, the rise in the membrane potential

causes the Na^+ conductance to inactivate by driving h towards zero. In addition, the depolarization activates the K^+ conductance by driving n towards a, resulting in a subsequent hyperpolarization.

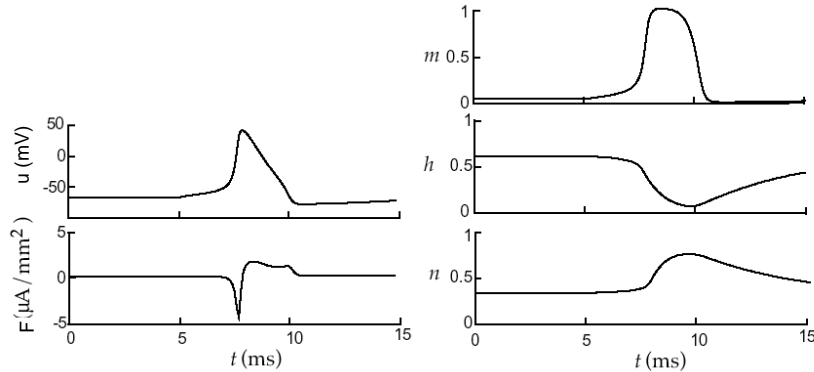FIGURE 2. The dynamics of u, n, m, h in the Hodgkin-Huxley model during the firing of an action potential induced by a current injection at $t = 5\ ms$.

Since the introduction of the Hodgkin-Huxley model, there has been considerable experimental progress in identifying the molecular mechanisms underlying the opening and closing of ion channels, and many other types of ion channels and associated currents have been discovered [3]. This has led to the development of more detailed conductance–based models that can account for a much wider variety of complex spiking behavior including bursting. In these lectures we mainly focus on regular spiking (§1.2 and §4) and irregular spiking behavior (§3). However, we do briefly describe some reduced integrate–and–fire models of bursting in §1.3. For extensive reviews of conductance–based models of bursting see [1] and the collection of articles in [9].

1.2. Periodically forced neural oscillator

We can generally formulate a conductance-based model of a neuron with constant input current as an M-dimensional ($M \geq 2$) system of ODEs

$$(1.7) \qquad \frac{d\mathbf{x}}{dt} = \mathbf{f}(\mathbf{x}), \qquad \mathbf{x} = (x_1, \ldots x_M).$$

Here x_1, say, represents the membrane potential of the neuron (treated as a point processor) and x_m, $m > 1$, represent various ionic channel gating variables. Suppose that the neuron has a stable periodic solution $\mathbf{x}(t) = \mathbf{x}(t + \Delta_0)$ where $\omega_0 = 2\pi/\Delta_0$ is the *natural frequency* of the oscillator. In *phase space* the solution is an isolated attractive trajectory called a *limit cycle*. The dynamics on the limit cycle can be described by a uniformly rotating phase such that

$$(1.8) \qquad \frac{d\phi}{dt} = \omega_0$$

and $\mathbf{x}(t) = \mathbf{g}(\phi(t))$ with $\mathbf{g}$ a 2π-periodic function. Note that the phase is *neutrally stable* with respect to perturbations along the limit cycle – this reflects invariance

of an autonomous dynamical system with respect to time shifts. Now suppose that a small external periodic input is applied to the oscillator such that

(1.9) $$\frac{d\mathbf{x}}{dt} = \mathbf{f}(\mathbf{x}) + \varepsilon\mathbf{p}(\mathbf{x}, t),$$

where $\mathbf{p}(\mathbf{x}, t) = \mathbf{p}(\mathbf{x}, t + \Delta)$ and $\omega = 2\pi/\Delta$ is the forcing frequency. If the amplitude ε is sufficiently small and the cycle is stable then deviations transverse to the limit cycle are small so that the main effect of the perturbation is to induce shifts in the phase. Therefore, we need to extend the definition of phase to a neighborhood of the limit cycle. We accomplish this using the notion of an *isochrone* [**10, 11, 12**].

Isochrones

Suppose that we observe the unperturbed system stroboscopically at time intervals of length Δ_0. This leads to a Poincare mapping

$$\mathbf{x}(t) \to \mathbf{x}(t + \Delta_0) \equiv \Phi(\mathbf{x}(t)).$$

This mapping has all points on limit cycle as fixed points. Choose a point $\mathbf{x}^*$ on the cycle and consider all points in the vicinity of $\mathbf{x}^*$ that are attracted to it under the action of Φ. They form an $(M-1)$-dimensional hypersurface I, called an isochrone, crossing the limit cycle at $\mathbf{x}^*$ (see Figure 3). A unique isochrone can be drawn through each point on the limit cycle so we can parametrize the isochrones by the phase $I = I(\phi)$. Finally, we extend the definition of phase by taking all points on $I(\phi)$ to have the same phase ϕ, which then rotates at the natural frequency ω_0.

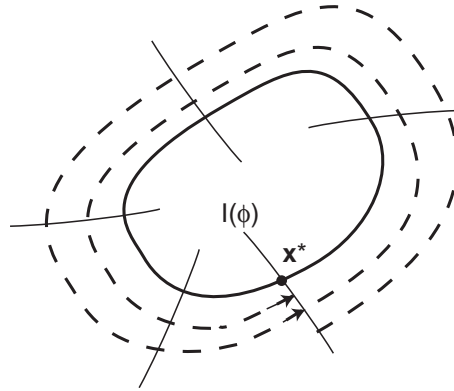FIGURE 3. Isochrones in the neighborhood of a stable limit cycle

Example: Limit cycle oscillator Consider as an example the amplitude equation that arises for a limit cycle oscillator close to a Hopf bifurcation [**13**]:

(1.10) $$\frac{dA}{dt} = (1 + i\eta)A - (1 + i\alpha)|A|^2 A.$$

In polar coordinates $A = Re^{i\theta}$,

$$\frac{dR}{dt} = R(1 - R^2), \quad \frac{d\theta}{dt} = \eta - \alpha R^2.$$

The solution for arbitrary initial data $R(0) = R_0$, $\theta(0) = \theta_0$ is

$$R(t) \;=\; \left[1 + \frac{1 - R_0^2}{R_0^2}\mathrm{e}^{-2t}\right]^{-1/2},$$

(1.11)

$$\theta(t) \;=\; \theta_0 + \omega_0 t - \frac{\alpha}{2}\log(R_0^2 + (1 - R_0^2)\mathrm{e}^{-2t}),$$

where $\omega_0 = \eta - \alpha$ is the natural frequency of the stable limit cycle at $R = 1$. Strobing the solution at times $t = n\Delta_0$, we see that

$$\lim_{n \to \infty} \theta(n\Delta_0) = \theta_0 - \alpha \ln R_0.$$

Hence, we can define a phase on the whole plane

(1.12) $\phi(R, \theta) = \theta - \alpha \ln R.$

It follows that the isochrones are logarithmic spirals with $\theta - \alpha \ln R = constant$.

Phase equation

For an unperturbed oscillator in the vicinity of the limit cycle we have

$$\omega_0 = \frac{d\phi(\mathbf{x})}{dt} = \sum_k \frac{\partial \phi}{\partial x_k}\frac{dx_k}{dt} = \sum_k \frac{\partial \phi}{\partial x_k} f_k(\mathbf{x}).$$

Now consider the perturbed system but with the unperturbed definition of the phase:

$$\frac{d\phi(\mathbf{x})}{dt} = \sum_k \frac{\partial \phi}{\partial x_k}(f_k(\mathbf{x}) + \varepsilon p_k(\mathbf{x}, t)) = \omega_0 + \varepsilon \sum_k \frac{\partial \phi}{\partial x_k} p_k(\mathbf{x}, t).$$

To a first approximation we can neglect deviations of $\mathbf{x}$ from the limit cycle which we denote by $\mathbf{x}^*$:

$$\frac{d\phi(\mathbf{x})}{dt} = \omega_0 + \varepsilon \sum_k \frac{\partial \phi(\mathbf{x}^*)}{\partial x_k} p_k(\mathbf{x}^*, t).$$

Finally, since points on the limit cycle are in 1:1 correspondence with the phase ϕ we obtain the closed phase equation

(1.13) $\dfrac{d\phi}{dt} = \omega_0 + \varepsilon Q(\phi, t),$

where

(1.14) $Q(\phi, t) = \sum_k \dfrac{\partial \phi(\mathbf{x}^*(\phi))}{\partial x_k} p_k(\mathbf{x}^*(\phi), t)$

is a 2π-periodic function of ϕ and a Δ-periodic function of t.

Example: forced limit cycle oscillator. Rewrite equation (1.10) in Cartesian coordinates

$$\frac{dx}{dt} \;=\; x - \eta y - (x^2 + y^2)(x - \alpha y) + \varepsilon \cos \omega t,$$

$$\frac{dy}{dt} \;=\; y + \eta y - (x^2 + y^2)(y + \alpha x),$$

where we have added a periodic modulation in the x-direction. Rewrite the phase (1.12) as

$$\phi = \tan^{-1}\frac{y}{x} - \frac{\alpha}{2}\log(x^2 + y^2)$$

so that

$$\frac{\partial\phi}{\partial x} = -\frac{y}{x^2 + y^2} - \alpha\frac{x}{x^2 + y^2}.$$

On the limit cycle $\mathbf{x}_0(\phi) = (\cos\phi, \sin\phi)$ and hence

$$\frac{\partial\phi(\mathbf{x}_0)}{\partial x} = -\sin\phi - \alpha\cos\phi.$$

It follows that the corresponding phase equation is

$$\frac{d\phi}{dt} = \omega_0 - \varepsilon(\alpha\cos\phi + \sin\phi)\cos\omega t.$$

Phase resetting curves for conductance-based models

The phase reduction method is particularly useful because the function $Q(\phi, t)$ can be related to an easily measurable property of a neural oscillator, namely its *phase resetting curve* (PRC), which we denote by the 2π-periodic function $R(\phi)$. The PRC is found experimentally (or numerically) by perturbing the oscillator with a brief depolarizing voltage stimulus at different times in its cycle and measuring the resulting phase-shift from the unperturbed system [**10, 12**]. Taking the coordinate x_1 as the membrane potential, it follows from equation (1.13) that

$$(1.15) \qquad \frac{d\phi}{dt} = \omega_0 + \varepsilon\frac{\partial\phi(\mathbf{x}^*(\phi))}{\partial x_1}\delta(t - t_0).$$

Integrating this equation over a small interval around t_0, we see that the impulse induces a phase-shift $\Delta\phi = \varepsilon R(\phi_0)$ where $R(\phi) = \partial\phi(\mathbf{x}^*(\phi))/\partial x_1$. Thus comparing the phase at large times for the unperturbed and perturbed cases generates the phase resetting curve. Given the phase resetting curve $R(\phi)$, the response of the neuron to a more general time-dependent voltage perturbation $\varepsilon P(t)$ is determined by the phase equation

$$(1.16) \qquad \frac{d\phi}{dt} = \omega_0 + \varepsilon R(\phi)P(t).$$

We can also express the PRC in terms of the firing times of a neuron (assuming fast reconvergence to the limit cycle). Suppose that there exists a well-defined threshold κ signalling the onset of fast somatic membrane depolarization and the subsequent firing of an action potential spike. If T^n denotes the nth firing time of the neuron then

$$(1.17) \qquad u(T^n) = \kappa, \quad \frac{du}{dt}(T^n) > 0,$$

where $u(t)$ is the membrane potential at time t. (Alternatively we could define the firing times in terms of when the neuron reaches its maximum depolarization). Since $u(t) = x_1(\phi(t))$, the threshold corresponds to a particular phase of the limit cycle, which we choose to be $\phi = 0$. Since $\phi(t) = 2\pi t/\Delta_0$ in the absence of perturbations, the firing times are $T^n = n\Delta_0$ where Δ_0 is the natural period of oscillation. On the other hand, a small perturbation applied at the point ϕ on the limit cycle at

time $t, T^n < t < T^{n+1}$, induces a phase-shift that changes the next time of firing according to (see Figure 4)

(1.18)
$$\frac{T^{n+1} - T^n}{\Delta_0} = 1 - \frac{R(\phi)}{2\pi\Delta_0}.$$

For certain types of neuron a depolarizing stimulus always advances the onset of
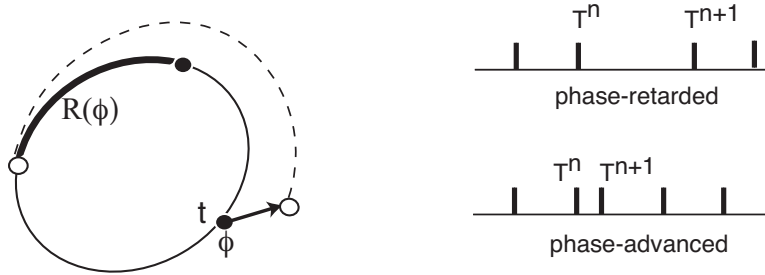
FIGURE 4. Phase-shift $R(\phi)$ induced by a small perturbation of the membrane potential applied at time $t = 0$ when the phase of the limit cycle is ϕ

the next spike, that is, the PRC is always positive, whereas for others the stimulus may also delay the next spike. We refer to models with a strictly positive PRC as Type I and those for which the PRC has a negative regime as Type II.

Example: Morris-Lecar model. A numerical example illustrating both types of PRC is shown in Figure 5(a) for the Morris–Lecar model of a neuron, which was originally introduced to describe how under constant current injection barnacle muscle fibers
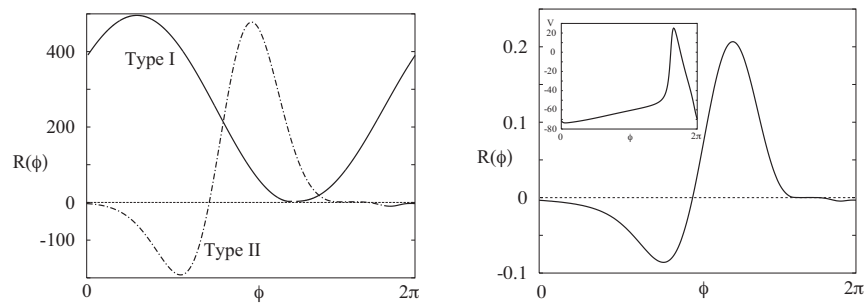
FIGURE 5. (a) Morris-Lecar model showing two different response types. In both cases $u_k = -0.7$, $u_L = -0.5$, $u_{Ca} = 1$, $g_K = 2$, $g_L = 0.5$, $u_1 = -0.01$, $u_2 = 0.15$. For a type I response, $g_{Ca} = 1.33$, $u_3 = 0.1$, $u_4 = 0.145$, $\phi = 1/3$ and $I = 0.0695$. For a type II response, $g_{Ca} = 1.1$, $u_3 = 0$, $u_4 = 0.3$, $\phi = 0.2$ and $I = 0.25$. Responses have been scaled to the same ranges. (b) Hodgkin-Huxley model with external drive $I = 10$ showing Type II phase resetting curve. Corresponding orbit over a single cycle is shown in the inset.

respond with a host of oscillatory voltage waveforms [**14**]. It takes the form

$$\frac{\mathrm{d}u}{\mathrm{d}t} = I - g_L(u - u_L) - g_K w(u - u_K) - g_{Ca}m_\infty(u)(u - u_{Ca}),$$

(1.19)
$$\frac{\mathrm{d}w}{\mathrm{d}t} = \lambda(u)(w_\infty(u) - U),$$

with

$$m_\infty(u) = 0.5(1 + \tanh[(u - u_1)/u_2]),$$
$$w_\infty(u) = 0.5(1 + \tanh[(u - u_3)/u_4]),$$
$$\lambda(u) = \phi\cosh[(u - u_3)/(2u_4)].$$

Here g_L is the leakage conductance, g_K, g_{Ca} are potassium and calcium conductances, u_L, u_K, u_{Ca} are corresponding reversal potentials, $m_\infty(u)$, $w_\infty(u)$ are voltage-dependent gating functions and $\lambda(u)$ is a voltage-dependent rate. The Type II PRC for the Hodgkin-Huxley model is shown in Figure 5(b)

Averaging theorem

Expand $Q(\phi, t)$ in the phase equation (1.13) as a double Fourier series

$$Q(\phi, t) = \sum_{l,k} a_{l,k}\mathrm{e}^{ik\phi + il\omega t}.$$

Substitute for ϕ using the zero-order approximation $\phi = \omega_0 t + \phi_0$:

$$Q(\phi, t) = \sum_{l,k} a_{l,k}\mathrm{e}^{ik\phi_0 + i(k\omega_0 + l\omega)t}.$$

It follows that Q contains fast oscillating terms (compared to the time-scale $1/\varepsilon$) together with slowly varying terms that satisfy the *resonance condition*

(1.20)
$$k\omega_0 + l\omega \approx 0.$$

Only the latter will lead to large variations in the phase, so we can average the forcing term Q keeping only the resonant terms. The simplest case is $\omega \approx \omega_0$ for which the resonant terms satisfy $l = -k$ and

(1.21)
$$Q(\phi, t) \rightarrow \sum_k a_{-k,k}\mathrm{e}^{ik(\phi - \omega t)} = q(\phi - \omega t).$$

The phase equation then becomes

$$\frac{d\phi}{dt} = \omega_0 + \varepsilon q(\phi - \omega t).$$

The phase difference between the oscillator and external drive, $\psi = \phi - \omega t$, then satisfies the equation

(1.22)
$$\frac{d\psi}{dt} = -\Delta\omega + \varepsilon q(\psi),$$

where $\Delta\omega = \omega - \omega_0$ is the degree of *frequency detuning*. Similarly, if $\omega \approx m\omega_0/n$ then

(1.23)
$$Q(\phi, t) \rightarrow \sum_k a_{-nj,mj}\mathrm{e}^{ij(m\phi - n\omega t)} = \hat{q}(m\phi - n\omega t)$$

and

(1.24)
$$\frac{d\psi}{dt} = m\omega_0 - n\omega + \varepsilon m\hat{q}(\psi),$$

where $\psi = m\phi - n\omega t$.

The above is an example of an application of the averaging theorem [**13**]. Assuming that $\Delta\omega = \omega - \omega_0 = \mathcal{O}(\varepsilon)$ and defining $\psi = \phi - \omega t$ we have

$$(1.25) \qquad \frac{d\psi}{dt} = -\Delta\omega + \varepsilon Q(\psi + \omega t, t) = \mathcal{O}(\varepsilon).$$

Define

$$(1.26) \qquad q(\psi) = \lim_{T\to\infty} \frac{1}{T} \int_0^T Q(\psi + \omega t, t)dt,$$

and consider the averaged equation

$$(1.27) \qquad \frac{d\psi}{dt} = -\Delta\omega + \varepsilon q(\psi).$$

It is easy to establish that q only contains the resonant terms of Q as above. The averaging theorem states that there exists a change of variables that maps solutions of the full equation to those of the averaged equation. The question then remains as to what extent solutions of the averaged equations are a good approximation to the solutions of the full equation. In general, one can only establish that a solution of the full equation is ε-close to a corresponding solution of the averaged system for times of $\mathcal{O}(\varepsilon^{-1})$. No such problem occurs however for hyperbolic fixed points corresponding to phase-locked states.

Phase-locking and synchronization

Suppose that the 2π-periodic function $q(\psi)$ has a unique maximum q_{max} and a unique minimum q_{min} in the interval $[0, 2\pi)$. We can then distinguish between two regimes:

Synchronization regime: If the degree of detuning for a given drive amplitude is sufficiently small,

$$\varepsilon q_{min} < \Delta\omega < \varepsilon q_{\max},$$

then there exists at least one pair of stable/unstable fixed points (ψ_s, ψ_u). (This follows from the fact that $q(\psi)$ is 2π-periodic and thus has to cross any horizontal line an even number of times). The system evolves to the synchronized state

$$\phi(t) = \omega t + \psi_s,$$

in which the oscillator is *phase-locked* to the external drive and is *frequency entrained*. Note that the stability of a phase-locked state is determined by the sign of $q'(\psi)$ with $q'(\psi_s) < 0$ and $q'(\psi_u) > 0$ (see Figure 6(a)).
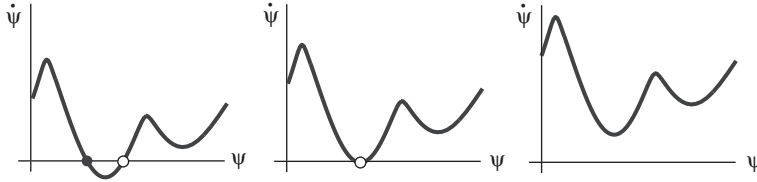

FIGURE 6. Saddle-node bifurcation signalling transition from a synchronized to a drifting state as size of frequency detuning $|\Delta\omega|$ increases.

Drift regime: As $|\Delta\omega|$ increases it approaches one of the critical values $\varepsilon q_{min,max}$ where the two fixed points coalesce in a saddle-node bifurcation and phase-locking disappears, see Figure 6(b,c). Hence, if the degree of tuning is large then $d\psi/dt$ never changes sign and the oscillation frequency differs from the drive frequency ω. The phase $\psi(t)$ rotates through 2π with period

$$(1.28) \qquad T_\psi = \left| \int_0^{2\pi} \frac{d\psi}{\varepsilon q(\psi) - \Delta\omega} \right|.$$

The mean frequency of rotation is thus $\Omega = \omega + \Omega_\psi$ where $\Omega_\psi = 2\pi/T_\psi$ is known as the *beat frequency*. One is often interested in how the behavior varies in the $(\Delta\omega, \varepsilon)$-plane (see Figure 7). First the boundary between the two regimes consists of the two straight lines $\Delta\omega = \varepsilon q_{max,min}$. Second, close to the boundary Ω_ψ has a characteristic form. Suppose, for example, that $\Delta\omega - \Delta\omega_{max}$ is small for fixed ε with $\Delta\omega_{max} = \varepsilon q_{max}$. The integral in equation (1.28) is then dominated by a small region around ψ_{max}. Expanding $q(\psi)$ as a Taylor series,

$$\begin{aligned}
\Omega_\psi = \frac{2\pi}{T_\psi} &\approx 2\pi \left| \int_{-\infty}^{\infty} \frac{d\psi}{\varepsilon q''(\psi_{max})\psi^2 - (\Delta\omega - \Delta\omega_{max})} \right|^{-1} \\
&= \sqrt{\varepsilon |q''(\psi_{max})|(\Delta\omega - \Delta\omega_{max})}.
\end{aligned}$$

(1.29)
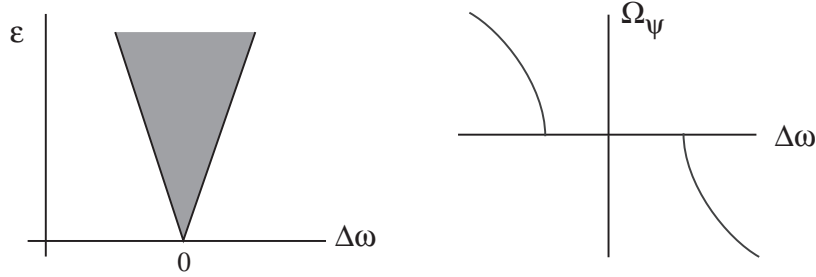
FIGURE 7. (a) Synchronization regime (shaded) in $(\Delta\omega, \varepsilon)$-plane. (b) Variation of beat frequency with $\Delta\omega$ for fixed ε.

1.3. Integrate–and–fire models

Integrate–and–fire (IF) neuron models neglect details regarding the spike generation process by reducing the latter to an all–or–nothing threshold event. That is, whenever the membrane potential crosses a firing threshold, the neuron fires a spike, typically modeled as a Dirac delta function, and the membrane potential is reset to some subthreshold value. The output of a spiking neuron can thus be characterized in terms of the sequence of threshold–crossing or firing times. Although they are less realistic than conductance–based models, they have provided a very useful platform for exploring computational issues such as neural coding and spike train statistics (see §3).

Leaky integrate–and–fire model

The simplest example of a spiking neuron is the so–called leaky integrate–and–fire (LIF) model [**15**]. The basic circuit of the LIF model consists of a capacitor C in parallel with a resistor R driven by a total current $I(t) = I_{\mathrm{ext}}(t) + I_{\mathrm{syn}}(t)$. The voltage $u(t)$ across the resistor then satisfies the differential equation

$$(1.30) \qquad \frac{du}{dt} = -\frac{u(t)}{\tau} + \frac{I_{\mathrm{ext}}(t) + I_{\mathrm{syn}}(t)}{C},$$

where $\tau = RC$ is the membrane time constant of the cell. The form of the action potential is not described explicitly. Spikes are formal events characterized by the ordered sequence of firing times $\{T^m, m \in \mathbf{Z}\}$ determined by the threshold crossing conditions

$$(1.31) \qquad T^m = \inf\{t | u(t) = u_\kappa, t > T^{m-1}\},$$

where u_κ is the firing threshold. Immediately after firing, the potential is reset to a value $u_r < u_\kappa$,

$$(1.32) \qquad \lim_{t \to T^m_+} u(t) = u_r.$$

For simplicity we set $u_\kappa = 1$, $u_r = 0$ and $C = 1$.

One of the useful features of the LIF model is that one can analyze the response of a neuron to external and synaptic input currents without requiring that the inputs are sufficiently small as in phase reduction methods. We will illustrate this in the case of periodic forcing. Suppose that $I_{\mathrm{syn}}(t) = 0$ and decompose the external drive as $I_{\mathrm{ext}}(t) = I_0 + \varepsilon I_1(t)$ with $I_1(t)$ assumed to be Δ-periodic. Integrate the LIF equation between successive firing times T^n and T^{n+1} using $u(T^n_+) = 0$ and $u(T^{n+1}_-) = 1$:

$$(1.33) \qquad \mathrm{e}^{T^{n+1}/\tau} = \tau I_0 \left[\mathrm{e}^{T^{n+1}/\tau} - \mathrm{e}^{T^n/\tau} \right] + \varepsilon \int_{T^n}^{T^{n+1}} \mathrm{e}^{t/\tau} I_1(t) dt.$$

When $\varepsilon = 0$ this equation can be solved explicitly to give

$$(1.34) \qquad T^{n+1} - T^n = \tau \log \frac{\tau I_0}{\tau I_0 - 1} \equiv \Delta_0,$$

which describes an oscillator that fires at uniform time intervals of length Δ_0 (provided that $\tau I_0 > 1$), see Figure 8(a). We interpret $\omega_0 = 2\pi/\Delta_0$ as the natural

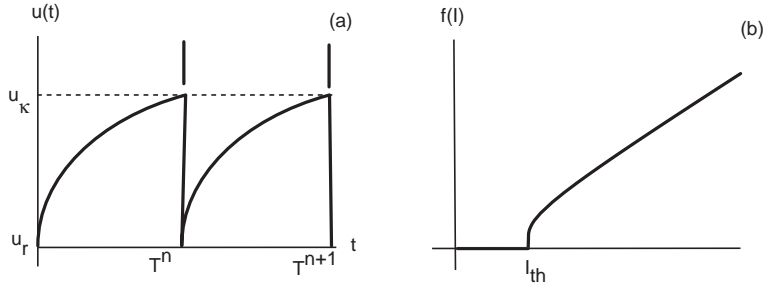

FIGURE 8. Integrate-and-fire oscillator. (a) Plot of $u(t)$ as a function of time t for constant current I. (b) Firing rate r as a function of current injection I with $I_{th} = 1/\tau$ when $u_\kappa = 1, u_r = 0$.

frequency of the LIF oscillator. The so–called $f - I$ curve relating the steady–state firing rate as a function of input current I_0 is then given by the firing rate function

$$(1.35) \qquad f(I_0) = \frac{1}{\tau} \left[\frac{1}{\log(\tau I_0 / [\tau I_0 - 1])} \right]_+ .$$

where $[x]_+ = 1$ if $x > 0$ and zero otherwise. The firing rate function f is plotted in Figure 8(b).

In order to analyze the case $\varepsilon \neq 0$, it is useful to introduce the function

$$(1.36) \qquad F(t) = [\tau I_0 - 1] e^{t/\tau} + \varepsilon \int_{-\infty}^{t} e^{s/\tau} I_1(s) ds$$

such that the iterative firing time map can be written in the form

$$(1.37) \qquad F(T^{n+1}) = F(T^n) + e^{T^n/\tau}.$$

This equation has been studied in great detail by Keener *et al* [**15**] for the particular case of the sinusoidal forcing $I(t) = I_0 + \epsilon \sin(2\pi t)$. Here the time-scale has been chosen so that the forcing period $\Delta = 1$. The function F then has the explicit form

$$(1.38) \qquad F(t) = e^{t/\tau} \left(\tau I_0 - 1 + \frac{\epsilon \tau}{\sqrt{1 + 4\pi^2 \tau^2}} \sin(2\pi t - \eta) \right),$$

where $\tan \eta = 2\pi\tau$. Keener *et al* [**15**] showed that major differences in behavior occur depending upon whether or not F is invertible. If F is invertible then we have an explicit first–order map

$$(1.39) \qquad T^{n+1} = \Psi(T^n) \equiv F^{-1} \left[F(T^n) + e^{T^n/\tau} \right].$$

The condition for invertibility is that $F'(t) \neq 0$ for all t, which implies that

$$(1.40) \qquad I_0 - \frac{1}{\tau} > \varepsilon \max_t \{ -I_1(t) \}.$$

The invertibility condition reduces to $I_0 - \tau^{-1} > \varepsilon$ in the case of sinusoidal forcing. Since (for $\Delta = 1$)

$$F(\Psi(t+1)) = e^{1/\tau} [F(t) + e^{t/\tau}] = e^{1/\tau} F(\Psi(t)) = F(\Psi(t) + 1),$$

it follows that $\Psi(t + 1) = \Psi(t) + 1$. By identifying the interval $0 \leq t < 1$ with the unit circle we thus obtain a smooth invertible circle map. When F is not invertible, the mapping $T^n \to T^{n+1}$ of equation (1.37) can still be defined provided that F^{-1} is taken to be the smallest branch of the inverse of F, that is, T^{n+1} is taken to be the smallest value of $t, t > T^n$, for which equation (1.37) is satisfied. The dynamics is now described by a discontinuous, piecewise monotonic circle map.

The qualitative dynamics of the equivalent circle map can be characterized in terms of its rotation number ρ. This is defined according to [**15**]

$$(1.41) \qquad \rho = \lim_{n \to \infty} \frac{T^n - T^0}{n},$$

and measures the mean inter-spike interval (time between successive firings). It can be shown that ρ is independent of the initial state T^0 and is a continuous function of parameters in both the invertible and non–invertible regimes. If ρ is rational , that is, $\rho = p/q$ for integers p, q, then every sequence of firing times converges to a periodic orbit on which $T^{n+p} = T^n + q$, and $p : q$ phase–locking is said to occur. In the invertible regime, ρ is irrational on a parameter set of positive Lebesgue
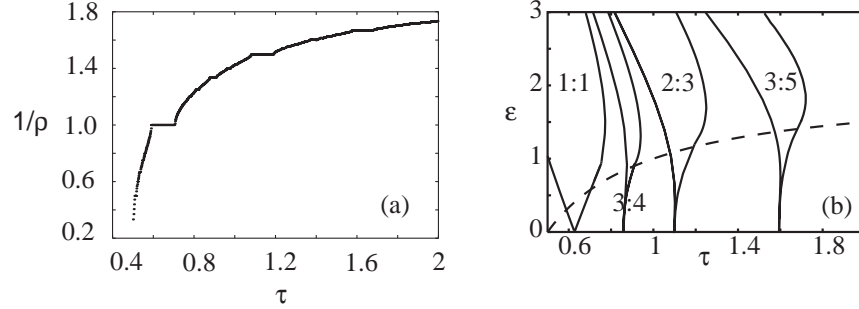
FIGURE 9. (a) Plot of the inverse mean firing period as a function of the membrane time constant τ for $I_0 - \epsilon = \tau^{-1}$ with $I_0 = 2$. Note that the dominant solutions are $1:1$, $3:4$, $2:3$ and $3:5$ (with increasing τ). (b) The Arnold tongue structure for the dominant modes. The dashed curve shows the boundary between invertible and non-invertible regimes of the firing time map

measure and the resulting quasiperiodic solutions are ergodic, that is, the sequence $T_n \mod 1$ is dense in the interval $[0, 1)$. On the other hand, in the noninvertible regime, ρ is irrational on a set of Lebesgue measure zero and the quasiperiodic orbits are no longer ergodic in $[0, 1)$. In Figure 9(a) we plot $1/\rho$ as a function of τ for $\varepsilon = I_0 - \tau^{-1}$. The resulting devil's staircase structure shows that the preferred mode-locked solutions are those with low ratios of q to p. In Figure 9(b) we plot the borders of the Arnold tongues where these dominant modes become unstable in the (τ, ϵ)-plane. In the invertible regime both boundaries are associated with the disappearance of a phase–locked state via a smooth saddle-node bifurcation, whereas in the noninvertible regime the left–hand boundary signals the non-smooth disappearance of a stable phase-locked state [**15**].

Weak periodic forcing and phase averaging

For sufficiently small ε, the conditions for mode–locking reduce to those obtained using the phase reduction method of §1.2. Consider an LIF neuron with a weak periodic input $\varepsilon I(t)$ evolving as

$$\frac{du}{dt} = f(u) + \varepsilon I(t),$$

where $f(u) = I_0 - u$ and we have set $\tau = 1$. Taking $u_r = 0$ and $u_\kappa = 1$ the period of oscillation for $\varepsilon = 0$ is

$$T_0 = \int_0^1 \frac{dx'}{f(x')} = \log[I_0/(I_0 - 1)].$$

Introducing the phase variable

(1.42) $$\theta(t) = \frac{2\pi}{T_0} \int_0^u \frac{dx'}{f(x')},$$

we can transform the LIF equation to a phase equation identical in form to (1.16)

$$\frac{d\theta(t)}{dt} = \omega_0 + \varepsilon R(\theta) I(t),$$

where $\omega_0 = 2\pi/T_0$ and

$$(1.43) \qquad R(\theta) = \frac{2\pi}{I_0 T_0} e^{T_0 \theta/2\pi}, \quad 0 \leq \theta < 2\pi.$$

We identify the 2π–periodic function $R(\theta)$ as the PRC of an LIF neuron (see §1.2). Suppose that the input $I(t) = \cos \omega t$ with $\omega - \omega_0 = \mathcal{O}(\varepsilon)$. Introduce the slowly varying phase variable $\psi(t) = \theta(t) - \omega t$ such that

$$\frac{d\psi(t)}{dt} = \varepsilon \left[\Delta\omega + R(\psi + \omega t) \cos(\omega t) \right],$$

with $\omega - \omega_0 = \varepsilon \Delta\omega$. From the averaging theorem [13], solutions of this equation can be approximated by solutions of the reduced equation (at least up to times of order $1/\varepsilon$)

$$\frac{d\psi(t)}{dt} = \varepsilon \left[\Delta\omega + q(\psi)) \right],$$

where

$$q(\psi) = \frac{1}{T} \int_0^T R(\psi + \omega t) \cos(\omega t) dt$$

and $\omega = 2\pi/T$. A fixed point of the reduced phase equation corresponds to a $1:1$ mode–locked solution, and from this the boundaries of the $1:1$ Arnold tongue can be deduced for small ε.

Spike response model

The LIF model assumes that it is the capacitative nature of the cell that in conjunction with a simple thresholding process dominates the production of spikes. The spike response (SR) model is a more general framework that can accommodate the apparent reduced excitability (or increased threshold) of a neuron after the emission of a spike [16, 17, 7]. Spike reception and spike generation are combined with the use of two separate response functions. The first, $\eta(t)$, describes the postsynaptic response to an incoming spike in a similar fashion to the LIF model, whereas the second, $\eta(t)$, mimics the effect of refractoriness. The refractory function $\eta(t)$ can in principle be related to the detailed dynamics underlying the description of ionic channels. In practice an idealized functional form is often used, although numerical fits to the Hodgkin-Huxley equations during the spiking process are also possible [18]. In more detail, a sequence of incoming spikes $\{T^m\}$ evokes a postsynaptic potential in the neuron of the form $u_s(t) = \sum_m \epsilon(t - T^m)$ where $\epsilon(t)$ incorporates details of axonal, synaptic and dendritic processing (see §2). The total membrane potential of the neuron is then taken to be

$$(1.44) \qquad u(t) = \sum_p \eta(t - \widehat{T}^p) + \sum_m \epsilon(t - T^m),$$

where $\{\widehat{T}^p\}$ is the sequence of output firing times and $\eta(t)$ is the the refractory function reflecting the reduced excitability seen after firing. Since the reset condition of the LIF model is equivalent to a sequence of current pulses, $-(u_\kappa - u_r) \sum_p \delta(\widehat{T}^p)$, the LIF model is a special case of the SR model. More specifically, integrating the LIF equation (1.30) in the case of a synaptic input of the form $I(t) = \sum_m g_{\text{syn}}(t - T^m)$,

we obtain the equivalent formulation (1.44) with

$$(1.45)\ \eta(t) = -(u_\kappa - u_r)\mathrm{e}^{-t/\tau}, \quad \epsilon(t) = \int_0^t \mathrm{e}^{-(t-t')/\tau} g_{\mathrm{syn}}(t')\mathrm{d}t', \quad t > 0.$$

Nonlinear IF model and parabolic bursting

In a general nonlinear IF model, equation (1.30) is replaced by [**19**]

$$(1.46)\qquad\qquad \tau\frac{du}{dt} = F(u) + G(u)I.$$

(Note that one can always eliminate the nonlinear factor $G(u)$ by a change of variables). A specific example of a nonlinear IF model is the quadratic model

$$(1.47)\qquad\qquad \tau\frac{du}{dt} = a_0(u - u_{\mathrm{rest}})(u - u_c) + RI,$$

with $a_0 > 0$ and $u_c > u_{\mathrm{rest}}$. For $I = 0$ and initial condition $u < u_c$, the voltage decays to the resting potential u_{rest}. For $u > u_c$ it increases to infinity in a finite time due to the quadratic nonlinearity, which defines when a spike is emitted. Immediately after firing, the neuron is reset to $-\infty$. Again the quadratic nonlinearity ensures that the membrane potential returns to a finite value in a finite time.

After shifting the voltage and current variables, the quadratic IF model can be rewritten as

$$(1.48)\qquad\qquad \frac{\mathrm{d}u}{\mathrm{d}t} = \left(p + qu^2\right),$$

which represents the normal form of any neuron exhibiting a saddle–node on a limit cycle bifurcation [**20, 21**], see Figure 10. Such a neuron displays Class I excitability, which is characterized by the appearance of oscillations with arbitrary low frequency; the frequency increases with increasing injected current. This should be contrasted with Class II excitability for which the onset of repetitive firing occurs at a non-zero frequency that is relatively insensitive to changes in the applied current. Class II excitability is usually associated with a Hopf bifurcation. The

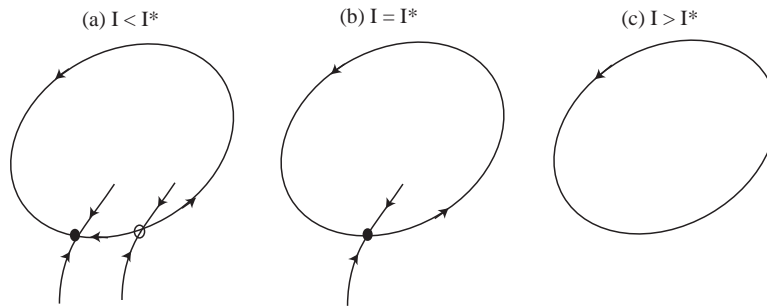FIGURE 10. Schematic diagram of a saddle-node bifurcation on a limit cycle occurring as the applied current I is increased. (a) For $I < I^*$ there is a unique asymptotically stable fixed point and a saddle-point with a one-dimensional unstable manifold whose branches form a closed loop. (b) At criticality, $I = I^*$, the node and saddle coalesce. (c) For $I > I^*$ all that remains is a limit cycle

behavior of the model becomes more transparent by performing the change of variables $u = \tan(\theta/2)$ which gives the so–called theta model [22]

$$(1.49) \qquad \frac{\mathrm{d}\theta}{\mathrm{d}t} = q(1 - \cos(\theta)) + p(1 + \cos(\theta)).$$

If q and p have opposite signs then equation (1.49) has two fixed points, one stable and the other unstable, and the neuron is in an excitable state. On the other hand, if q and p have the same sign (which we take to be positive) then there are no fixed points and the phase monotonically increases with time. In fact, one can solve equation (1.49) explicitly to obtain the solution

$$(1.50) \qquad \theta(t) = 2 \tan^{-1} \left[\sqrt{\frac{p}{q}} \tan\left(\sqrt{pq}\, t + \phi \right) \right]$$

for some arbitrary phase ϕ. It follows that the frequency of rotation is $\omega = 2\sqrt{pq}$. Each time $\theta(t)$ passes through π the potential $u(t)$ 'blows up' thus signalling the firing of a single spike in the full system.

A simple extension of the above canonical model of a Class I excitable neuron can be used to describe what is known as a parabolic burster [20]. *Bursting* is the rhythmic generation of several action potentials during a short time, followed by a period of inactivity. There are a wide variety of burst phenomena, but it appears that many are due to a similar underlying mechanism. We first note that the various chemical and electrical dynamics of the neuron operate on many time-scales, and for some neurons one can *dissect* their full dynamics into a fast system coupled to a slowly oscillating sub-system [23, 1, 4, 5]. Typically the fast system has a time-scale of milliseconds and models the membrane potential, and hence spike generation. The slow sub-system operates on a time-scale that varies from hundreds of milliseconds to tens of seconds and typically models trans-membrane ionic currents. For many types of bursting, the fast subsystem exhibits bistability between a quiescent fixed point and an active oscillatory state. At least one slow variable is then required to alternate back and forth through the region of bistability such that the neuron periodically jumps between the active and quiescent phases along a hysteresis loop. It is also possible to generate bursting without bistability in the fast subsystem, as in the case of parabolic bursting, provided there are at least two variables in the slow subsystem that periodically sweep the fast subsystem through a sequence of bifurcations. Both cases are illustrated in Figure 11.

Ermentrout and Kopell [20] showed how parabolic bursting models can be reduced to the following canonical form

$$(1.51) \qquad \dot{\theta} = [1 - \cos(\theta)] + [1 + \cos(\theta)]\, g(\phi), \quad \dot{\phi} = \omega$$

where $(\phi, \theta) \in S^1 \times S^1$ is on a torus, the frequency of the slow oscillations is $\omega \ll 1$, and $g : S^1 \to \mathbf{R}$ is a continuous function describing the influence of ϕ on the fast variable θ. If g is negative for all ϕ then the fast variable is quiescent, and there is no bursting. If $g(\phi) > 0$ the fast variable fires all the time and is never quiescent. Bursting occurs when g changes sign over the interval $\phi \in [0, 2\pi)$. A typical choice of g is $g(\phi) = a + b\cos\phi$ resulting in the so called atoll model. Typical activity of this system in the (θ, ϕ) plane is shown in Figure 12 for $(a, b) = (0, 1)$.
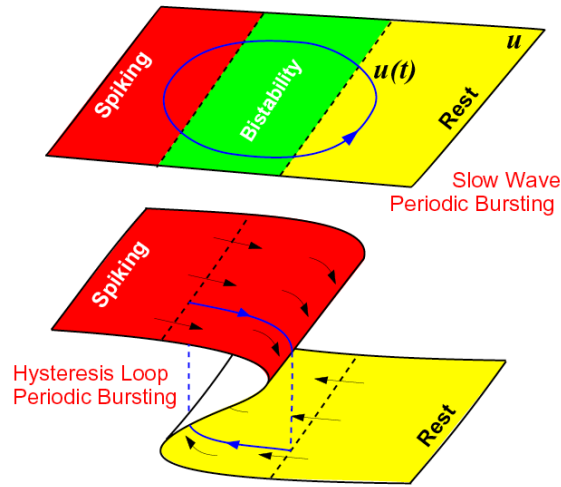
FIGURE 11. Slow variation in the parameter s switches the neuron between quiescent and spiking states resulting in bursting. In the case of slow wave bursting the periodic variation of s is independent of the fast system, whereas in hysteresis type bursting the slow and fast systems are mutually coupled. [Reprinted from [1], figure 9.17, by permission of the MIT Press.]
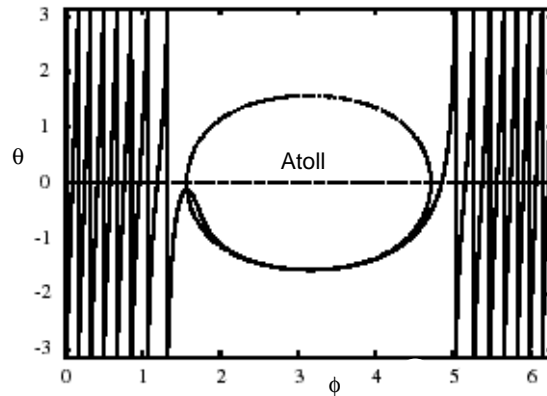
FIGURE 12. Activity of the atoll model for $\omega = 0.05, a = 0, b = 1$. The dashed circle is the set of equilibria for the fast variable θ. Outside the atoll region, θ completes full 2π rotations, so that the neuron fires action potentials whereas within the atoll θ is attracted to a fixed point and the neuron is quiescent. The system periodically enters and leaves the atoll due to the periodic rotation of the slow phase variable ϕ.

Integrate-and-fire-or-burst model

Several models of bursting neurons include a low-threshold calcium T-current [24]. Such a current is slowly de–inactivated when the neuron is sufficiently hyperpolarized so that it can cause the neuron to fire a burst of action potentials when released

from sustained inhibition, so-called *post-inhibitory* rebound. Recently the integrate-and-fire model has been extended to incorporate this slow acting T-current leading to the aptly named *integrate-and-fire-or-burst* (IFB) model [**25**]. The current balance equation for the model is

$$(1.52) \qquad C\frac{du}{dt} = -I - I_L - I_T,$$

where C is a membrane capacitance, I represents external or synaptic current, $g_L(u - u_L)$ is a leakage current with constant conductance g_L and reversal potential u_L. The low-threshold Ca^{2+} current is given by

$$(1.53) \qquad I_T = g_T h(t)(u - u_T)H(u - u_h),$$

where H is a Heaviside function and the slow variable h has the dynamics

$$(1.54) \qquad \frac{dh}{dt} = \left\{ \begin{array}{ll} -h/\tau_-, & u \geq u_h \\ (1-h)/\tau_+, & u < u_h \end{array} \right. .$$

The variable h, which represents slow de-inactivation of the low-threshold Ca^{2+} conductance, relaxes to zero with time constant τ_- when $u \geq u_h$ and relaxes to unity with time constant τ_+ when $u < u_h$. Assuming $u_h < u_r < u_\kappa$, where u_κ is the firing threshold, it follows that sustained hyperpolarization is required in order that the potential crosses the u_h boundary from above resulting in an increase in h. If the cell is then released from inhibition so that u recrosses the threshold u_h from below, a non-zero I_T current is generated that can depolarize the cell and produce a burst of spikes. In the absence of such hyperpolarization, the system acts as a regular integrate-and-fire neuron. Also note that if $u_r < u_h < u_\kappa$ then bursting can be induced by direct excitation, as occurs for inhibitory reticular cells (see below). In the case of a constant external input, it is possible to obtain an exact solution of the IFB model in terms of characteristic curves in the (u, h)–plane [**26**]. The Arnold tongue structure for the IFB model under periodic forcing has also been determined [**27**].

One particular structure where calcium T–currents are thought to be important is the thalamus. The thalamus is the primary relay station for most of the sensory information on route to the cerebral cortex. Oscillations at 7-14 Hz (spindles) and 4-7 Hz (delta) are common in cortex and thalamus during various stages of non-REM sleep [**28, 29**]. The EEG spindles are typical of brain electrical synchronization at the onset of sleep associated with the loss of perceptual awareness. It has been established that these oscillations are generated as the result of synaptic interactions between excitatory thalamocortical cells and GABA inhibitory neurons of the thalamic reticular nucleus. The latter is a thin sheet of inhibitory cells between the thalamus and cortex that is uniquely placed to play a regulatory role in levels of awareness. From a computational perspective, one can basically reduce sleep into two phases that correspond roughly speaking to two modes of firing of thalamic cells. During the slow oscillations of non-REM sleep, thalamic cells are in a bursting mode in which there is sufficient hyperpolarization to de-inactivate the low-threshold calcium current. Rather than communicating information about the sensory world, the thalamocortical neurons participate in a globally synchronized bursting state mediated by the corticothalamic loop. Such a coherent brain state may perform the function of consolidating memory traces acquired during wakefulness [**28**]. However, it can also lead to hypersynchronous episodes similar to those observed in some epileptic seizures. During REM sleep, the thalamic neurons are

more depolarized such that the calcium current is inactivated. The neurons now fire in a tonic (regular spiking) rather than a bursting mode and may exhibit high frequency γ oscillations similar to the awake state. Transitions between non-REM sleep, REM sleep, and arousal are controlled by a variety of neurotransmitters released from brain stem nuclei including acetylcholine, norepinephrine and serotonin [31]. Until recently, it was thought that during wakefulness the thalamic cells only operate in tonic mode, which relays sensory information to the cortex. However, recent experimental studies indicate that burst firing can also serve as an effective relay mode in the awake state [30], see Figure 13. In particular burst firing is more effective than tonic firing in detecting weak signals in background noise. It
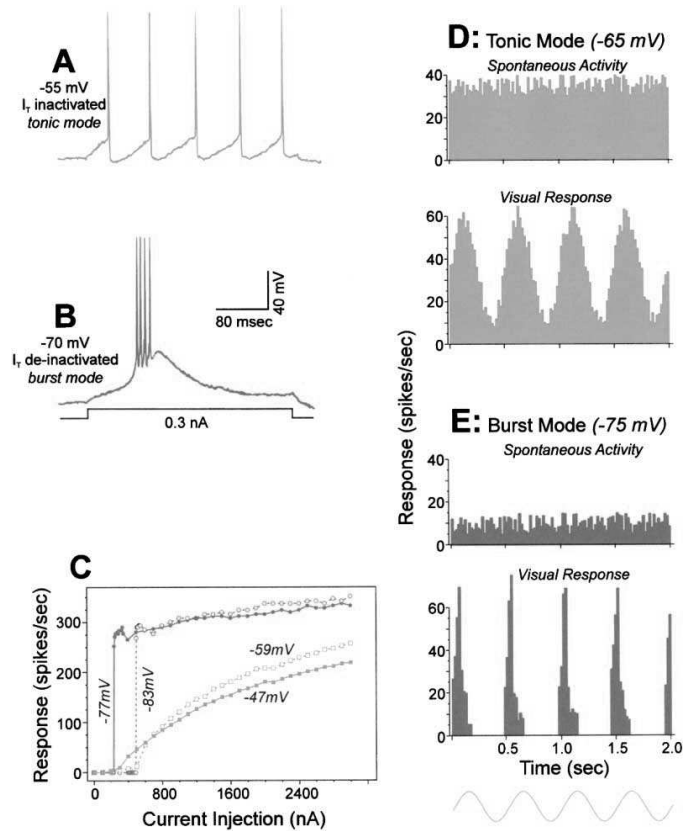
FIGURE 13. Two modes of firing in thalamic cells during the wake state. (A) Tonic firing with T–current inactivated. (B) Burst firing when the T–current is de-inactivated. (C) Firing rate as a function of current injection in the tonic mode (at -47 and -59 mV) and in the burst mode (-77 and -83 mV). The former is approximately linear whereas the latter is approximately a step function. (D) Peri-stimulus time histograms of a neuron in tonic mode showing response to a periodic stimuli and spontaneous activity in the absence of the stimulus. (E) Corresponding histograms in burst mode. [Reprinted from [30], with permission of Elsevier.]

is also possible that bursting is more effective in stimulating neurons downstream. This has led to the suggestion that the burst mode is used to detect novel stimuli. Once the change is detected, the neuron switches to tonic mode so that the new object can be analyzed more faithfully. Recently, IFB models have been used to investigate both bursting and tonic firing in models of thalamic tissue [**32, 33**].

Synaptic and Dendritic Processing

In the single neuron models discussed in §1, we decomposed the total input current into an external part $I_{\text{ext}}(t)$ and a synaptic part $I_{\text{syn}}(t)$. In order to develop recurrent network models, it is necessary to consider the detailed form of the synaptic current $I_{\text{syn}}(t)$ that mediates neuronal interactions. In this lecture we begin by considering a single synapse and the sequence of events underlying conductance changes in the postsynaptic membrane due to the arrival of an action potential at the presynaptic terminal. We then show how these conductance changes can be modeled in terms of a kinetic scheme describing the opening and closing of ion channels in the postsynaptic membrane. Typically, a single neuron in cerebral cortex has up to 10,000 synapses, which are spatially distributed along the dendritic tree (and perhaps on the cell body and proximal part of the axon). In order to find the total synaptic current $I_{\text{syn}}(t)$ entering the cell body, it is necessary to determine how the various local currents flow along the dendritic tree and combine at the soma. We show that if the dendrites are modeled as passive electrical cables, then the dendritic tree acts as a linear spatio-temporal filter of synaptic currents. We end the lecture by describing some biophysical models of synaptic plasticity, in which the strength or weight of a synapse is modifiable by experience. (The synaptic weight can be identified as the maximal conductance change induced by a single action potential). In particular, we consider the phenomenon of spike timing–dependent plasticity (STDP), where changes in synaptic weights depend on the precise timing of pre– and post–synaptic spikes at the millisecond level. STDP is emerging as an important paradigm in computational approaches to adaptive behavior and learning.

2.1. Excitatory and inhibitory synapses

The basic stages of synaptic processing induced by the arrival of an action potential at an axon terminal are shown in Figure 1. (See [**3**] for a more detailed description). An action potential arriving at the terminal of a presynaptic axon causes voltage-gated Ca^2+ channels within an active zone to open. The influx of Ca^2+ produces a high concentration of Ca^2+ near the active zone [**34, 35**], which in turn causes vesicles containing neurotransmitter to fuse with the presynaptic cell membrane and release their contents into the synaptic cleft (a process known as exocytosis). The released neurotransmitter molecules then diffuse across the synaptic cleft and bind to specific receptors on the post-synaptic membrane. These receptors cause ion channels to open, thereby changing the membrane conductance and membrane potential of the postsynaptic cell. A single synaptic event due to the arrival of an action potential at time T induces a synaptic current of the form

$$(2.1) \qquad I_{\text{syn}}(t) = g_{\text{syn}}(t - T)(u_{\text{syn}} - u(t)),$$

where u is the voltage of the postsynaptic neuron, u_{syn} is the synaptic reversal potential and $g_{\mathrm{syn}}(t)$ is the change in synaptic conductance with $g_{\mathrm{syn}}(t) = 0$ for $t < 0$. The sign of u_{syn} relative to the resting potential u_{rest} (typically $u_{\mathrm{rest}} \approx -65mV$) determines whether the synapse is excitatory ($u_{\mathrm{syn}} > u_{\mathrm{rest}}$) or inhibitory ($u_{\mathrm{syn}} < u_{\mathrm{rest}}$). For simplicity, it is often assumed that a neuron spends most of its time close to rest such that $u_{\mathrm{syn}} - u \approx u_{\mathrm{syn}} - u_{\mathrm{rest}}$, with the factor $u_{\mathrm{syn}} - u_{\mathrm{rest}}$ absorbed into g_{syn} (see also §3.3). One is then effectively taking the arrival of a spike as generating a synaptic current rather than a change in conductance.
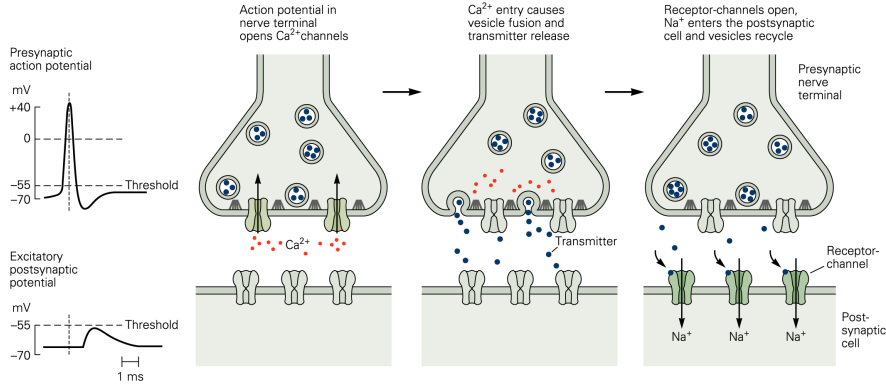
FIGURE 1. Basic stages of synaptic processing shown for an excitatory synapse. See text for details. [Adapted from Kandel *et al* [**36**]]

The predominant fast, excitatory neurotransmitter of the vertebrate central nervous system is the amino acid *glutamate*, whereas in the peripheral nervous system it is *acetylcholine*. Glutamate-sensitive receptors in the post-synaptic membrane can be subdivided into two major types, namely, NMDA and AMPA [**3**]. At an AMPA receptor the postsynaptic channels open very rapidly. The resulting increase in conductance peaks within a few hundred microseconds, with an exponential decay of around 1 msec. The time course of the synaptic conductance change can be modeled in terms of an nth state Markov process [**37**] (see §2.2). Usually a simplified representation of $g_{\mathrm{syn}}(t)$ is used that is given by the difference of exponentials

$$(2.2) \qquad g_{\mathrm{syn}}(t) = \bar{g} \left(\frac{1}{\tau_2} - \frac{1}{\tau_1} \right) (\mathrm{e}^{-t/\tau_1} - \mathrm{e}^{-t/\tau_2}) H(t),$$

with $H(t)$ the Heaviside function. In the limit $\tau_2 \to \tau_1 = \alpha^{-1}$, equation (2.2) reduces to the well known α function

$$(2.3) \qquad g_{\mathrm{syn}}(t) = \bar{g} \alpha^2 t \mathrm{e}^{-\alpha t} H(t).$$

These expressions for the conductance are also used for GABA inhibitory synapses (see below). In contrast to an AMPA receptor, the NMDA receptor operates about 10 times slower and the amplitude of the conductance change depends on the postsynaptic membrane potential, see Figure 2. If the postsynaptic potential is at rest and glutamate is bound to the NMDA receptor then the channel opens but it is physically obstructed by Mg^{2+} ions. As the membrane is depolarized, the Mg^{2+} ions move out and the channel becomes permeable to Na^+ and Ca^{2+} ions. The

rapid influx of calcium ions due to the opening NMDA channels is thought to be the critical trigger for the onset of *long term potentiation* or LTP, a major component of synaptic plasticity (see §2.4).
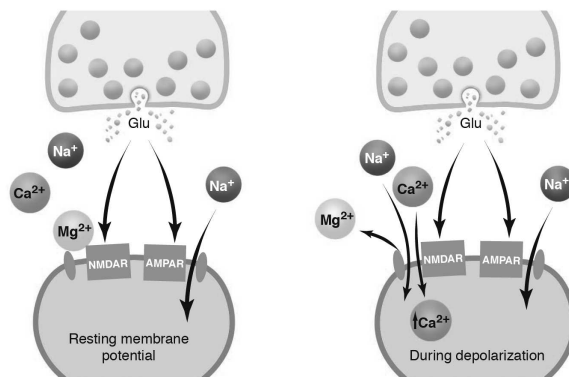
FIGURE 2. An NMDA synapse. Arrival of an action potential at the presynaptic terminal induces vesicles containing glutamate to merge with the cell membrane and release the neurotransmitter into the synaptic cleft. This binds to NMDA and AMPA receptors on the postsynaptic cell membrane. The AMPA associated channel opens but the NMDA channel is blocked by magnesium. Depolarization of the postsynaptic membrane unblocks magnesium allowing the influx of calcium. Depolarization may be caused by a back propagating action potential (BPAP) that travels up the dendrites.[Reprinted from [**38**], with permission from AAAS.]

The most common inhibitory neurotransmitter in the central nervous system of both vertebrates and invertebrates appears to be GABA. There are two major forms of postsynaptic receptors termed A and B. The $GABA_A$ receptors opens channels selective to chloride ions, whose reversal potential $u_{\mathrm{syn}} = -70mV$ is close to that of the resting potential. The postsynaptic conductance change is quite fast, rising within 1 msec and decaying within 10-20 msec. $GABA_B$ receptors are at least 10 times slower and open ion channels selective for K^+ ions. Thus they tend to be considerably more hyperpolarizing with $u_{\mathrm{syn}} \approx -100mV$. The two receptor classes tend to be segregated with $GABA_A$ occurring at or close to the soma and $GABA_B$ further out on the dendrites. Another way to distinguish between $GABA_A$ and $GABA_B$ receptors is that the former is ionotropic (as are NMDA and AMPA) whilst the latter is metabotropic [**3**]. Neurotransmitter binding to an ionotropic receptor directly opens an ion channel through a series of conformational changes of the receptor. On the other hand, neurotransmitter binding to a metabotropic receptor indirectly opens an ion channel elsewhere in the membrane through a sequence of biochemical steps.

Synaptic facilitation and depression
A single synaptic event due to the arrival of an action potential at time T induces a synaptic current of the form (2.1). As a crude approximation we might try summing individual responses to model the synaptic current arising from a train of action

potentials arriving at times T^m, integer m:

$$(2.4) \qquad I_{\text{syn}}(t) = \sum_m g_{\text{syn}}(t - T^m)(u_{\text{syn}} - u(t)).$$

Note that this sum only includes spikes for which $T^m < t$ since $g_{\text{syn}}(t) = 0$ for $t < 0$ (causality condition). For many synapses such a simple ansatz does not hold, since processes such as synaptic facilitation and short-term depression cause the amplitude of the response to depend on the previous history of presynaptic firing [**39, 40**]. One way to incorporate these history–dependent effects is to take [**41**]

$$(2.5) \qquad I_{\text{syn}}(t) = \left[\sum_m A(T^m) g_{\text{syn}}(t - T^m) \right] (u_{\text{syn}} - u(t)),$$

where the factor $A(T^m)$ scales the response evoked by an action potential by an amount that depends upon the details of the previous spike train data. One interpretation of the factor A is that it represents short-term (reversible) changes in the release probability for synaptic transmission. One possible mechanism for synaptic depression is a depletion in the number of vesicles that can readily fuse with the cell membrane, whereas facilitation is thought to be due to residual calcium remaining in active fusion regions [**42**].

A common phenomenological model of facilitation or depression is to assume that between spikes $A(t)$ relaxes at a rate τ_A to its steady state value of one, but that directly after the arrival of a spike it changes discontinuously. τ_A can vary between around 100msecs and a few seconds [**40**]. For facilitation A is increased, whilst for depression it is decreased. It is mathematically convenient to model the former as an additive process and the latter as a multiplicative process in order to avoid possible divergences. That is, $A \to A + \gamma - 1$ with $\gamma > 1$ for facilitation, and $A \to \gamma A$ with $\gamma < 1$ for depression. The two models may be written succinctly as

$$(2.6) \qquad \tau_A \frac{dA}{dt} = (1 - A) + (\gamma - 1) \sum_n A^\beta \delta(t - T^n), \quad A(0) = 1$$

with $\beta = 1$ for the multiplicative model and $\beta = 0$ for the additive model. They have solutions of the form

$$(2.7) \qquad A(T^m) = 1 + (\gamma - 1) \sum_{n < m} \hat{\gamma}^{[m-n-1]\beta} \mathrm{e}^{-(T^m - T^n)/\tau_A},$$

where $\hat{\gamma} = \gamma$ (depression) and $\hat{\gamma} = 1$ (facilitation). Assuming a regular sequence of incoming spikes $T^n - T^{n-1} = \Delta$ for all n we find that the asymptotic amplitude $A_\infty(\Delta) \equiv \lim_{m \to \infty} A(T^m)$ is given by

$$(2.8) \qquad A_\infty(\Delta) = 1 + \frac{(\gamma - 1)}{(\mathrm{e}^{\Delta/\tau_A} - 1)} \qquad \text{(facilitation)},$$

and

$$(2.9) \qquad A_\infty(\Delta) = \frac{1 - \mathrm{e}^{-\Delta/\tau_A}}{1 - \gamma \mathrm{e}^{-\Delta/\tau_A}} \qquad \text{(depression)}.$$

One possible computational role for synaptic depression is as a mechanism for cortical gain control [**40**]. The basic idea can be understood from the dependence

of the asymptotic amplitude $A_\infty(\Delta)$ on the stimulus frequency $f = \Delta^{-1}$. Assuming that $\tau_A \gg \Delta$, we can Taylor expand A_∞ in equation (2.9) to find that

$$(2.10) \qquad A_\infty(f) \approx \frac{\Gamma}{f},$$

where $\Gamma = \tau_A/(1-\gamma)$. The main point to note is that the postsynaptic response per unit time is approximately independent of f (assuming that each spike elicits the same response in the steady-state). This means that the synapse is very sensitive to changes in the stimulus frequency. The instantaneous response to a rapid increase Δf in the stimulus rate is given by $\Gamma \Delta f/f$. In other words, the synapse responds to relative rather than absolute changes in the rate of input stimulation.

2.2. Kinetic model of a synapse

Let $g_{\mathrm{syn}}(t) \sim s(t)$ where $s(t)$ is the fraction of synaptic receptor channels that are in an open conducting state. The probability of being in an open state depends on the presence and concentration $\mathcal{T}$ of neurotransmitter released by the presynaptic neuron. Assuming a first order kinetic scheme, in which a closed receptor in the presence of a concentration of neurotransmitter $\mathcal{T}$ equilibrates with the open receptor state, we have

$$C \underset{r_2(u)}{\overset{r_1(u,\mathcal{T})}{\rightleftharpoons}} O,$$

where C and O represent the closed and open states of the channel and $r_1(u, \mathcal{T})$ and $r_2(u)$ are the associated rate constants. However, in many cases synaptic channels are found to have time dependent properties that are more accurately modeled with a second order kinetic scheme. In fact the presence of one or more receptor sites on a channel allows the possibility of transitions to *desensitized states*. Such states are equivalent to the inactivated states of voltage-dependent channels. The addition of such a desensitized state to the first order process generates a second order scheme:

$$\frac{\mathrm{d}s}{\mathrm{d}t} = r_1(u, \mathcal{T})(1 - s - z) - [r_2(u) + r_3(u)]s + r_4(u)z,$$

$$(2.11) \qquad \frac{\mathrm{d}z}{\mathrm{d}t} = r_6(u, \mathcal{T})(1 - s - z) - [r_4(u) + r_5(u)]z + r_3(u)s,$$

where z is the fraction of channels in the desensitized state. All neurotransmitter dependent rate constants have the form $r_i(u, \mathcal{T}) = r_i(u)\mathcal{T}$. It is common for detailed Markov models of voltage-gated channels to assume that the voltage dependence of all rates takes a simple exponential form. However, it has been shown that the number of states needed by a model to more accurately reproduce the behavior of a channel may be reduced by adopting sigmoidal functions for the voltage-dependent transition rates (see Destexhe *et al* [**37**] for a discussion), so that we write

$$(2.12) \qquad r_i(u) = \frac{a_i}{1 + \exp\left[-(u - c_i)/b_i\right]}.$$

The a_i set the maximum transition rate, b_i the steepness of the voltage dependence and c_i the voltage at which the half-maximal rate is reached. Furthermore, the concentration of neurotransmitter can also often be successfully approximated by a sigmoidal function of the presynaptic potential u_{pre}:

$$(2.13) \qquad \mathcal{T}(u_{\mathrm{pre}}) = \frac{\mathcal{T}_{\mathrm{max}}}{1 + \exp[-(u_{\mathrm{pre}} - u_\Delta)/\Delta]}.$$

Here $\mathcal{T}_{\max}$ is the maximal concentration of transmitter in the synaptic cleft, u_{pre} is the presynaptic voltage, Δ gives the steepness and u_{Δ} sets the value at which the function is half activated. It is common to take $\Delta = 5\mathrm{mV}$ and $u_{\Delta} = 2\mathrm{mV}$. One of the main advantages of using an expression such as (2.13) is that it provides a smooth transformation between presynaptic voltage and transmitter concentration from which postsynaptic currents can be easily calculated from (2.1), (2.11) (2.12) and (2.13).

Now consider the following second-order gating scheme

$$
\begin{array}{ccc}
C & \overset{r_1(\mathcal{T})}{\underset{r_2}{\rightleftharpoons}} & C_1 \\
\scriptstyle r_4 \searrow & & \swarrow \scriptstyle r_3 \\
& O &
\end{array}
$$
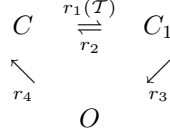
where C and C_1 are the closed forms of the receptor, O is the open (conducting) form, and the r_i are voltage independent transition rates. Under certain assumptions it may be shown that this particular second order scheme describes the so-called alpha function response commonly used in synaptic modeling. The following approximations are required: (i) The transmitter concentration ($\mathcal{T}$) occurs as a pulse $\delta(t-t_0)$ for a release event occurring at time $t = t_0$. Then $r_1(\mathcal{T}) = r_1\delta(t-t_0)$ and (ii) The fraction of channels in C is considered constant and ~ 1. Then the kinetic equations (2.11) reduce to

$$
\frac{\mathrm{d}\mathbf{p}(t)}{\mathrm{d}t} = \mathbf{Q}\mathbf{p}(t) + \mathbf{I}(t)
$$

(assuming $\mathbf{p}(0) = \mathbf{0}$) where

$$
\mathbf{Q} = \begin{pmatrix} -\frac{1}{\tau_1} & 0 \\ r_3 & -\frac{1}{\tau_2} \end{pmatrix}, \quad \mathbf{I}(t) = \begin{pmatrix} r_1\delta(t-t_0) \\ 0 \end{pmatrix}, \quad \mathbf{p} = \begin{pmatrix} z \\ s \end{pmatrix}
$$

and $\tau_1 = 1/(r_2 + r_3)$, $\tau_2 = 1/r_4$ and z and s represent the fraction of receptors in the forms C_1 and O respectively. This Markov chain system has a solution of the form

$$
\mathbf{p}(t) = \int_0^t \mathbf{G}(t-s)\mathbf{I}(s)\mathrm{d}s, \quad \mathbf{G}(t) = \mathrm{e}^{t\mathbf{Q}}.
$$

The eigenvectors of $\mathbf{Q}$ are $(1, r_3/(\tau_2^{-1} - \tau_1^{-1}))$ and $(0,1)$ with associated eigenvalues $-1/\tau_1$ and $-1/\tau_2$ respectively. Hence, one finds that

$$
s(t) = r_1 r_3 \left(\frac{1}{\tau_2} - \frac{1}{\tau_1} \right)^{-1} (\mathrm{e}^{-(t-t_0)/\tau_1} - \mathrm{e}^{-(t-t_0)/\tau_2}), \quad t > t_0.
$$

In the limit $\tau_2 \to \tau_1 \to \tau_s$ this reduces to an alpha function

$$
s(t) = r_1 r_3 (t - t_0)\mathrm{e}^{-(t-t_0)/\tau_s}, \quad t > t_0.
$$

This kinetic derivation of the alpha function only holds for $s \ll 1$ in order to remain consistent with condition (ii).

The time course of some ion channel open and closed states seem to follow a power law rather than multiexponential law at large times [**43**]. In order to understand such power law behavior, consider an ion channel with N closed states

such that the transition to an open state can only take place from state 1 at one end of a chain

$$0 \overset{\alpha}{\leftarrow} 1 \underset{\beta_1}{\overset{\gamma_1}{\rightleftharpoons}} 2 \ldots \underset{\gamma_{N-1}}{\overset{\beta_{N-1}}{\rightleftharpoons}} N.$$
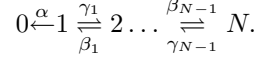
The corresponding kinetic equations are

$$\frac{dp_1}{dt} = \beta_1 p_2 - (\gamma_1 + \alpha)p_1,$$

$$\frac{dp_n}{dt} = \gamma_{n-1}p_{n-1} + \beta_n p_{n+1} - (\gamma_n + \beta_{n-1})p_n, \quad 1 < n < N,$$

$$\frac{dp_N}{dt} = \gamma_{N-1}p_{N-1} - \beta_{N-1}p_N.$$

In the following we take $\gamma_n = \beta_n = 1$ for all n and $\alpha = 1$, so that the system of equations describes a discrete diffusion process along a chain with a reflecting boundary at $n = N$ and an absorbing boundary at $n = 0$. In the large N limit, it can be shown that given the initial condition $p_n(0) = \delta_{n,1}$, the exact solution is

$$(2.14) \qquad\qquad p_n(t) = e^{-2t}[I_{n-1}(t) - I_{n+1}(t)],$$

where $I_n(t)$ is the modified Bessel function of integer order:

$$I_n(t) = \int_{-\pi}^{\pi} e^{ink} e^{2t \cos(k)} \frac{dk}{2\pi}.$$

By carrying out an asymptotic expansion for large t, it can be shown that

$$p_n(t) \approx \frac{n}{2\pi^{1/2} t^{3/2}}.$$

Define $F(t)$ to be the total probability of finding the system in a closed state:

$$F(t) = \sum_{n=1}^{N} p_n(t).$$

It follows that $dF/dt = -\alpha p_1$ and, hence, $F(t) \approx (\pi t)^{-1/2}$ for large N, t and $\alpha = 1$. More recently, it has been suggested that synapses with multiple states, which exhibit dynamics over a wide-range of time-scales and show power–law like behavior, could have some interesting computational properties [**44, 45**]. For example, it has been suggested that such synapses could provide a way of combining high levels of memory storage with long retention times [**44**].

Stochastic model of receptor binding

In the above kinetic scheme, the stochastic opening and closing of ion channels was modeled in terms of deterministic rate equations that keep track of the mean number of channels in each available state. An implicit assumption of such a model is that the number of ion channels is sufficiently large so that one can ignore fluctuations. In order take into account such fluctuations, it is necessary to consider the associated master equation. We will illustrate this by considering a simple first order kinetic scheme, in which the opening or closing of a channel is equivalent to the binding or unbinding a neurotransmitter to a postsynaptic receptor. For simplicity, we will assume that there is a fixed, uniform concentration $\mathcal{T}$ of neurotransmitter in the synaptic cleft. Consider a cell surface with a fixed number N of receptors. Let k_+ and k_- denote the binding and disassociation rates of neurotransmitter

molecules. If B denotes the mean fraction of bound receptors then the standard kinetic binding equations is (from the law of mass action)

$$\frac{dB}{dt} = k_+ \mathcal{T}(1 - B) - k_- B.$$

However, this equation ignores fluctuations in the number of bound receptors, which become significant when N is sufficiently small. A stochastic version of the binding problem is described by an associated master equation for transitions between bound and unbound states. More specifically, if $P(n,t)$ denotes the probability that n out of N receptors are bound at time t, then the master equation takes the form

$$\frac{\partial P}{\partial t} = \lambda_+(n-1)P(n-1,t) + \lambda_-(n+1)P(n+1,t) - [\lambda_+(n) + \lambda_-(n)]P(n,t),$$

with

$$\lambda_+(n) = (N - n)k_+ \mathcal{T}, \quad \lambda_-(n) = nk_-.$$

Define the mean number of bound receptors at time t by

$$\overline{n}(t) = \sum_{n=0}^{N} np(n,t).$$

By differentiating both sides with respect to t and using the master equation, it can be shown that in the limit of large N (where the upper limit in the sum can be taken to be ∞) we recover the kinetic equation with $B = \overline{n}/N$.

The steady-state solution $P_s(n)$ satisfies $J(n) = J(n+1)$ with

$$J(n) = \lambda_-(n)P_s(n) - \lambda_+(n-1)P_s(n-1).$$

Using the fact that n is a nonnegative integer, that is, $P_s(n) = 0$ for $n < 0$, it follows that $J(n) = 0$ for all n. Hence, by iteration,

$$(2.15) \qquad P_s(n) = P_s(0) \prod_{m=1}^{n} \frac{\lambda_+(m-1)}{\lambda_-(m)} = P_s(0) \left[\frac{k_+ \mathcal{T}}{k_-}\right]^n \frac{N!}{n!(N-n)!}.$$

Taking logs of both sides of this equation and use Stirling's formula $\log(n!) \approx n\log n - n$ it can be shown that for large n, N, $P_s(n) \approx p(\phi)$ where $\phi = n/N$,

$$(2.16) \qquad\qquad\qquad p(\phi) = p(0)e^{NA(\phi)}$$

and

$$A(\phi) = \phi \log(k_+ \mathcal{T}/k_-) - \phi \log(\phi) - (1 - \phi)\log(1 - \phi).$$

Let ϕ^* be the (unique) stationary solution, that is, $A'(\phi^*) = 0$. Since N is large, the method of steepest descent leads to the Gaussian approximation

$$(2.17) \qquad p(\phi) \approx p(0)\exp\left[NA(\phi^*) + NA''(\phi^*)(\phi - \phi^*)^2/2\right].$$

Under this approximation, the mean and variance of the fraction of bound receptors are given by

$$(2.18) \qquad \langle\phi\rangle = \phi^* = \frac{k_+ \mathcal{T}}{k_- + k_+ \mathcal{T}}, \quad \langle(\phi - \phi^*)^2\rangle = \frac{\phi^*(1 - \phi^*)}{N}.$$

It is clear that fluctuations become negligible in the large–N limit.

2.3. Dendritic filtering of synaptic inputs

So far we have neglected the fact that the synapses of a neuron are spatially distributed across the neuron's dendritic tree, see Figure 3(a). At the simplest level, the dendritic tree can be treated as a passive electrical medium that filters incoming synaptic stimuli in a diffusive manner. The current flow and potential changes along a branch of the tree may be described with a second–order, linear partial differential equation commonly known as the *cable equation* [**46, 2**]. The cable equation is based on a number of approximations: (i) magnetic fields due to the movement of electric charge can be neglected, (ii) changes in ionic concentrations are sufficiently small so that Ohm's law holds, (iii) radial and angular components of voltage can be ignored so that the cable can be treated as one-dimensional medium, and (iv) dendritic membrane properties are voltage-independent, that is, there are no active elements. Given a distribution of synaptic inputs innervating the dendritic tree, what is the net synaptic current I_{syn} entering the soma or cell body of a neuron? In order to address this problem we consider, for simplicity, a semi-infinite uniform dendritic cable, $0 \leq x < \infty$, with the soma located at the end $x = 0$, see Figure 3(b). We model the soma as a LIF neuron that is passively coupled to the dendritic cable via a resistor with conductance σ,

$$(2.19) \qquad \tau\frac{\mathrm{d}u}{\mathrm{d}t} = -u + RI_{\text{ext}} + \sigma[v(0,t) - u(t)],$$
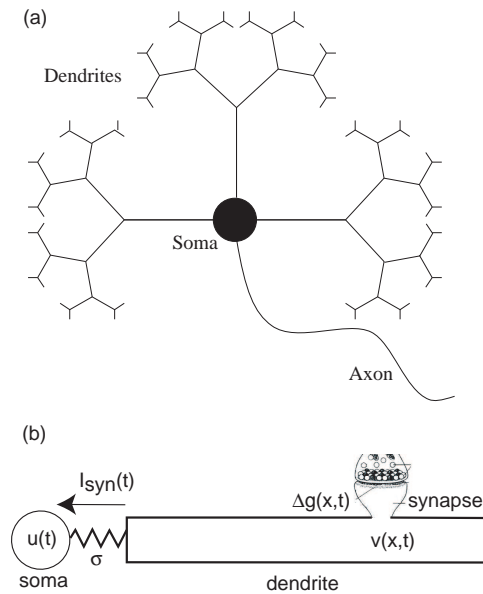

FIGURE 3. (a) Branching dendritic tree of an idealized single neuron. (b) Schematic diagram of a neuron consisting of a soma resistively coupled to one end of a dendritic cable. A synaptic conductance change $\Delta g(x,t)$ at position x on the cable induces a synaptic current into the soma at $x = 0$.

where $\sigma[v(0,t) - u(t)]$ is the net current density flowing into the soma from the dendritic cable at $x = 0$ and $v(x,t)$ is the membrane potential of the cable at position x. The dendritic potential $v(x,t)$ evolves according to the cable equation

$$(2.20) \qquad \widehat{\tau}\frac{\partial v(x,t)}{\partial t} = -v(x,t) + \lambda^2\frac{\partial^2 v(x,t)}{\partial x^2} + I(x,t),$$

where $\widehat{\tau}$ is the dendritic membrane time constant and λ is the corresponding space constant, both of which are determined by the passive electrical properties of the cable. Here $I(x,t)$ is the synaptic input at location x at time t:

$$(2.21) \qquad I(x,t) = g(x)[V_{\text{syn}} - v(x,t)]\sum_{m}\alpha(t - T^m(x)),$$

where $\alpha(t)$ is an α function, say, $g(x)$ determines the maximal conductance and $\{T^m(x)\}$ is the sequence of spikes arriving into the synapses located at x. It follows from current conservation that we also have the boundary condition

$$(2.22) \qquad -\frac{1}{r}\frac{\partial v}{\partial x}(0,t) = \sigma[v(0,t) - u(t)],$$

where r is the intracellular resistance per unit length of cable. Since we can eliminate the term $-\sigma u(t)$ in equation (2.19) by shifting the somatic membrane time constant τ, it follows that the total synaptic current into the soma is $I_{\text{syn}}(t) = \sigma v(0,t)$.

Under the approximations $V_{\text{syn}} \gg v$, we can formally solve the inhomogeneous boundary value problem for $v(0,t)$ using the Green's function G for the semi-infinite cable with a closed boundary [**47**]:

$$
\begin{aligned}
v(0,t) \quad = \quad & V_{\text{syn}}\int_{-\infty}^{t}\int_{0}^{\infty}G(0,x',t-t')I(x',t')dx'dt' \\
& -\sigma\int_{-\infty}^{t}G(0,0,t-t')[v(0,t') - u(t')]dt',
\end{aligned}
$$
$$(2.23)$$

with

$$(2.24) \qquad G(x,y,t) = G_0(x-y,t) + G_0(x+y,t),$$

and

$$(2.25) \qquad G_0(x,t) = \frac{1}{2\lambda\sqrt{\pi t/\widehat{\tau}}}\mathrm{e}^{-t/\widehat{\tau}}\mathrm{e}^{-\widehat{\tau}x^2/4\lambda^2 t}$$

is the Green's function of the cable equation on an infinite domain. We see that the effective synaptic current I_{syn} flowing into the soma will itself be affected by the cell firing an action potential, due to the dependence of $v(0,t)$ on $u(t)$. This could be taken into account within the spike response model framework by using an effective reset function [**7**]. Here we will assume for simplicity that the second term on the r.h.s. of equation (2.23) is small compared to the first term arising from synaptic inputs. This approximation corresponds to imposing the homogeneous boundary condition $\partial v/\partial x|_{x=0} = 0$. It then follows that the total synaptic input into the soma is

$$(2.26) \qquad I_{\text{syn}}(t) = \sigma V_{\text{syn}}\int_{-\infty}^{t}\int_{0}^{\infty}G(0,x',t-t')I(x',t')dx'dt'.$$

A similar analysis can also be carried out for more general dendritic topologies with the soma coupled to one of the terminals of the tree. We conclude that under the given approximations, the passive dendritic tree acts like a spatio-temporal linear

filter on incoming spike trains, whose properties are determined by the underlying Green's function on the tree. The effects of the dendritic filtering of synaptic inputs on network dynamics is reviewed in some detail by Bressloff and Coombes [**48**].

Dendritic spines

The majority of excitatory synapses that occur in the cortex are located on tiny specialized protoplasmic protuberances called dendritic *spines* [**49**], see Figure 4. They typically occupy 20–70% of the total dendritic membrane. Since the input impedance of a spine head is typically large, a small excitatory synaptic current can produce a large local depolarization. Moreover, the thin stem neck connecting the spine to the main body of the dendrite provides an axial resistance that partially decouples the spine-head dynamics from the dendritic tree. Hence, it has long been theorized that the dendritic spine is a favorable site for the initiation of an action potential [**50, 51**], and is thus a possible substrate for local computations [**52**]. Modeling studies also suggest that if the heads of dendritic spines have excitable membrane properties, then the spread of current from one spine along the dendrites could bring adjacent spines to their thresholds for impulse generation. The result would be a sequence of spine-head action potentials, representing a saltatory propagating wave in the distal dendritic branches [**53, 54**]. Calcium imaging experiments provide strong evidence that the spine heads are endowed with voltage-dependent Ca^{2+} channels that can indeed support an all-or-nothing response to an excitatory synaptic input [**55**].
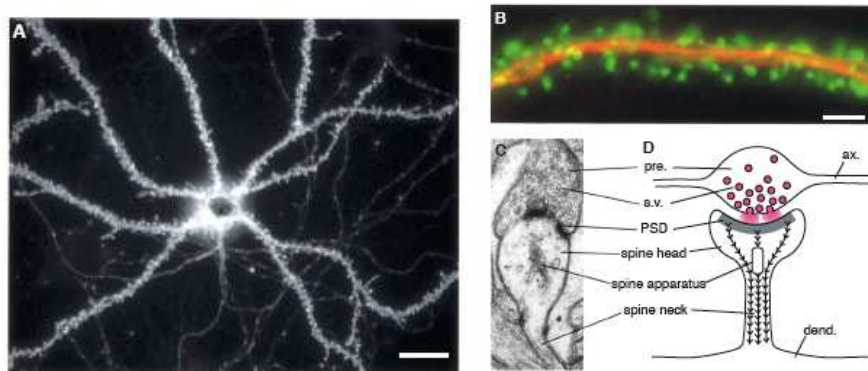
FIGURE 4. Dendritic spines. (A,B) Dendritic spines of a cultured hippocampal neuron revealed by green fluorescent protein (GFP) tagged actin.   (C) A single spine revealed by electron microscopy.   (D) Schematic diagram of a spine with barbed lines representing actin filaments.[Reprinted from Matus [**56**], with permission of AAAS.]

Early theoretical studies of spines also considered their potential role in synaptic plasticity and Hebbian learning. This was motivated by the idea that small changes in spine morphology, such as changes in the width of the spine neck, could lead to large changes in the amplitude of response to excitatory synaptic inputs on to the spine. It is now known that spines are rich in actin filaments, which have the capacity to drive such changes in spine shape [**56**]. Moreover, there is increasing experimental evidence that the growth and removal of spines provides an important

substrate for structural changes during brain development [**57, 58, 59**]. It is less clear whether changes in spine morphology play a significant role in adult plasticity. Nevertheless, the basic geometry of a spine does provide an isolated biochemical microenvironment for Ca^{2+} to accumulate, and Ca^{2+} is thought to be a major chemical signal for the induction of synaptic plasticity [**60, 61**], see §2.4. The dynamics of calcium diffusion in dendritic spines has been explored in a number of computational models [**62, 63**].

2.4. Synaptic plasticity

An important property of a synapse is its effective strength, which can be identified as the maximal conductance change induced by the arrival of a single action potential eg. the factor $\bar{g}$ in equation (2.3). A great deal of experimental evidence has accumulated that these synaptic weights can undergo experience–dependent persistent changes over time. Such changes are thought to be the neural correlates of learning and memory. Most experimental studies of synaptic plasticity have focused on refining the original theoretical postulate due to Hebb [**64**]: *When an axon of cell A is near enough to excite cell B or repeatedly or persistently takes part in firing it, some growth process or metabolic change takes place in one or both cells such that A's efficiency, as one of the cells firing B, is increased.* A more modern interpretation of this postulate is that synaptic modification is driven by correlations in the firing activity of presynaptic and postsynaptic neurons.

In many regions of the brain, neurons are found to exhibit bidirectional plasticity in which the strength of a synapse can increase or decrease depending on the stimulus protocol [**65, 66, 67, 68, 69**]. Long term potentiation (LTP) is a persistent increase in synaptic efficacy produced by high-frequency stimulation of presynaptic afferents or by the pairing of low frequency presynaptic stimulation with robust postsynaptic depolarization. Long–term synaptic depression (LTD) is a long-lasting decrease in synaptic strength induced by low-frequency stimulation of presynaptic afferents. More recent experimental studies suggest that both the sign and degree of synaptic modification arising from repeated pairing of pre- and post-synaptic action potentials depend on their relative timing [**70, 71, 72**]. Long-term strengthening of synapses occurs if presynaptic action potentials precede postsynaptic firing by no more than about 50 ms. Presynaptic action potentials that follow postsynaptic spikes produce long-term weakening of synapses. The largest changes in synaptic efficacy occur when the time difference between pre- and postsynaptic action potentials is small, and there is a sharp transition from strengthening to weakening. This phenomenon of spike timing–dependent plasticity (STDP) is illustrated in Figure 5. In the following, we consider some of the molecular mechanisms underlying bidirectional synaptic plasticity and how they can be modeled. Before proceeding, however, it is useful to distinguish between the induction, expression and maintenance of LTP and other forms of synaptic plasticity. LTP induction refers to the early steps that trigger the modification process, LTP expression is the proximal cause of synaptic modifications that may last hours or days, and LTP maintenance concerns the more general problem of how a synaptic change can endure over longer periods in the face of constant molecular turnover. The maintenance of synaptic plasticity, which requires modifications in gene expression and protein synthesis, is still poorly understood and will not be discussed further here.
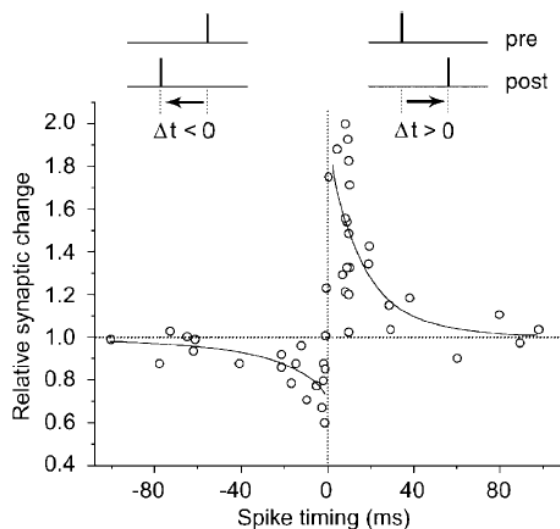
FIGURE 5. Spike-timing-dependent synaptic plasticity observed in hip-
pocampal neurons. Each data point represents the relative change in the
amplitude of evoked postsynaptic current after repetitive application of
pre- and postsynaptic spiking pairs (1 Hz for 60 s) with fixed spike timing
Δt, which is defined as the time interval between pre- and postsynaptic
spiking within each pair. Long-term potentiation (LTP) and depression
(LTD) windows are each fitted with an exponential function. [Reprinted
from Bi and Poo [73], with permission from J. Neurosci.]

NMDA receptors and calcium influx

Calcium has long been suggested as a major signaling agent for the induction of
LTP and LTD [74, 75, 66, 76], and more recently for STDP [72]. However, the
details of the induction mechanism depend on the type of synapse and the stim-
ulus protocol. We will focus on NMDA–dependent mechanisms, which arise in
the most commonly studied synapses, namely those connecting the axons of the
Schaffer collateral/commissural system to pyramidal neurons in the CA1 region of
the hippocampus. As illustrated in Figure 2, calcium can enter these cells through
channels controlled by NMDA receptors. Two conditions are necessary for the open-
ing of such channels: (i) arrival of an action potential at the presynaptic terminal
releases the excitatory neurotransmitter glutamate which then binds to NMDA re-
ceptors and (ii) the postsynaptic cell is sufficiently depolarized so that magnesium
ions are unblocked from the NMDA channels allowing the influx of calcium. One
source of strong depolarization is the back propagation of an action potential into
the dendritic tree, which is a signature that the postsynaptic neuron has fired a
spike. Given that calcium ions can enter the cell only if glutamate has been released
by presynaptic activity *and* if the postsynaptic membrane is sufficiently depolar-
ized, it follows that the NMDA receptor is a natural candidate for the biophysical
implementation of a Hebbian–like mechanism for detecting correlations between
presynaptic and postsynaptic activity.

Recently Shouval *et al* [**77**] have proposed a mechanism for calcium–induced bidirectional synaptic plasticity, based on the idea that the maximum level of postsynaptic calcium concentration determines whether LTP or LTD occurs. That is, at intermediate calcium levels LTD occurs whereas at high calcium levels LTP occurs. Suppose that a presynaptic spike arrives at an NMDA synapse at time T and the postsynaptic membrane potential is $u(t)$. The calcium current through an NMDA receptor–controlled channel is taken to be of the form [**77**]

$$(2.27) \qquad I_{Ca}(t) = \bar{g}_{Ca}\alpha(t - T)[u(t) - u_{Ca}]B(u(t)),$$

where $\bar{g}_{Ca}$ is the maximal conductance of the channel and u_{Ca} is the reversal potential of calcium $(130mV)$. The function $\alpha(t-T)$ describes the time course of binding to NMDA receptors and is typically taken to be the sum of a fast $(\tau_f = 50ms)$ and a slow $(\tau_s = 200ms)$ exponential:

$$(2.28) \qquad \alpha(t) = I_f e^{-t/\tau_f} + I_s e^{-t/\tau_s}, \quad t > 0.$$

The experimentally fitted function

$$(2.29) \qquad B(u) = \frac{1}{1 + \eta[Mg^{2+}]e^{-\gamma u}},$$

with $\gamma = 0.062, \eta = 1/3.57$, describes the unblocking of the channel at depolarized levels of membrane potential [**78**]. The extracellular magnesium concentration is approximately $1mM$ $(10^{-3}$ molars or moles per liter). If there are several presynaptic spikes within 100ms then calcium accumulates inside the cell. The change in the calcium concentration $[Ca^{2+}]$ can be described by the simple first order kinetic equation

$$(2.30) \qquad \frac{d[Ca^{2+}]}{dt} = I_{Ca}(t) - \frac{[Ca^{2+}]}{\tau_{Ca}}$$

with $\tau_{Ca} = 50ms$.

In order to completely determine the calcium current, it is necessary to specify the dynamics of the postsynaptic membrane potential $u(t)$. In the case of STDP, the main source of depolarization is thought to arise from a back propagating action potential (although this might not be the whole story [**79**]). This can be modeled by taking [**77**]

$$(2.31) \qquad u(t) = \eta(t - \widehat{T}), \quad \eta(t) = U\left(\widehat{I}_s e^{-t/\hat{\tau}_s} + \widehat{I}_f e^{-t/\hat{\tau}_f}\right)$$

where $\widehat{T}$ is the last firing time of the postsynaptic cell and $\eta(t)$ is the profile of the BPAP, which is taken to be the sum of a fast $(\hat{\tau}_s = 5ms)$ and a slow $(\hat{\tau}_f = 25ms)$ exponential. Equations (2.27), (2.30) and (2.31) determine how the maximum level of calcium influx depends on the relative timing of presynaptic and postsynaptic spikes, and hence whether LTP or LTD occurs (see Figure 6) [**77**]. One potential problem with this particular calcium control mechanism for STDP is that it predicts LTD can also be induced by a sequence of pre–post spikes if the separation between spikes is larger than about $\Delta t = 40ms$. The reason is that in this case the removal of the magnesium block (induced by the BPAP) occurs at a time when the probability of glutamate binding is reduced. As a consequence less calcium enters the cell so that only the LTD threshold is reached. There is currently no convincing experimental evidence for such a form of LTD. This has motivated a more detailed

biophysical model in which the time course of the calcium current rather than just its level acts as signal for STDP [**80**].
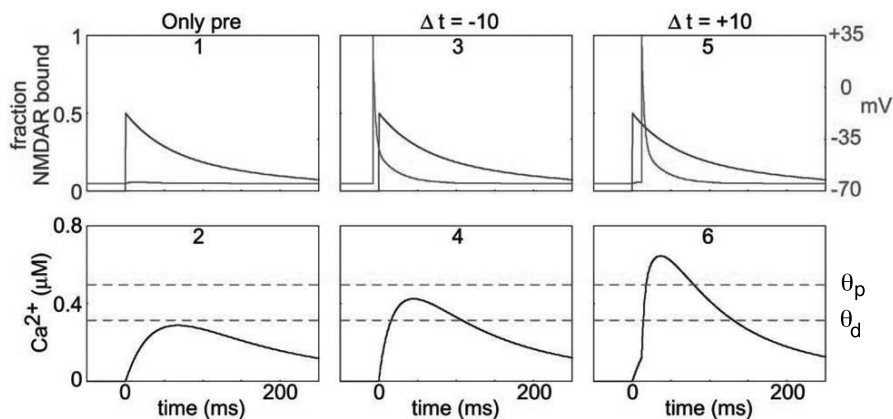

FIGURE 6. (1,2) Presynaptic stimulation alone results in the binding of glutamate to NMDA receptors but only a small depolarization so that there is only moderate calcium influx. (3,4) Post–pre stimulation ($\Delta t = -10ms$) results in a large brief depolarization due to a BPAP, which partially overlaps with the onset of glutamate binding to NMDA receptors. The calcium influx is increased so that it crosses the threshold θ_d for LTD and there is a negative weight change. (5,6) Pre–post stimulation ($\Delta t = +10ms$) results in a large brief depolarization that completely overlaps with the period of significant glutamate binding to NMDA receptors. The resulting calcium influx is well above the threshold θ_p for LTP and there is a positive weight change. [Reprinted from Shouval *et al* [**77**], with permission of the National Academy of Sciences.]

Regulation of AMPA receptors

There is growing experimental evidence that a major component of the postsynaptic expression of LTP and LTD is the regulation of AMPA receptor trafficking, which results in changes in receptor number at the postsynaptic membrane, and hence modifications in synaptic strength [**81, 82, 83**]. The total number of synaptic AMPA receptors is determined by a nonequilibrium steady–state, in which the flux of receptors between the synaptic and extrasynaptic regions of the postsynaptic membrane is balanced by the rate of exchange of receptors with intracellular recycling pools (see Figure 7).

A mathematical model of AMPA receptor trafficking has recently been constructed [**84**] in terms of a simplified two-compartment model of a dendritic spine's surface membrane (see Figure 8). The first compartment represents the postsynaptic density (PSD) of the spine head, which is the protein-rich domain in the postsynaptic membrane of a dendritic spine that is directly apposed to the presynaptic active zone, and the second compartment represents the extrasynaptic membrane (ESM) of the remaining spine head and neck. AMPA receptors are assumed to diffuse freely in the extrasynaptic membrane. Within and near the PSD, however, AMPA receptor diffusion proceeds in a highly obstructed fashion. This is
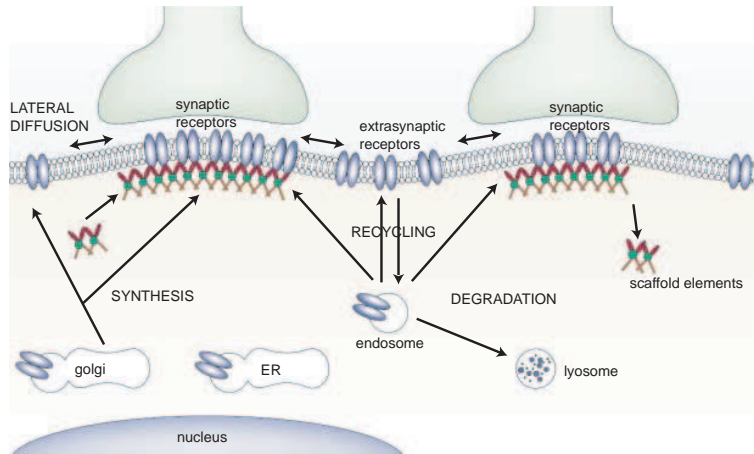
FIGURE 7. AMPA receptor trafficking involves exchanges between synaptic, extrasynaptic and intracellular compartments. The extrasynaptic diffusive receptors are immobilized by the scaffold-cytoskeleton complex at postsynaptic densities (PSDs). The extrasynaptic receptors are also exchanged with the intracellular recycling pool. Increasing or diminishing the number (or affinity) of scaffold molecules at the synapse changes proportionally the confinement capabilities, and subsequently the number of receptors at steady state. [Reprinted from Choquet and Triller [**82**], with permission from Macmillan Publishing Ltd: *Nature Reviews Neuroscience*, copyright 2003.]
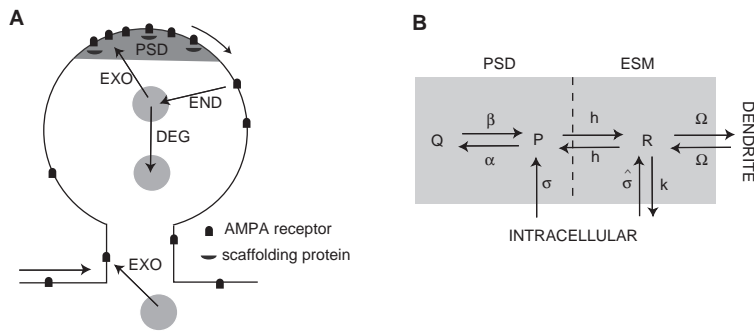
FIGURE 8. Compartmental model of AMPA receptor trafficking. (A) Schematic of AMPA receptor trafficking at a dendritic spine. Receptors stored in intracellular pools are continually exchanged with surface receptors through exo/endocytosis (EXO/END) and sorted for degradation (DEG). Surface receptors diffuse in the dendritic membrane and can be immobilized at the PSD through interactions with scaffolding proteins. (B) Simplified two-compartment model of a dendritic spine. Free receptors (P) bind to scaffolding proteins within the PSD to form bound receptors (Q) at a rate α and unbind at a rate β. Free receptors flow between the the PSD and ESM at a hopping rate h, and flow between the ESM and surface of the dendritic cable at a rate Ω. Free receptors (R) within the ESM are internalized at a rate k. Receptors are inserted into the PSD at a rate σ.

probably due to a number of factors including the attraction and binding of re-
ceptors to scaffolding proteins, the transient corralling of receptors to restricted
domains by the underlying actin cytoskeleton, and the repulsion of receptors by
picket-like transmembrane proteins. Single-particle tracking data suggests that the
PSD acts as a confinement domain for diffusing receptors, and that about half of
the AMPA receptors within the PSD are mobile [**82**]. Experimental estimates for
the diffusivity D in the PSD and ESM range from 0.01 to 0.5 $\mu m^2 s^{-1}$. Given
that the typical length–scale of a spine is $\ell_{sp} = 1\mu m$, it follows that the time–scale
$\sqrt{\ell_{sp}^2/D}$ for diffusion within each compartment is 1-10 sec, which is faster than
the typical time–scale (minutes) for the expression of LTP/LTD. Thus, assuming
that each compartment is homogeneous, the corresponding free receptor concen-
tration can be taken to be spatially uniform. In order to model the confinement
of diffusing particles within the PSD, the boundary between the PSD and ESM
compartments is treated as a potential barrier over which receptors must hop in
order to enter or exit the PSD. For simplicity, the net flux across the boundary
is taken to be proportional to the difference in concentrations on either side of
the barrier, with the hopping rate dependent on the barrier height. Receptors can
also hop between the ESM and the surrounding membrane of the dendritic cable,
with the net flux proportional to the difference between the free receptor concen-
trations in the ESM and dendrite. The latter is taken to have a fixed background
receptor density. The hopping rate between the ESM and dendrite incorporates
the effects of spine neck geometry on restricting the flow of receptors. In addition
to the lateral movement of AMPA receptors within the plasma membrane, there
is a continual exchange of surface receptors with pools of intracellular receptors
through exo/endocytosis. Experimentally it is found that under basal conditions,
the rates of receptor exo/endocytosis are of the order 10-30 minutes. (In fact there
are at least two separate sources of intracellular AMPA receptors, one consisting of
GluR1/2 heteromers that are inserted into the ESM during LTP and the other con-
sisting of GluR2/3 heteromers that are inserted into the PSD during constitutive
recycling. Here we do not distinguish between the two receptor types.)

Let P, Q denote the concentration of free and bound receptors in the PSD
and R denote the corresponding free receptor concentration in the ESM. It is also
assumed that there is a fixed concentration L of active binding sites within the PSD.
Receptor trafficking in the PSD is then described in terms of the kinetic equations
[**84**]

$$(2.32) \qquad \frac{dP}{dt} = \sigma - \alpha[L - Q]P + \beta Q - h[P - R]$$

$$(2.33) \qquad \frac{dQ}{dt} = \alpha[L - Q]P - \beta Q$$

where σ is the rate of exocytosis of receptors into the PSD, and α, β denote the
rates at which receptors bind and unbind to scaffolding proteins. The corresponding
kinetic equation for the receptor concentration in the ESM is given by

$$(2.34) \qquad \frac{dR}{dt} = \hat{\sigma} - kR + h[P - R] - \Omega[R - \overline{R}]$$

where $\hat{\sigma}$ is the rate of exocytosis into the ESM and k is the rate of endocytosis.
The last term on the right–hand side of equation (2.34) represents the hopping of
receptors between the ESM and surrounding dendritic cable with hopping rate Ω.

The fixed background receptor concentration in the dendritic membrane is denoted by $\overline{R}$. Two basic assumptions of the model are (1) the strength of a synapse can be identified with the number of synaptic receptors $(P + Q)$ and (2) there is a separation of time-scales between the activation of the signaling pathways by the postsynaptic calcium signal during the induction of LTP/LTD (seconds) and the subsequent expression of LTP/LTD via receptor trafficking (minutes). One can then determine the time–dependent variation in receptor number induced by rapid modifications in one or more model parameters and compare these with experimentally measured time courses for LTP/LTD. Good agreement is obtained for physiologically reasonable choices of parameters provided that changes in receptor trafficking are correlated with changes in the concentration L of binding sites (see [84] for more details)

Model of a CaMKII switch

One of the major challenges concerning synaptic plasticity is unraveling the signaling pathways that convert a transient elevation in Ca^{2+} concentration, which can last for just a few hundred milliseconds, to a persistent change in synaptic strength, which can last for hours or even days. One molecule that appears to play a critical role in LTP is calcium/calmodulin–dependent protein kinase II (CaMKII). It has been shown that CaMKII activation is persistent, is required for LTP and can by itself produce potentiation (see [85] for a review). Further evidence that CaMKII may serve as a memory molecule is provided by the finding that it has autocatalytic properties that would allow it to act as a bistable molecular switch. The basic biochemical autocatalytic mechanism is as follows (see Figure 9(a,b)). CaMKII is composed of two rings, each with six kinase subunits. Each subunit has a single phosphorylation site that, when activated, makes the subunit active independently
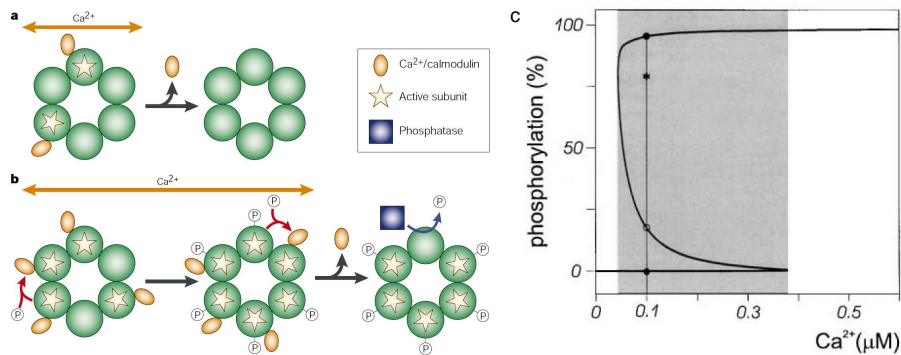
FIGURE 9. (a) At low Ca^{2+} concentrations there is little autophosphorylation, so that subunits of CaMKII are only active if bound by Ca^{2+}/calmodulin. (b) A transient increase in Ca^{2+} concentration causes an increase in the rate of phosphorylation leading to persistent activity after Ca^{2+} falls. [Reprinted from Lisman *et al* [85], with permission from Macmillan Ltd: *Nature Reviews Neuroscience*, copyright 2002.] (c) Steady–state levels of phosphorylation as a function of Ca^{2+} concentration calculated using a biophysical model [86]. A pair of stable states exists over a range of concentrations.

of Ca^{2+}. In the absence of phosphorylation, a subunit is only active when bound by a calcium binding protein known as Ca^{2+}/calmodulin. Initial autophosphorylation of a CaMKII ring requires the binding of two Ca^{2+}/calmodulin molecules, one to activate a catalytic subunit and another to expose the phosphorylation site of a neighboring substrate subunit. At the resting Ca^{2+} concentration, this process is slow with an average rate of one initial autophosphorylation every few hours. Once one or more sites of a ring are phosphorylated, subsequent phosphorylation is much faster since only a single Ca^{2+}/calmodulin molecule is required, namely, to expose the phosphorylation site on a substrate subunit adjacent to an already activated subunit.

A recent biophysical model [**86, 87, 88**] has shown how the interplay between autophosphorylation and dephosphorylation by phosphotase-1 (PP1) enzymes can generate two stable states of phosphorylation at resting levels of Ca^{2+}, see Figure 9(c). A transient increase of Ca^{2+}, induced for example by an LTP stimulus protocol, can switch the system from an unphosphorylated (DOWN) state to a persistent, highly phosphorylated (UP) state. Such a persistent change in the activation of CaMKII following LTP induction could then mediate persistent changes in synaptic strength. The system of equations describing the reaction kinetics takes the following form [**86, 87**]:

$$\frac{dP_0}{dt} = -v_1 M P_0 + v_3 P_1$$
$$\frac{dP_1}{dt} = v_1 M P_0 - v_3 P_1 - v_2 P_1 + v_3 2 P_2$$
$$\frac{dP_j}{dt} = v_2 w_{j-1} P_{j-1} - v_3 j P_j - v_2 w_j P_j + v_3 (j+1) P_{j+1}$$
$$\frac{dP_M}{dt} = v_2 P_{M-1} - v_3 M P_M$$

where P_j denotes the concentration of j–fold phosphorylated rings, M is the number of subunits on a ring, v_1 is the initial per site rate of autophosphorylation, v_2 is the per site rate of autophosphorylation of partially phosphorylated CaMKII, and v_3 is the rate of dephosphorylation by PP1. The factors w_j count the number of ring configurations that can undergo the transition $P_j \rightarrow P_{j+1}$. The autophosphorylation rates v_1 and v_2 are taken to depend on calcium concentration according to

$$(2.35) \qquad v_1 = \frac{k_1([Ca^{2+}]/K_{H1})^8}{(1 + ([Ca^{2+}]/K_{H1})^4)^2}, \qquad v_2 = \frac{k_1([Ca^{2+}]/K_H 1)^4}{1 + ([Ca^{2+}]/K_{H1})^4}$$

where k_1 is a rate constant, and the resting Ca^{2+} concentration ($100nM$) is well below the constant K_{H1} ($0.7\mu M$). Dephosphorylation proceeds according to a Michaelis-Menten scheme:

$$SP + E \rightleftharpoons SPE \rightarrow E + S,$$

where S is an unphosphorylated subunit, SP is a phosphorylated subunit, and E denotes the enzyme PP1. Thus

$$(2.36) \qquad\qquad v_3 = \frac{k_2[E]}{K_M + \sum_{j=1}^{M} j P_j}$$

for constants k_2, K_M. The concentration $[E]$ of PP1 is itself modulated by calcium concentration as detailed elsewhere [86]. The resulting full system of equations can be solved numerically to determine the steady state levels of phosphorylation as a function of Ca^{2+} concentration, and hence establish bistability.

Recall from §2.2 that certain care has to be taken in using rate equations when the number of reacting molecules is small, since stochastic fluctuations become important. Recent measurements indicate that for a typical postsynaptic density the number of CaMKII molecules is only around 30 [89]. In order to determine the stability of the CaMKII switch with respect to fluctuations, Monte Carlo simulations of the full stochastic chemical equations have recently been carried out. These simulations suggest that even a small number of molecular switches can maintain stable persistent activation [88].

Computational role of STDP

One of the problems with standard formulations of Hebbian learning is that without additional constraints, the level of activity in a network can grow or shrink in an uncontrolled manner. The observation that LTP and LTD can occur at the same synapse depending on the pre-post correlations suggests that STDP can provide a mechanism for self-stabilization of weights and firing rates in a network. A second important requirement of any learning scheme is that networks need to operate competitively. Thus, normally it does not make sense to drive all synapses into similar states through learning, because the network will then no longer contain inner structure. Instead, most real networks in the brain are highly structured, forming maps or other subdivisions. There have been a number of recent theoretical studies exploring the possible role of STDP in stability and competition during learning (see [7] for a review). We end this lecture by briefly describing another potential application of STDP, namely to prediction and reward learning [90]. Animals in the environment often have to react quickly to the earliest signs of harmful stimuli or potential prey. That is, they have to predict or anticipate future events. STDP provides a hint at how a simple form of predictive coding could be implemented at the cellular level. Consider as an example a single neuron receiving inputs from a set of N presynaptic cells that fire sequentially (see Figure 10). This could be the result of a moving stimulus. Initially all synapses have the same weight $w_j = w_0$ for all $j = 1, \ldots N$. Suppose that the postsynaptic neuron initially fires at time T during the presentation of the sequence. All synapses that have been activated prior to the postsynaptic spike are strengthened while synapses that have been activated immediately afterward are depressed. After many trials, the firing time of the postsynaptic neuron within the sequence has shifted by an amount $-\Delta t$. Interestingly, this effective shift in the distribution of synaptic connections is consistent with experimental observations of a shift in the place fields of hippocampal neurons [91].

The shift of responses towards earlier predictors plays a central role in classical conditioning as exemplified by Pavlov's dog. An unconditioned stimulus (US) – food – is preceded by a conditioned stimulus (CS) – a bell – at a fixed time interval ΔT. Before learning the US evokes an immediate response – salivation – wheres the CS evokes no response. After learning, the dog starts to salivate in response to the CS. Thus the reaction has moved from the US to the CS, which reliably predicts the US. STDP can replicate this result if the time difference ΔT between two stimuli is less than the width of the learning window. The mechanism is identical to the
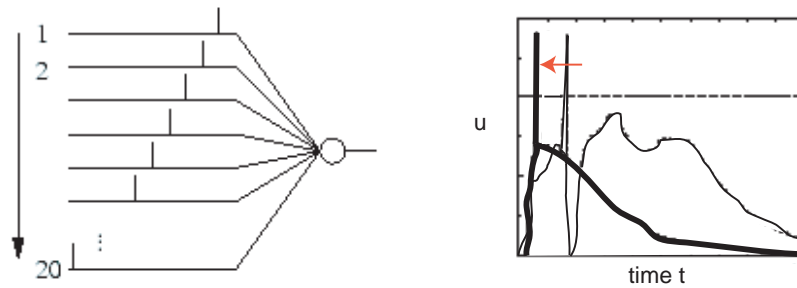
FIGURE 10. A) A sequence of presynaptic spikes is presented to a single neuron. Such a sequence could be generated by a moving stimulus. B) After many trials the synapses in the early part of the sequence have been strengthened so that the neuron fires earlier by an amount Δt. Initial response is shown by thin lines and adapted response by thick lines

previous example illustrated in Figure 10, except that the inputs are clustered into two groups corresponding to US and CS. A shift to early predictors is also observed experimentally in recordings from dopamine neurons in the basal ganglia concerned with reward processing [92]. Before learning some dopamine neurons respond to an unpredicted reward. During learning this response decreases and the neurons now increase their firing to a reward-predicting stimulus. The more predictable the reward becomes, the less strongly the neurons fire when it appears, and if it does not appear the neurons are inhibited. There are in fact a number of different types of reward–predicting dopamine neurons with distinct responses. For example, some neurons fire a prolonged discharge following a trigger stimulus until a reward is delivered. Dopamine neurons have a central role in guiding our behavior and thoughts [93]. Their performance is impaired by every addictive drug and in mental illness. They are also lost in dramatically impairing illnesses such as Parkinson's disease. If dopamine systems are overstimulated, we may hear voices, experience elaborate bizarre cognitive distortions, or engage excessively in dangerous goal-directed behavior. Dopamine function is also central to the way that we value our world, including the way that we value money and other human beings.

Firing Rates, Spike Statistics and the Neural Code

A major debate in the neuroscience literature is whether neurons use a rate code or a spike code to carry out information processing [**94, 95**]. The former is some form of smoothed version of the sequence of spikes obtained by averaging with respect to time, experimental trials or populations of neurons. The latter on the other hand preserves temporal information at the level of individual spikes, that is, on a millisecond time scale. Since generating a rate code requires averaging over a distribution of spikes, it is necessary to specify the associated spike statistics. It turns out that in many cases the output spike train of a single neuron can be modeled quite well by an inhomogeneous Poisson process. Such a spike train generates a stochastic input current to other neurons via synaptic coupling. Hence, it is important to understand how neurons respond to stochastic inputs at both the single neuron and network levels. In the latter case, the degree of cross–correlation between spike trains of distinct neurons is an important factor in determining the appropriate description of network dynamics. In cases where the spike trains are incoherent, it is often possible to carry out some form of population averaging, leading to a rate–based description of network dynamics (see §5). On the other hand, when there is a high level of coherence across spike trains the rate reduction procedure breaks down. One situation where this occurs is when the individual neurons act as intrinsic oscillators along the lines of §1.2. One can then use phase reduction methods to investigate network oscillations and synchrony as outlined in §4. In this third lecture, we focus on some of the basic issues regarding neural coding and noise.

3.1. The neural code

Rate codes

The most commonly used definition of a firing rate $\nu(t)$ refers to a *temporal average*. Suppose that we represent a sequence of spikes at times $\{T^1, \ldots, T^n\}$ in terms of the sum of delta functions

$$(3.1) \qquad \rho(t) = \sum_m \delta(t - T^m).$$

Introducing a temporal filter function $K(t)$ with $K(t) = 0$ for $t < 0$, we set

$$(3.2) \qquad \nu(t) = \int_{-\infty}^{\infty} K(t - \tau)\rho(\tau)d\tau = \sum_m K(t - T^m).$$

The degree of smoothing will depend on the choice of K as illustrated in Figure 1. Note that if $K(t) = T^{-1}$ for $0 \le t < T$ and is zero otherwise, then $\nu(t)$ is simply the mean number of spikes within the time interval $[t - T, t]$. There are a number of problems with the idea that neurons use a time–averaged rate code [**97**]. From
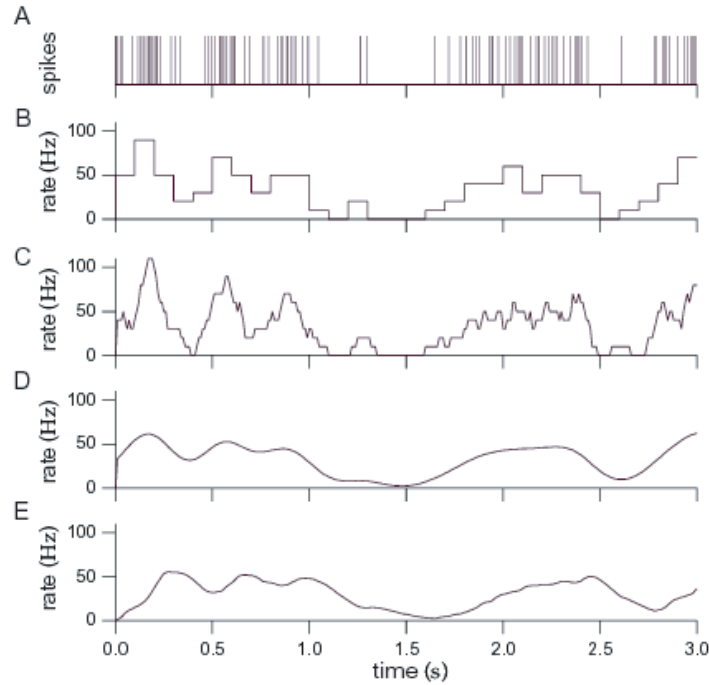
49

FIGURE 1. Firing rates obtained by filtering a spike train with various convolution functions $K(t)$. (A) Spike train recorded from a neuron in the inferotemporal lobe of a monkey. (B) Discrete-time firing rate obtained by binning time and counting spikes with $\Delta t = 100$ ms. (C) Filtering with a step function of width 100 ms. (D) Filtering with a Gaussian $K(t) = (2\pi\sigma^2)^{-1/2}e^{-t^2/2\sigma^2}$ with $\sigma^{-1} = 100$ ms. (E) Filtering with an alpha function having $\alpha^{-1} = 100ms$. [Reprinted from Baddeley, et al [96], with permission from the Royal Society.]

behavioral experiments it is known that reaction times tend to be too short for neurons to sample over a sufficient number of spikes. For example, a fly can react to new stimuli and change the direction of flight within $30 - 40$ ms [94]. Moreover, humans can recognize certain aspects of visual scenes in just a few hundred milliseconds [98], even though recognition is believed to involve several processing stages. (See, however, Rossum *et al* [99] who show how fast computation through a number of processing levels can be achieved using a population rate code). Finally, given that real spike trains are highly irregular, a reliable estimate of the mean firing rate requires averaging over a larger number of spikes.

There is a second definition of rate, which is more applicable to time-dependent stimuli. This is constructed by averaging over *experimental trials* and representing the data in a Peri-Stimulus-Time-Histogram (PSTH). For each trial the time interval is divided into bins of size Δt and the number of spikes appearing in each bin is counted. Summing over the N trials, the total number of spikes $n(t, t + \Delta)$ in the

interval $[t, t + \Delta t)$ is

$$(3.3) \qquad n(t, t + \Delta t) = \sum_{j=1}^{N} \int_{t}^{t+\Delta t} \rho_j(t)dt,$$

where j, $j = 1, \ldots, N$, labels trials. That is, $\rho_j(t) = \sum_m \delta(t - T_j^m)$ where T_j^m is the mth firing time of the jth trial. We then identify the rate with the *spike density*

$$(3.4) \qquad \nu(t) = \frac{1}{\Delta t} \frac{n(t, t + \Delta t)}{N} = \langle \rho(t) \rangle,$$

where $\langle \rangle$ denotes trial averaging. Sometimes this is combined with time averaging to obtain a smooth rate variable. An obvious problem with this approach is that it cannot be used by neurons in the brain – a frog does not catch a fly by waiting for the insect to fly repeatedly along exactly the same trajectory; it has to act on a single trial! Nevertheless, the spike density can make sense experimentally if there is a large population of independent neurons that respond to the same stimulus. Instead of recording from the population of N neurons in a single run, it is experimentally easier to record from a single neuron and average over many trials. This leads to the third definition of rate based on *population averaging*. Given a homogeneous population of N identical neurons, the rate is defined by equations (3.3) and (3.4) except that now $j = 1, \ldots N$ labels the neurons within the population and T_j^m is the mth firing time of the jth neuron. One of the useful properties of the population activity is that it can respond very quickly to changes in inputs [**100**], see §3.4. However, it does require that the population is sufficiently homogeneous. Population rate codes are used extensively in modeling the large–scale spatio-temporal dynamics of cortex [**101, 102**], see §5.

Spike codes
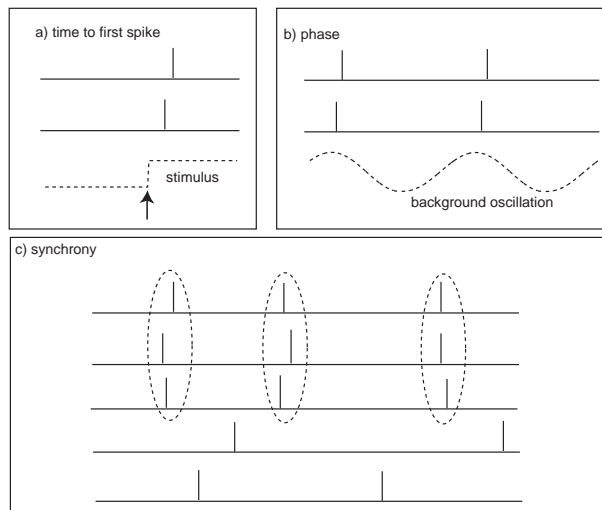Three possible coding strategies based on spike timing are shown in Figure 2:

FIGURE 2. Three examples of spike codes

Time-to-first-spike: Suppose that there is a rapid change of input at a time t_0. Such an abrupt change could be due to a saccade, for example, in which an animal's gaze jumps to a new location. One can then imagine a code based on how quickly a neuron fires after t_0, with a shorter latency signalling a stronger stimulus. This form of coding scheme has been advocated as a means of carrying out fast computations [98]. However, as we have already mentioned, it is also possible to achieve fast computations using a population code. Moreover, one expects there to be a correlation between the time-to-first-spike and the firing rate of a neuron.

Phase: A second coding strategy is based on the timing of spikes relative to some reference background oscillation. For example, extensive studies of rodents have demonstrated direct behavioral correlates of hippocampal neuronal activity, the most robust of which is the selective activation of certain hippocampal cells at particular locations in space called place fields [103]. When a rodent is exploring its environment (or is in REM sleep) cells in the hippocampus participate in 4-10 Hz theta rhythms. A key observation is that the spike activity of a hippocampal place cell advances to earlier phases of the theta cycle as the animal passes through the cell's place field [103]. One possible interpretation of this phase advance is that it reflects a prediction of the sequence of upcoming locations based on the rat's current position [104], that is, it is part of a path integration system. Theta oscillations are superimposed upon faster gamma (40 Hz) oscillations, and these may organize the readout of sequential locations during a theta cycle.

Correlations/Synchrony: Various experimental studies have shown that correlations in the firing patterns of groups of neurons are stimulus-dependent. For example, neurons in the antennal lobe of insects are typically synchronized by 20 Hz oscillations – when such synchronization is artificially disrupted the specificity of downstream responses to different odors decreases [105]. Stimulus-induced oscillations have also been observed in the olfactory lobe of mollusks and rabbits [106], and the visual cortex of cats [107]. Correlated activity between neurons can also be considered without reference to intrinsic oscillations. For example, analysis of the activity of visual neurons in the lateral geniculate nucleus has shown that significantly more information about the stimulus can be extracted from their spike trains if coincident spikes are taken into account separately from the non-coincident ones [108]. Similarly, recordings from primary auditory cortex indicate that when a stimulus is turned on, neurons respond by changing their firing rates and their correlations; in many cases, the firing rate modulations are transient whereas the evoked changes in correlations can be sustained [109]. The possible role of stimulus-induced correlated or synchronous activity is still unclear. One suggestion is that synchrony between pairs of neurons in the visual cortex provides a mechanism for signalling whether or not such neurons are responding to a single object or two distinct objects that induce the same firing rates [110]. Indeed, stimulus-induced phase synchronization has been proposed as a solution to the so-called binding problem, that is, how to bind together the multitude of different representations (color, form, location) of an object, although it remains a controversial issue [111, 112]. An alternative suggestion is that correlations do not contain information about the nature of a stimulus, but provide an attentional gating mechanism that controls the flow of information [113]. The issue of network oscillations and synchrony will be considered in §4.

Reverse correlation methods

One important question concerns how a spike or rate code is used to represent information about a stimulus. Reverse correlation methods provide a powerful tool for investigating stimulus encoding and decoding [**94, 95**]. Consider a neuron that is driven by a time dependent stimulus $s(t)$. Suppose that every time a spike occurs, we record the time course of the stimulus in a time window of about 100 msec immediately before the spike. Averaging the results for several spikes yields the typical time course of the stimulus just before a spike. Such a procedure is called a *reverse correlation* method. In contrast to the Peri-Stimulus-Time-Histogram (PSTH), which is constructed by averaging the neuron's response over several trials with the same stimulus, reverse correlation involves averaging the stimulus under the condition of the same response, that is, the firing of a single spike. The so-called spike-triggered average stimulus $C(\tau)$ is defined according to

$$(3.5) \qquad C(\tau) = \left\langle \frac{1}{M} \sum_{m=1}^{M} s(T^m - \tau) \right\rangle \approx \frac{1}{\langle M \rangle} \left\langle \sum_{m=1}^{M} s(T^m - \tau) \right\rangle$$

where the stimulus is first averaged over all M spikes $T^1, \dots, T^M$ in a given trial of length T and then it is averaged over trials. It is also assumed that for large N the total number of spikes on each trial is well approximated by the average number of spikes per trial, $M \approx \langle M \rangle$. Under such an approximation, we can rewrite $C(\tau)$ in the form

$$(3.6) \qquad C(\tau) = \frac{1}{\langle M \rangle} \int_0^T \langle \rho(t) s(t - \tau) \rangle dt = \frac{1}{\bar{\nu} T} \int_0^T \nu(t) s(t - \tau) dt$$

where $\rho(t) = \sum_m \delta(t - T^m)$, $\bar{\nu} = \langle M \rangle / T$ is the mean firing rate and

$$(3.7) \qquad \nu(t) = \langle \rho(t) \rangle = \frac{1}{N} \sum_{j=1}^{N} \sum_{m=1}^{M} \delta(t - T_j^m)$$

with j labeling the trial. A schematic illustration of the spike-triggered average is shown in Figure 3. One common application of spike–triggered averaging is to determine the linear response properties of a neuron. That is, using a white noise stimulus one can identify the resulting spike–triggered average as the optimal linear filter for modeling the relationship between an input stimulus and the output firing rate of a neuron [**95**]. Another interesting application has been to decoding the spike trains of the H1 neuron of the fly [**94**]. The H1 neuron detects the motion of visual images during flight in order to generate and guide stabilizing motor corrections. In experiments, the fly is usually held fixed while a visual image with a time-varying velocity is presented. The basic idea of spike decoding is to generate a linear estimate of a stimulus based on the neuron's firing times.

3.2. Spike statistics and the Poisson process

In vivo recordings of neuronal activity are characterized by a high degree of irregularity. One often finds that the statistics of neuronal spike trains can be modeled quite well by a Poisson process. Suppose that a neuron emits a sequence of spikes at times $T^1, T^2, \dots, T^n$. One way to characterize this sequence statistically is in terms of the probability density $\rho(T^1, \dots T^n)$ of finding such a sequence over many experimental trials. In other words, the probability of having a sequence of n spikes in the interval $[0, T]$ with the ith spike falling between the times T^i and $T^i + \Delta t$ is
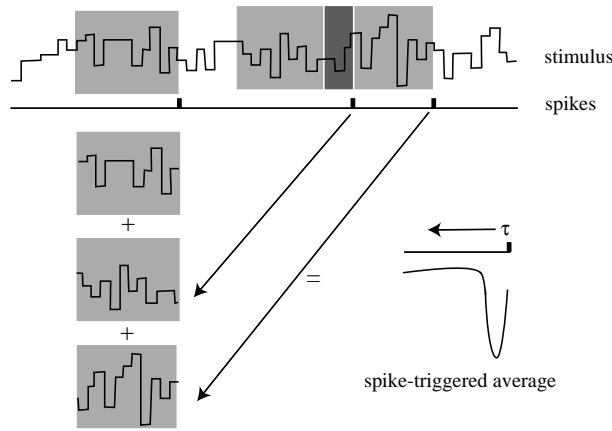
FIGURE 3. Schematic diagram illustrating the procedure for computing the spike-triggered average. Each gray rectangle contains the stimulus prior to one of the spikes shown along the time axis. These are averaged over spikes and trials to produce the waveform shown in the lower right.

$P[T^1, \ldots T^n] = \rho(T^1, \ldots T^n)(\Delta t)^n$. In principle, the probability of an event occurring, namely the firing of the next spike, could depend on the entire history of past spikes. If this dependence only extends to the previous spike so that the inter-spike intervals are statistically independent, then the stochastic process is said to be a *renewal process*. If there is no dependence at all on preceding spikes so that the firing times are themselves independent then we have a *Poisson process*.

Homogeneous Poisson process

Consider a sequence of spikes generated by a homogeneous Poisson process, that is, one with a time-independent mean firing rate r. Divide a given time interval T into M bins of size $\Delta t = T/M$ and assume that Δt is small enough so that the probability of finding two spikes within any one bin can be neglected. Then the probability $P_T[n]$ of finding n spikes over the interval T is given by

$$P_T[n] = \lim_{\Delta t \to 0} \frac{M!}{(M-n)!n!}(r\Delta t)^n(1 - r\Delta t)^{M-n}.$$

This consists of the probability $(r\Delta t)^n$ of finding n spikes in n specific bins multiplied by the probability $(1 - r\Delta t)^{M-n}$ of not finding spikes in the remaining bins. The binomial factor is the number of ways of choosing n out of M bins with spikes. Using the approximation $M - n \approx M = T/\Delta t$ and defining $\varepsilon = -r\Delta t$, we have that

$$\lim_{\Delta t \to 0}(1 - r\Delta t)^{M-n} = \lim_{\varepsilon \to 0}\left((1 + \varepsilon)^{1/\varepsilon}\right)^{-rT} = e^{-rT}.$$

For large M, $M!/(M-n)! \approx M^n = (T/\Delta t)^n$, so that we obtain the Poisson distribution

(3.8) $$P_T[n] = \frac{(rT)^n}{n!}e^{-rT}.$$

Given that there are n independent spikes over the interval $[0, T]$, the probability that these spikes lie within specified bins of size Δt is $n!(\Delta t/T)^n$. Hence

$$(3.9) \qquad \rho(T^1, \ldots T^n) = n! \left(\frac{1}{T}\right)^n P_T[n] = r^n \mathrm{e}^{-rT}.$$

Also note that the fastest way to generate a sequence of Poisson spikes for constant r is to iterate the firing times $T^{n+1} = T^n - \log(x_{rand})/r$ with x_{rand} uniformly distributed over $[0, 1]$. A simple method for calculating the moments of the Poisson distribution is to introduce the moment generating function

$$(3.10) \qquad G(s) = \sum_{n=0}^{\infty} P_T[n] \mathrm{e}^{sn}.$$

Differentiating with respect to s shows that

$$(3.11) \qquad \left. \frac{d^k G(s)}{ds^k} \right|_{s=0} = \langle n^k \rangle.$$

The generating function for the Poisson process can be evaluated explicitly as

$$(3.12) \qquad G(s) = \exp(-rT) \exp(rT \mathrm{e}^s),$$

from which we deduce that

$$(3.13) \qquad \langle n \rangle = rT, \quad \sigma_n^2 = rT.$$

Another useful quantity is the interspike-interval (ISI) distribution. Suppose that a spike was last fired at time T^n. The probability of a homogeneous Poisson process generating the next spike in the interval $T^n + \tau \leq T^{n+1} \leq T^n + \tau + \Delta\tau$ is equal to the probability that no spike is fired for a time τ, which is $P_\tau[0] = \mathrm{e}^{-r\tau}$ multiplied by the probability $r\Delta\tau$ of generating a spike within the following interval $\Delta\tau$:

$$\mathbf{Pr}[\tau \leq T^{n+1} - T^n \leq \tau + \Delta\tau] = r\Delta\tau \mathrm{e}^{-r\tau}.$$

The ISI probability density is thus an exponential, $\rho(\tau) = r\mathrm{e}^{-r\tau}$. It follows that the mean interspike interval is

$$\langle \tau \rangle = \int_0^\infty r\mathrm{e}^{-r\tau} \tau d\tau = \frac{1}{r}$$

and the variance is

$$\sigma_\tau^2 = \int_0^\infty r\mathrm{e}^{-r\tau} \tau^2 d\tau - \langle\tau\rangle^2 = \frac{1}{r^2}.$$

The ratio of the standard deviation to the mean is called the *coefficient of variation* $C_V = \sigma_\tau/\langle\tau\rangle$. It follows that for a homogeneous Poisson process $C_V = 1$.

How well do Poisson statistics describe experimentally measured spike trains? One often finds that for ISIs longer than about $10 msec$ the ISI distribution is indeed approximately exponential. However, for shorter intervals there is a rapid decrease in the distribution reflecting the fact that neurons are refractory immediately after firing. This is illustrated in Figure 4. The data can be fitted more accurately by a gamma distribution $\rho[\tau] = r(r\tau)^k \mathrm{e}^{-t\tau}/k!$. Alternatively, one can introduce a refractory period into a standard Poisson model. Note that C_V values extracted from the spike trains of cortical neurons also take values around unity, provided that the mean interspike interval is not too small [115].
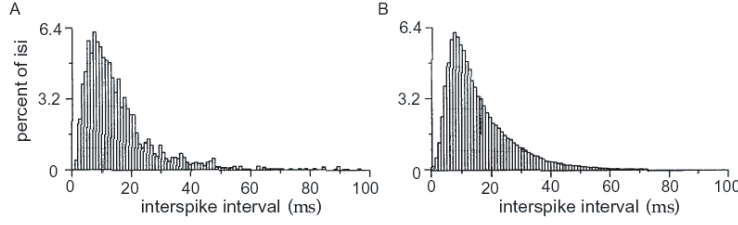
FIGURE 4. (A) Interspike interval distribution from a neuron from the MT cortical visual area of a macaque monkey responding to a moving image. (B) Interspike interval generated with a Poisson model with a stochastic refractory period. [Reprinted from [**114**], with permission from J. Neurosci.]

Inhomogeneous Poisson process

It is possible to generalize the above Poisson model to the case of a time-dependent rate $r(t)$. The simplest way to analyze this inhomogeneous Poisson process is to consider the probability distribution $\rho(T^1, \ldots T^n)$. This is given by the product of the probabilities $r(T^i)\Delta t$ that the neuron fires within the time intervals $T^i \le t \le T^i + \Delta t$ and the probabilities of not firing during the interspike intervals. The latter is given by

$$\mathbf{Pr}[\text{no spikes in } (T^i, T^{i+1})] = \prod_{m=1}^{M} (1 - r(T^i + m\Delta t)\Delta t),$$

where we have partitioned the interval (T^i, T^{i+1}) into M bins of size Δt. Taking the logarithm,

$$\log \mathbf{Pr}[\text{no spikes in } (T^i, T^{i+1})] = \sum_{m=1}^{M} \log(1 - r(T^i + m\Delta t)\Delta t)$$

$$\approx - \sum_{m=1}^{M} r(T^i + m\Delta t)\Delta t.$$

Taking the limit $\Delta t \to 0$ and exponentiating again shows that

$$\mathbf{Pr}[\text{no spikes in } (T^i, T^{i+1})] = \exp\left(- \int_{T^i}^{T^{i+1}} r(t)dt\right).$$

Hence

(3.14) $$\rho(T^1, \ldots T^n) = \prod_{i=1}^{n} r(t_i) \exp\left(- \int_0^T r(t)dt\right).$$

In the case of a time-dependent rate, one generates x_{rand} at each time step and a spike is fired if $r(t)\Delta t > x_{rand}$.

3.3. Stochastically driven IF neuron

The origin of neural irregularity is still not very well understood, and whether the variability is simply noise or some intricate neural encoding of information remains unclear. Nevertheless, one can distinguish between intrinsic sources of noise that

generate stochastic behavior at the level of single neuron dynamics, and extrinsic sources that arise from network effects. Examples of the former include thermal noise inducing membrane fluctuations, fluctuations in the opening and closing of ion channels in the postsynaptic cell membrane (see §2.2), and synaptic transmission failure. One way to model the effects of intrinsic noise is to define a noisy threshold in terms of an instantaneous escape rate, which depends on the distance of the membrane potential from the threshold [**7**]. Extrinsic noise reflects the fact that a typical neuron such as a pyramidal cell in the cerebral cortex receives input spikes from thousands of other neurons, which in turn receive input from their own presynaptic neurons and so forth. Rather than trying to model the brain as a single huge network, one typically focuses on a specific subset of neurons and treat inputs from other parts of the brain as a stochastic background. The stochastic arrival of excitatory and inhibitory pulses leads to a diffusion of the membrane potential that can be analyzed using Fokker–Planck equations [**116, 117, 118**]. We shall consider the effects of such diffusive noise on the dynamics of IF neurons.

Suppose that an IF neuron receives an external input $I_{\text{ext}}(t)$ together with a set of N spike trains generated by N background neurons. Denote the arrival times of the spikes from the kth presynaptic neuron by $\{T_k^n, n \in \mathbf{Z}\}$ for $k = 1, \ldots, N$. The membrane potential evolves according to the equation

$$(3.15) \qquad \tau \frac{du}{dt} = -u + R I_{\text{ext}} + \tau \sum_{n \in \mathbf{Z}} \sum_{k=1}^{N} w_k g_{\text{syn}}(t - T_k^n),$$

together with the reset condition that $u(t^+) = 0$ whenever $u(t) = 1$. Here $g_{\text{syn}}(t)$ represents a normalized synaptic conductance and w_k is the strength or efficacy of the kth synapse. Note that this equation treats input spikes as generating current rather than conductance fluctuations (ie. we have dropped the factor $u_{\text{syn}} - u$). The latter can be accounted for heuristically by introducing an input–dependent effective membrane time constant [**119**]. As a further simplification, we will ignore the shape of each postsynaptic potential by taking $g_{\text{syn}}(t) = \delta(t)$, where $\delta(t)$ is a Dirac delta function. Each input spike from the kth neuron then generates a change in the postsynaptic potential of the form

$$\Delta u(t) = w_k h(t - T_k^n), \quad h(t) = \mathrm{e}^{-t/\tau} H(t),$$

where $H(t)$ is the Heaviside function. Thus each spike induces a jump of size w_k, which represents the strength of the connection or synapse from the kth presynaptic neuron, and then decays exponentially. Suppose that the spikes at synapse k are generated by an inhomogeneous Poisson process with arrival rate $\nu_k(t)$. This means that in each small time interval $[t, t + \Delta t]$ the probability that a spike arrives on the kth synapse is $\nu_k(t)\Delta t$, and each spike is uncorrelated with any other. We will derive a Fokker–Planck equation for the probability density $p(u, t)$ for u evolving according to the stochastic ODE (3.15), assuming that the neuron last fired at $t = 0$. We also set $I_{\text{ext}} = 0$ for simplicity.

The probability that no spike arrives in a short time interval Δt is

$$(3.16) \qquad \text{Prob\{no spike in } [t, t + \Delta t]\} = 1 - \sum_k \nu_k(t)\Delta t.$$

If no spike arrives then the membrane potential changes from $u(t) = u'$ to $u(t + \Delta t) = u'\mathrm{e}^{-\Delta t/\tau}$. On the other hand, if a spike arrives at synapse k, the membrane

changes from u' to $u'e^{-t/\tau}+w_k$. Therefore, given a value u' at time t, the probability density of finding a membrane potential u at time $t + \Delta t$ is

$$P(u, t + \Delta t | u', t) = \left[1 - \Delta t \sum_k \nu_k(t)\right] \delta\left(u - u'e^{-\Delta t/\tau}\right)$$

(3.17)
$$+\Delta t \sum_k \nu_k(t)\delta\left(u - u'e^{-\Delta t/\tau} - w_k\right).$$

Since the input spikes are generated by a Poisson process, it follows that the random variable $u(t)$ evolves according to a Markov process:

(3.18) $$p(u, t + \Delta t) = \int P(u, t + \Delta t | u', t)p(u', t)du'.$$

Substituting for P using equation (3.17) shows that

$$p(u, t + \Delta) = \left[1 - \Delta t \sum_k \nu_k(t)\right] e^{\Delta t/\tau} p(e^{\Delta t/\tau}u, t)$$

(3.19)
$$+\Delta t \sum_k \nu_k(t)e^{\Delta t/\tau}p(e^{\Delta t/\tau}u - w_k, t).$$

Rearranging and taking the limit $\Delta t \to 0$ leads to the master equation

(3.20) $$\frac{\partial p}{\partial t} = \frac{1}{\tau}\frac{\partial}{\partial u}[up(u, t)] + \sum_k \nu_k(t)[p(u - w_k, t) - p(u, t)].$$

If the jump amplitudes w_k are sufficiently small, then we can formally Taylor expand the right–hand side of the master equation as a series in w_k corresponding to the so–called Kramers–Moyall expansion [117, 118]. Neglecting terms of order w_k^3 then leads to the Fokker–Planck equation

$$\frac{\partial p}{\partial t} = -\frac{1}{\tau}\frac{\partial}{\partial u}\left[-u + \tau \sum_k \nu_k(t)w_k\right] p(u, t) + \frac{1}{2}\left[\sum_k \nu_k(t)w_k^2\right] \frac{\partial^2}{\partial u^2}p(u, t).$$

(3.21)

The Fokker-Planck equation determines the time evolution of the probability density of a membrane potential evolving according to the equivalent stochastic differential equation (Langevin equation)

(3.22) $$\tau du = -u(t)dt + \mu(t)dt + d\xi(t).$$

Here $\mu(t)$ is the mean background synaptic input

(3.23) $$\mu(t) = \tau \sum_k \nu_k(t)w_k$$

and $\xi(t)$ is a Gaussian white noise process,

(3.24) $$\langle \xi(t) \rangle = 0, \quad \langle \xi(t)\xi(t') \rangle = \tau\sigma^2(t)\min(t, t'),$$

with the size of the membrane fluctuations given by

(3.25) $$\sigma^2(t) = \tau \sum_k \nu_k(t)w_k^2.$$

In the case of constant noise, the resulting Langevin equation describes the well known Ornstein–Uhlenbeck process. Note that in the derivation of the Fokker–Planck equation we have suppressed higher–order terms of the form

$$\sum_{n=3}^{\infty} \frac{(-1)^n}{n!} A_n(t) \frac{\partial^n}{\partial u^n} p(u,t),$$

with $A_n = \sum_k \nu_k(t) w_k^n$. This becomes exact in the so–called diffusion limit $w_k \to 0$ such that $\mu(t), \sigma^2(t)$ are unchanged and $A_n \to 0$ for $n \geq 3$.

First passage times

In our derivation of the Fokker–Planck equation we neglected the threshold u_κ. This can be incorporated as an absorbing boundary condition

(3.26)
$$p(u_\kappa, t) \equiv 0 \text{ for all } t.$$

We can then look for the solution $p = p(u,t|U,0)$ of the Fokker–Planck equation assuming the initial condition $p(u,0|U,0) = \delta(u-U)$. At any time $t > 0$, the probability that the neuron has not reached threshold is

(3.27)
$$S(U,t) = \int_{-\infty}^{u_\kappa} p(u,t|U,0)dt.$$

Let $\psi(U,t)\Delta t$ be the probability that the neuron fires its next spike between t and $t+\Delta t$. It follows that $\psi(U,t)\Delta t = S(U,t) - S(U,t+\Delta t)$ so that in the limit $\Delta t \to 0$,

(3.28)
$$\psi(U,t) = -\frac{d}{dt} \int_{-\infty}^{u_\kappa} p(u,t|U,0)du.$$

The density $\psi(U,t)$ determines the distribution of first passage times. When this is combined with the reset condition $U = u_r$, we see that it also determines the distribution of interspike intervals $\Delta^n = T^{n+1} - T^n$. Unfortunately, no general solution is known for the first passage time problem of the Ornstein–Uhlenbeck process. However, in the case of constant inputs such that $\mu(t) = \mu_0$ and $\sigma(t) = \sigma$, one can carry out a moment expansion of the first passage time distribution. In particular, a closed form expression for the mean first passage time can be obtained.

In the case of constant inputs, $p(u,t|U,0)$ evolves according to the Fokker–Planck equation

$$\tau \frac{\partial p}{\partial t} = -\frac{\partial}{\partial u}[-u+\mu_0]p + \frac{\sigma^2}{2} \frac{\partial^2 p}{\partial u^2},$$

with $p(u,0|U,0) = \delta(u-U)$ and absorbing boundary condition $p(u_\kappa, t|U,0) = 0$. It can then be shown that $S(U,t)$ satisfies the backwards FP equation [**116, 117**]

(3.29)
$$\tau \frac{\partial S}{\partial t} = [-U+\mu_0]\frac{\partial S}{\partial U} + \frac{\sigma^2}{2} \frac{\partial^2 S}{\partial U^2},$$

with $S(U,0) = 1$ for $U \leq u_\kappa$ and zero otherwise. Defining the mean first passage time (MFPT) by

$$T(U) = \int_0^\infty t\psi(U,t)dt,$$

it follows that $T(U)$ satisfies the ODE

(3.30)
$$-\tau = [-U+\mu_0]\frac{dT}{dU} + \frac{\sigma^2}{2} \frac{d^2T}{dU^2}.$$

The solution for $T(U)$ is then

$$(3.31) \qquad T(U) = \frac{2\tau}{\sigma^2} \int_U^{u_\kappa} du e^{2\Phi(u)/\sigma^2} \int_{-\infty}^u e^{-2\Phi(u')/\sigma^2} du',$$

where $\Phi(u) = u^2/2 - \mu_0 u$. Hence, we obtain the following expression for the MFTP of an IF neuron whose initial state is the reset potential, $U = u_r$:

$$(3.32) \qquad T(u_r) = \int_0^\infty s\psi(s)ds = \tau\sqrt{\pi} \int_{(u_r-\mu_0)/\sigma}^{(u_\kappa-\mu_0)/\sigma} e^{u^2}(1 + \text{erf}(u))du.$$

Subthreshold regime

A major aim of noisy neuron models is to try to understand the large variability of interspike intervals found *in vivo* [**97, 120**]. Given that a neuron receives a large number of inputs at any one time, one might expect the law of large numbers to apply so that the neuron's output reflects the average input activity and thus exhibits small fluctuations about a mean firing rate. This is certainly true if the neuron operates in the superthreshold regime, in which the total input to the neuron in the absence of noise drives it to fire. Diffusive noise has little influence other than slightly broadening the interspike interval distribution. On the other hand, if the noise–free input is subthreshold, that is, it generates a membrane potential that remains below the firing threshold, then diffusive noise has a significant effect. In the subthreshold regime spikes are generated by the fluctuations of the membrane potential, rather than by its mean, and the interspike interval distribution is broad. The differences between the two regimes are illustrated in Figure 5. Another interesting subthreshold effect is *stochastic resonance*. This refers to a range of phenomena in which noise improves the signal transmission properties of a system and this effect is optimal at a particular noise level [**121**]. Within the neural context, a subthreshold input stimulus without noise does not generate action potentials, so no information regarding the stimulus is transmitted. However, if noise is added then spikes occur and there is an optimal noise level for signal transmission [**122**]. A related phenomenon is *coherence resonance* [**123**]. Here it is assumed that an excitable neuron is at rest in the absence of noise, but fires a sequence of spikes when noise is added. The optimal noise level now corresponds to the condition under which the resulting spike train is most regular.

3.4. Homogeneous population of IF neurons

Let us now consider a large population of identical IF neurons each being driven by a set of Poisson distributed spike trains. We assume that the kth synapse of every neuron receives a Poisson spike train with the same instantaneous rate $\nu_k(t)$, but that the spike trains across the population are statistically independent. The derivation of the Fokker–Planck equation proceeds along very similar lines to the single neuron case, and takes the form

$$(3.33) \qquad \frac{\partial p}{\partial t} = -\frac{\partial}{\partial u}\left[\frac{-u + \mu(t) + RI_{\text{ext}}(t)}{\tau}\right]p(u,t) + \frac{\sigma^2(t)}{2\tau}\frac{\partial^2}{\partial u^2}p(u,t),$$

with $\mu(t), \sigma(t)$ given by equations (3.23) and (3.25) and we now include an external input. However, there are a number of important differences between the single neuron and population cases. First, $p(u,t)$ is now interpreted as the probability
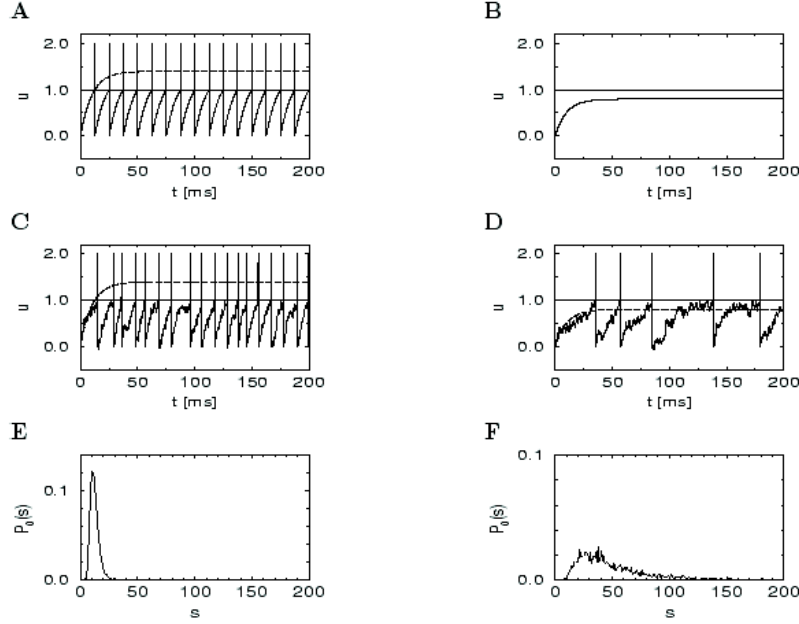
FIGURE 5. IF neuron with superthreshold (left column) and subthreshold (right column) inputs. (A,B) Noise–free case showing either regular firing or zero firing. (C,D) Spike trains in the presence of diffusive noise. (E,F) Corresponding interspike intervals. [Reprinted from [**7**], with permission of Cambridge University Press.]

density of membrane potentials across the population of neurons. Consequently, the normalization is different. In the case of a single neuron, the integrated density

$$\int_{-\infty}^{u_\kappa} p(u,t)du \leq 1$$

was interpreted as the probability that the neuron under consideration has not yet fired, which changes over time. On the other hand, if a neuron in the population fires, it remains part of the population so that we have the constant normalization

$$(3.34) \qquad \int_{-\infty}^{u_\kappa} p(u,t)du = 1.$$

The second major difference is that we now have to incorporate the reset condition explicitly in the evolution of the probability density. First, note that the Fokker–Planck equation can be rewritten as a continuity equation reflecting conservation of probability:

$$(3.35) \qquad \frac{\partial}{\partial t}p(u,t) = -\frac{\partial}{\partial u}J(u,t), \quad \text{for } u \neq u_\kappa, u_r,$$

where

$$(3.36) \qquad J(u,t) = \frac{1}{\tau}\left[-u + \mu(t) + RI_{\text{ext}}(t)\right]p(u,t) - \frac{\sigma^2(t)}{2\tau}\frac{\partial}{\partial u}p(u,t).$$

In a population of N neurons, the fraction of active neurons is calculated by counting the number of output spikes $n(t; t + \Delta t)$ in a small time interval Δt and dividing by N. Further division by Δt yields the population activity

$$(3.37) \qquad \nu(t) = \lim_{\Delta t \to 0} \frac{1}{\Delta t} \frac{n(t, t + \Delta t)}{N} = \frac{1}{N} \sum_{j=1}^{N} \sum_{m} \delta(t - T_j^m).$$

The double sum runs over all firing times T_j^m of all neurons in the population. The fraction of neurons that flow across the threshold per unit time should then be equal to the population averaged activity $\nu(t)$, that is, $\nu(t) = J(u_\kappa, t)$. Equation (3.36) together with the absorbing boundary condition

$$(3.38) \qquad p(u_\kappa, t) = 0$$

implies that

$$(3.39) \qquad \frac{\partial}{\partial u} p(u_\kappa, t) = -\frac{2\nu(t)\tau}{\sigma^2(t)}.$$

Due to the reset condition, the neurons that "disappear" across threshold are reinjected at the reset potential u_r, which implies that there is a discontinuity in the flux at u_r, $J(u_r^+, t) - J(u_r^-, t) = \nu(t)$. Continuity of p,

$$(3.40) \qquad p(u_r^+, t) - p(u_r^-, t) = 0,$$

together with equation (3.36) then shows that there is a discontinuity in the first derivative of $p(u, t)$ at $u = u_r$:

$$(3.41) \qquad \frac{\partial}{\partial u} p(u_r^+, t) - \frac{\partial}{\partial u} p(u_r^-, t) = -\frac{2\nu(t)\tau}{\sigma^2(t)}.$$

In summary, one has to solve the Fokker–Planck equation (3.33) together with the boundary conditions (3.38), (3.39), (3.40) and (3.41).

Steady–state solution
Suppose that the background rates ν_k and external input I_{ext} are time–independent so that the total mean input

$$(3.42) \qquad h_0 = RI_0 + \tau \sum_k \nu_k w_k$$

is a constant. The steady–state Fokker–Planck equation implies that the flux

$$(3.43) \qquad J(u) = \frac{-u + h_0}{\tau} p(u) - \frac{1}{2} \frac{\sigma^2}{\tau} \frac{\partial}{\partial u} p(u)$$

is constant except at $u = u_r$ where it jumps by an amount ν_0, which is the steady–state population activity. Taking $J(u) = 0$ for $u < u_r$ we can solve equation (3.43) to obtain the Gaussian distribution

$$(3.44) \qquad p_0(u) = \frac{c_1}{\sigma} \exp\left[-\frac{(u - h_0)^2}{\sigma^2}\right], \quad \text{for } u \leq u_r$$

for some constant c_1. However, such a solution cannot be valid for $u > u_r$, since it does not satisfy the absorbing boundary condition $p_0(u_\kappa) = 0$. It turns out that in this domain the solution is of the form [**124**]

$$(3.45) \quad p_0(u) = \frac{c_2}{\sigma^2} \exp\left[-\frac{(u - h_0)^2}{\sigma^2}\right] \int_u^{u_\kappa} \exp\left[\frac{(x - h_0)^2}{\sigma^2}\right] dx, \quad \text{for } u_r < u \leq u_\kappa$$

for some constant c_2. Equation (3.43) shows that $c_2 = 2\tau J(u)$ for $u_r < u \leq u_\kappa$ with $J(u) = \nu_0$. Continuity of the solution at $u = u_r$ implies that

$$(3.46) \qquad c_1 = \frac{c_2}{\sigma} \int_u^{u_\kappa} \exp\left[\frac{(x - h_0)^2}{\sigma^2}\right] dx.$$

Finally, the constant c_2 is determined by the normalization condition (3.34). On setting $\nu_0 = c_2/2\tau$, one finds a firing rate that is consistent with the MFPT of equation (3.32):

$$(3.47) \qquad \nu_0 = \left[\tau\sqrt{\pi} \int_{(u_r-h_0)/\sigma}^{(u_\kappa-h_0)/\sigma} e^{u^2}(1 + \mathrm{erf}(u))du\right]^{-1} \equiv f(h_0),$$

where f is the so–called gain function for the population.

Asynchronous firing in recurrent networks

The above analysis assumed that the neurons were independent of each other so that the only synaptic inputs were from some stochastic background. Now suppose that we have a fully connected network such that there is an additional contribution to the synaptic current into each neuron of the form

$$(3.48) \qquad I_{\rec}(t) = \frac{\tau}{R}\frac{\Gamma_0}{N} \sum_{j=1}^N \sum_m \delta(t - T_j^m) = \tau\Gamma_0\nu(t)/R,$$

where Γ_0/N is the strength of connection between any pair of neurons within the population, and we have used the definition (3.37) of the population activity $\nu(t)$. Suppose that the neuronal population is in a macroscopic state with constant activity $\nu(t) = \nu_0$, which is referred to as a state of asynchronous firing. The steady–state activity can then be determined self–consistently from equation (3.47) by setting

$$(3.49) \qquad h_0 = RI_0 + \tau\left[\sum_k \nu_k w_k + \Gamma_0\nu_0\right].$$

This is illustrated in Figure 6(a). One can also determine the stability of the asynchronous state by considering small perturbations of the steady–state probability distribution. One finds that in the limit of low noise, the asynchronous state is unstable and the neurons tend to split up into several synchronized groups that fire alternately. The overall activity then oscillates several times faster than the individual neurons [**125, 126, 124**], see §4.3. One of the interesting properties of the asynchronous state from a computational perspective is that the population activity can respond rapidly to a step input [**7**], as illustrated in Figure 6(b). The basic intuition behind this is that in the asynchronous state there will always be a significant fraction of neurons that are sitting close to the firing threshold so that as soon as a step increase in input current occurs they can respond immediately. However, the size of the step has to be at least as large as the noise amplitude σ, since the threshold acts as an absorbing boundary, that is, the density of neurons vanishes as $u \to u_\kappa$.

In the above example noise is added explicitly in the form of stochastic background activity. It is also possible for a network of deterministic neurons with fixed random connections to generate its own noise [**124, 127, 128, 129**]. In particular, suppose that each neuron in the population of N neurons receives input from C randomly selected neurons in the population with $C \ll N$. The assumption of
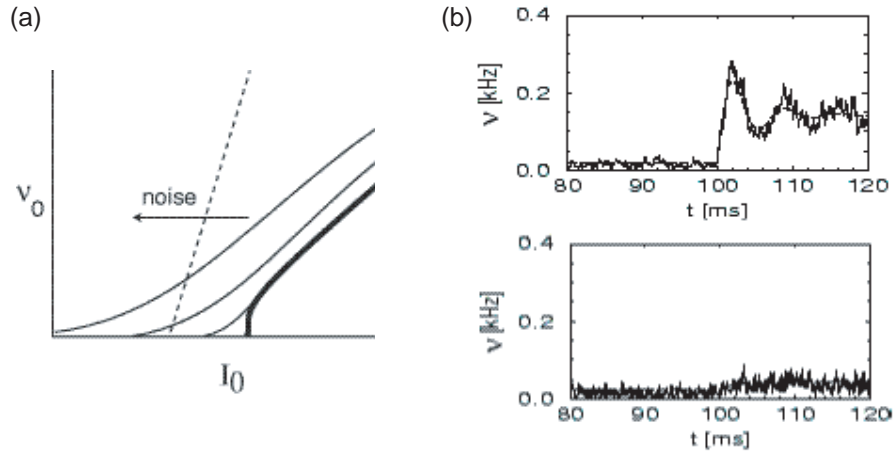
(a)

(b)

FIGURE 6. (a) Steady–state population activity ν_0 as a function of external input I_0 for different levels of noise (increasing from right to left). Thick curve shows firing rate function for a single noiseless IF neuron. Intersection with the dashed line of slope $1/\Gamma_0$ gives possible solutions for the stationary activity in a population with excitatory coupling Γ_0. (b) Response of a network of 1000 IF neurons with diffusive noise to a step current input. Rapid response to a large current step for low noise (upper figure). Slow response to a small current step for high noise (lower figure). [Reprinted from [7], with permission of Cambridge University Press.]

sparse connectivity means that two neurons share only a small number of common inputs. Hence, if the presynaptic neurons fire stochastically then the input spike trains that arrive at distinct postsynaptic neurons can be treated as statistically independent. Since the presynaptic neurons belong to the same population, it follows that each neuron's output should itself be stochastic in the sense that it should have a sufficiently broad distribution of interspike intervals. This will tend to occur if the neurons operate in a subthreshold regime, that is, the mean total input is below threshold so that threshold crossings are fluctuation driven. Finally, note that there have been a number of studies of recurrent network dynamics based on extensions of the single neuron master equation (3.20) to neural populations. In the case of large populations, numerical solutions of the resulting master equation compare very well with direct simulations of the full network equations, capturing fine details not possible under the diffusion approximation [130]. In certain special cases, it is also possible to obtain analytical solutions [131]. One recent application of the master equation approach has been to the study of fluctuation–driven dynamics in recurrent network models of primary visual cortex [132].

Network Oscillations and Synchrony

Synchronized neural activity appears to be prevalent in many areas of the brain including sensory cortices, thalamus and hippocampus. Synchrony can occur on the spike-to-spike level or on the bursting level, and is usually associated with oscillatory activity. Oscillations may be generated by intrinsic properties of single cells or may arise through excitatory and inhibitory synaptic interactions within a local population of cells. In this lecture we explore some of the mechanisms underlying oscillatory activity and synchronization at the network level by considering populations of synaptically coupled spiking neurons. From a theoretical perspective there are a number of issues that need to be addressed: Is the basic oscillatory unit a single neuron or a local population of neurons? What are the roles of recurrent excitatory and inhibitory connections in determining the patterns of oscillations? How are the patterns affected by the intrinsic ionic properties of the neurons? Which conditions determine whether synchronous activity is at the level of spikes, bursts or firing rates, and in which frequency range? How are synchronous states affected by external inputs? Under what conditions does one expect to observe traveling (phase) waves rather than synchronous oscillations?

One popular approach to tackling some of these issues is to assume that each neuron (or group of neurons) is intrinsically oscillatory, and that interactions among the neurons, or groups of neurons that comprise an oscillator unit, are weak. The phase reduction method outlined in §1 can then be applied at the network level. This leads to a system of coupled equations for the phases of the oscillators in the network, in which the effective phase interaction function H depends on both the nature of the synaptic interactions and the intrinsic properties of each oscillator as expressed through its phase resetting curve. For simplicity, we shall take the fundamental oscillatory unit to be a single neuron that transmits a regular sequence of spikes to other neurons in the network (see Figure 1). The relative shift in the spike trains of two oscillating neurons will then depend on the relative phases of the two oscillators. Note, however, that the phase reduction techniques outlined below can also be applied to models in which the basic oscillator consists of more than one neuron. For example, when modeling spindle oscillations in thalamus, the minimal oscillator might consist of an excitatory thalamocortical neuron and an inhibitory reticular neuron. As another example, we note that stimulus-induced oscillations in visual cortex are likely to arise at the level of a cortical column, involving several thousand excitatory and inhibitory neurons that form the basic oscillatory unit. In this case it is more appropriate to express the output of the oscillator in terms of a population-averaged firing rate (see §3). Networks of weakly interacting cortical columns can then be described in terms of a set of coupled phase equations, whose phase interaction function is stimulus–dependent [**133, 134**]. Note

that oscillations at the population level can occur, even when the individual neurons are not themselves intrinsic oscillators, due to the combined effects of external stimuli and recurrent synaptic interactions. One particular network mechanism for stimulus–induced oscillations is through a Hopf bifurcation of a stationary activity bump, leading to the formation of a spatially–localized oscillation or breather that is aligned with the stimulus [**135, 136**]. Activity bumps are discussed in §5.3.
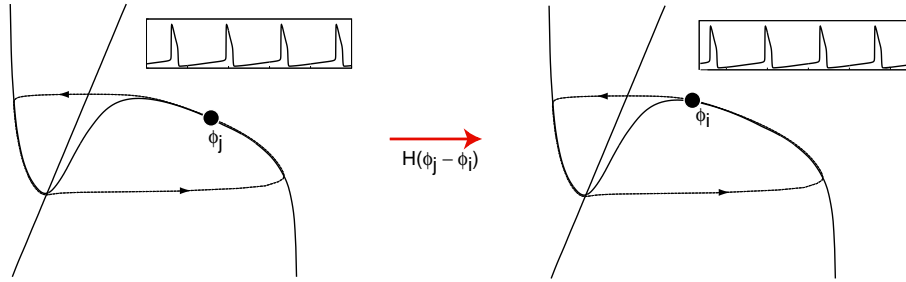

FIGURE 1. A system of two synaptically coupled limit cycle oscillators can be reduced to a pair of phase equations involving an effective phase interaction function H. See text for details.

4.1. Phase reduction for synaptically coupled neural oscillators

Let us consider a network of N neural oscillators labeled $i = 1, \dots, N$. Denoting the state of the ith neuron by $\mathbf{x}_i \in \mathbf{R}^m$, the general form of the network dynamics is the coupled system of ODEs

$$(4.1) \qquad \frac{d\mathbf{x}_i}{dt} = \mathbf{f}(\mathbf{x}_i) + \varepsilon \sum_{j=1}^{N} w_{ij} \mathbf{P}(\mathbf{x}_i, \mathbf{x}_j),$$

where $w_{ij}\mathbf{P}(\mathbf{x}_i, \mathbf{x}_j)$ represents the synaptic input from the jth to the ith neuron. We assume that the synaptic interactions are identical in form but are allowed to have different relative strengths or weights w_{ij}. (It is straightforward to extend the analysis to non-identical oscillators with different intrinsic frequencies for example). If the coupling between the oscillators is weak then one can derive closed equations for the phases of the oscillators. We shall establish this using the method of isochrones [**11**], following along similar lines to the analysis of a periodically forced oscillator described in §1. An alternative derivation based on the Fredholm alternative is described at the end of the section.

Method of isochrones
Suppose that in the absence of interactions each neuron has a stable limit cycle $\mathbf{X}$ with natural frequency ω_0. For each oscillator we introduce the phase variable ϕ_i such that

$$(4.2) \qquad \frac{d\phi_i}{dt} = \omega_0,$$

and there is a one-to-one mapping $\phi_i \rightarrow \mathbf{X}(\phi_i)$. The definition of the phase is then extended into a neighborhood of the limit cycle using isochrones. That is, we

associate with any point $\mathbf{x}_i$ in the vicinity of the ith limit cycle a phase $\phi_i(\mathbf{x}_i)$ such that

$$\frac{d\phi_i(\mathbf{x}_i)}{dt} = \omega_0 + \varepsilon \frac{\partial \phi_i}{\partial \mathbf{x}_i} . \sum_{j=1}^{N} w_{ij} \mathbf{P}(\mathbf{x}_i, \mathbf{x}_j).$$

To a first approximation we can evaluate the r.h.s on the unperturbed limit cycles $\mathbf{X}$. Since these are defined uniquely by the phase we obtain the coupled phase equations

$$(4.3) \qquad \frac{d\phi_i}{dt} = \omega_0 + \varepsilon \sum_{j=1}^{N} w_{ij} Q(\phi_i, \phi_j),$$

where

$$(4.4) \qquad Q(\phi_i, \phi_j) = \frac{\partial \phi_i}{\partial \mathbf{x}_i}(\mathbf{X}(\phi_i)) . \mathbf{P}(\mathbf{X}(\phi_i), \mathbf{X}(\phi_j)).$$

Q is a 2π-periodic function of the phases.

It remains the specify the structure of $\mathbf{P}$. The first point to note is that the coupling term only contributes to the equation for the membrane potential $u_i = [\mathbf{x}_i]_1$ so that $P_k = \delta_{1,k} P$ and we can write

$$(4.5) \qquad Q(\phi_i, \phi_j) = R(\phi_i) P(\mathbf{X}(\phi_i), \mathbf{X}(\phi_j)),$$

where R is the phase response curve of the oscillator, see §1.2. If we neglect dendritic processes and synaptic depression then the synaptic input from the jth to the ith neuron is of the form

$$(4.6) \qquad I_{syn}(t) = w_{ij} \sum_{m} g_{\text{syn}}(t - T_j^m - \tau_a)[u_{syn} - u_i(t)],$$

where the sum is taken over all the spikes emitted by neuron j at the firing times T_j^m, $g_{\text{syn}}(t)$ is the alpha function (2.3) and τ_a is a discrete axonal delay. The firing times can be related to the phase of the oscillators as follows. Assume that the neuron fires whenever the phase ϕ_j crosses zero. The firing times then satisfy the condition

$$(4.7) \qquad \phi_j(T_j^m) = 2\pi m, \quad \dot{\phi}_j(T_j^m) > 0.$$

If we now set $\psi_j = \phi_j - \omega_0 t$ then ψ_i is a slowly varying function of time so that to a first approximation

$$(4.8) \qquad T_j^m = (m - \psi_j/2\pi)\Delta_0 = t + (m - \phi_j(t)/2\pi)\Delta_0.$$

Hence
$$(4.9)$$
$$P(\phi_i, \phi_j) \equiv P(\mathbf{X}(\phi_i), \mathbf{X}(\phi_j)) = \sum_{m} g_{\text{syn}}((\phi_j/2\pi - m)\Delta_0 - \tau_a)[u_{syn} - u^*(\phi_i)].$$

Thus we can rewrite Q as

$$(4.10) \qquad Q(\phi_i, \phi_j) = \widehat{R}(\phi_i)\widehat{P}(\phi_j - \omega_0\tau_a),$$

where

$$(4.11) \qquad \widehat{R}(\phi_i) = [u_{syn} - u^*(\phi_i)]R(\phi_i), \quad \widehat{P}(\phi_j) = \sum_{m} g_{\text{syn}}((\phi_j/2\pi - m)\Delta_0).$$

The final step of the analysis is to use the method of averaging to obtain effective interactions that depend only on phase differences. Substituting $\psi_i = \phi_i - \omega_0 t$ into the phase equation (4.3) gives

$$(4.12) \qquad \frac{d\psi_i}{dt} = \varepsilon \sum_{j=1}^{N} w_{ij} Q(\psi_i + \omega_0 t, \psi_j + \omega_0 t).$$

The corresponding averaged equation is then

$$(4.13) \qquad \frac{d\psi_i}{dt} = \varepsilon \sum_{j=1}^{N} w_{ij} H(\psi_j - \psi_i - \omega_0 \tau_a),$$

where

$$
\begin{aligned}
H(\psi_j - \psi_i) &= \frac{1}{\Delta_0} \int_0^{\Delta_0} \widehat{R}(\psi_i + \omega_0 t) \widehat{P}(\psi_j + \omega_0 t]) dt \\
(4.14) \qquad &= \frac{1}{2\pi} \int_0^{2\pi} \widehat{R}(\phi + \psi_i - \psi_j) \widehat{P}(\phi) d\phi,
\end{aligned}
$$

and we have exploited the periodicity of the functions $\widehat{R}, \widehat{P}$. A useful alternative expression for H is obtained by substituting for $\widehat{P}$:

$$
\begin{aligned}
H(\psi) &= \frac{1}{2\pi} \int_0^{2\pi} \widehat{R}(\phi - \psi) \sum_m g_{\text{syn}}([\phi/2\pi - m]\Delta_0) d\phi \\
(4.15) \qquad &= \frac{1}{2\pi} \int_0^{\infty} \widehat{R}(\phi - \psi) g_{\text{syn}}(\phi \Delta_0 / 2\pi) d\phi.
\end{aligned}
$$

Our analysis also establishes that averaging in the weak coupling regime reduces the effect of an axonal delay to that of an additional phase-shift.

Fredholm alternative

An alternative derivation of the phase equation (4.13) involves the Fredholm alternative and perturbation theory [**137, 138**]. To simplify the notation we set $\Delta_0 = 2\pi$. The basic idea is to seek solutions of equation (4.1) of the form

$$(4.16) \qquad \mathbf{x}_i = \mathbf{X}(t + \psi_i(\tau)) + \varepsilon \mathbf{U}_i(t, \tau, \varepsilon),$$

where $\mathbf{X}(t)$ represents the 2π-periodic solution of the uncoupled equation. Substituting into equation (4.1) yields at order ε

$$
\begin{aligned}
(4.17) \qquad \mathbf{f}(\mathbf{X}(t + \psi_i)) & \frac{d\psi_i}{d\tau} + \frac{d\mathbf{U}_i(t, \tau, 0)}{dt} \\
&= \mathcal{D}\mathbf{f}(\mathbf{X}(t + \psi_i))\mathbf{U}_i(t, \tau, 0) + \sum_{j=1}^{N} w_{ij} \mathbf{P}(\mathbf{X}(t + \psi_i), \mathbf{X}(t + \psi_j)),
\end{aligned}
$$

where $\mathcal{D}\mathbf{f}$ is the Jacobian of $\mathbf{f}$. This equation may be rewritten in the more suggestive form

$$(4.18) \quad \mathcal{L}(t + \psi_i)\mathbf{U}_i(t, \tau, 0) \equiv \left[\frac{d}{dt} - \mathcal{D}\mathbf{f}(\mathbf{X}(t + \psi_i)) \right] \mathbf{U}_i(t, \tau, 0) = \mathbf{b}_i(t, \tau),$$

where

$$(4.19) \quad \mathbf{b}_i(t, \tau) = -\mathbf{f}(\mathbf{X}(t + \psi_i)) \frac{d\psi_i}{d\tau} + \sum_{j=1}^{N} w_{ij} \mathbf{P}(\mathbf{X}(t + \psi_i), \mathbf{X}(t + \psi_j)).$$

Using the Fredholm alternative, the inhomogeneous linear equation (4.18) has a periodic solution if and only if

$$(4.20) \qquad \frac{1}{\Delta_0} \int_0^{\Delta_0} \overline{\mathbf{Z}}(t + \psi_i).\mathbf{b}_i(\omega_0 t, \tau)dt = 0,$$

where $\mathbf{Z}(t)$ is the unique 2π-periodic solution of the adjoint homogeneous equation

$$(4.21) \qquad \left[\frac{d}{dt} + \mathcal{D}\mathbf{f}(\mathbf{X}(t))^\dagger \right] \mathbf{Z}(t) = 0$$

with chosen normalization

$$(4.22) \qquad \frac{1}{2\pi} \int_0^{2\pi} \overline{\mathbf{Z}}(t).\mathbf{f}(\mathbf{X}(t))dt = 1.$$

Using this normalization condition and the expression for $\mathbf{b}_i$, we conclude that equation (4.18) has a solution if and only if

$$(4.23) \qquad \frac{d\psi_i}{d\tau} = \frac{1}{2\pi} \int_0^{2\pi} \overline{\mathbf{Z}}(t + \psi_i).\sum_{j=1}^N w_{ij}\mathbf{P}(\mathbf{X}(t + \psi_i), \mathbf{X}(t + \psi_j))dt.$$

Exploiting the periodicity of the functions on the r.h.s, we can shift t to obtain the phase-difference equation (4.13) with H given by

$$(4.24) \qquad H(\psi_j - \psi_i) = \frac{1}{2\pi} \int_0^{2\pi} \overline{\mathbf{Z}}(t).\mathbf{P}(\mathbf{X}(t), \mathbf{X}(t + \psi_j - \psi_i))dt.$$

Equation (4.24) can be further reduced by substituting the explicit form for the synaptic interactions $\mathbf{P}$ as given by equation (4.9). One then recovers equation (4.14) with $\overline{Z}_1$ replacing the phase resetting curve R. (The two forms of H are equivalent to lowest order in ε). Note that the adjoint solution can be determined using standard numerical methods. On the other hand, the phase resetting curve has a more direct physical interpretation, and hence we will adopt the version given by equation (4.14) in our subsequent analysis.

4.2. Phase-locked solutions

We define a $1 : 1$ phase-locked solution of the phase equation (4.13) to be of the form

$$(4.25) \qquad \psi_i(t) = \Delta\omega\ t + \bar{\psi}_i,$$

where $\omega = \omega_0 + \Delta\omega$ is the *collective frequency* of the coupled oscillators and $\Psi = (\bar{\psi}_1, \dots, \bar{\psi}_n)$ is a set of constant phases. Substitution into equation (4.13) leads to the fixed point equations

$$(4.26) \qquad \Delta\omega = \varepsilon \sum_j w_{ij}H(\bar{\psi}_j - \bar{\psi}_i), \quad j = 1, \dots, N.$$

After choosing some reference oscillator, the N phase equations determine the collective period ω and $N - 1$ relative phases with the latter independent of ϵ. In order to analyze the local stability of a phase-locked solution Ψ, we linearize equation (4.13) by setting $\psi_i(t) = \bar{\psi}_i + \Delta\omega t + \Delta\psi_i(t)$ and expanding to first-order in

$\widetilde{\psi}_i$:

$$(4.27) \qquad \frac{\mathrm{d}\Delta\psi_i}{\mathrm{d}t} = \epsilon \sum_{j=1}^{N} \widehat{\mathcal{H}}_{ij}(\Phi)\Delta\psi_j,$$

where

$$(4.28) \qquad \widehat{\mathcal{H}}_{ij}(\Phi) = w_{ij}H'(\bar{\psi}_j - \bar{\psi}_i) - \delta_{i,j}\sum_k w_{ik}H'(\bar{\psi}_k - \bar{\psi}_i),$$

and $H'(\psi) = dH(\psi)/d\psi$. One of the eigenvalues of the Jacobian $\widehat{\mathcal{H}}$ is always zero, and the corresponding eigenvector points in the direction of the flow, that is $(1, 1, \ldots, 1)$. The phase-locked solution will be stable provided that all other eigenvalues have a negative real part [139].

Pair of identical neural oscillators

Consider the case of two identical oscillators ($N = 2$) that are symmetrically coupled, in other words $w_{12} = w_{21} = 1$ and $w_{11} = w_{22} = 0$. The phase difference $\psi = \psi_2 - \psi_1$ satisfies the simple equation

$$(4.29) \qquad \frac{d\psi}{dt} = \varepsilon H^-(\psi),$$

where $H^-(\psi) = H(-\psi) - H(\psi)$. Phase-locked states are then given by the zeros of the odd function H^-:

$$(4.30) \qquad H^-(\psi) = 0.$$

A given phase-locked state is stable provided that

$$(4.31) \qquad \epsilon\frac{\mathrm{d}H^-(\psi)}{\mathrm{d}\psi} < 0.$$

Note that by symmetry both the in-phase ($\psi = 0$) and anti-phase ($\psi = \pi$) states are guaranteed to exist [140]. However, there may be additional fixed points depending on the parameters. The collective frequency of oscillation is determined by the even part of H, $H^+(\psi) = H(\psi) + H(-\psi)$:

$$(4.32) \qquad \omega = \omega_0 + \frac{\varepsilon}{2}H^+(\psi).$$

It turns out that the stability of the in-phase state for a pair of neurons depends on a number of factors [141, 142]: whether the synapses are excitatory ($u_{syn} > 0$) or inhibitory ($u_{syn} > 0$), whether the kinetics are fast (large α) or slow (small α), whether the phase resetting curve is Type I or Type II, and the size of axonal delays. We shall illustrate this by considering two simple examples with $\widehat{R}(\phi) \approx u_{syn}R(\phi)$ and u_{syn} absorbed into ε: the sign of ε will then determine whether the neurons are excitatory or inhibitory.

Example: Hodgkin-Huxley neuron. In Figure 2 we show a typical phase-resetting curve $R(\phi)$ for the Hodgkin-Huxley model together with the resulting phase interaction function $H(\psi)$ for an α function synapse, calculated using equation (4.15),
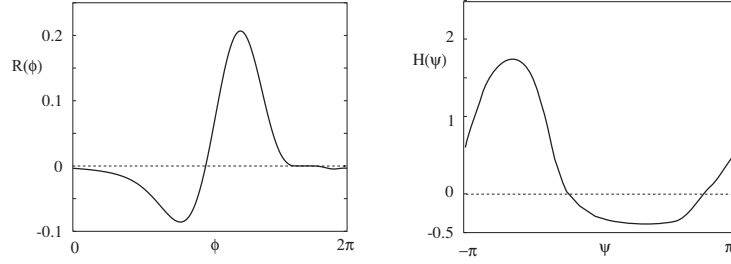
FIGURE 2. Plot of Type II phase resetting curve $R(\phi)$ for the Hodgkin-Huxley model together with effective phase interaction function $H(\psi)$.

and zero axonal delays. If we approximate the PRC by $R(\phi) = -\sin \phi$ then

$$
\begin{aligned}
H(\psi) &= \frac{1}{2\pi} \int_0^\infty R(\phi - \psi) P(\phi \Delta_0 / 2\pi) d\phi \\
&= \frac{\alpha^2}{2\pi} \frac{d}{d\alpha} \int_0^\infty \sin(\phi - \psi) e^{-\alpha\phi\Delta_0/2\pi} d\phi \\
&= \frac{\alpha^2}{2\pi} \mathrm{Im} \frac{d}{d\alpha} \int_0^\infty e^{i(\phi - \psi)} e^{-\alpha\phi\Delta_0/2\pi} d\phi.
\end{aligned}
$$

Now

$$
\text{(4.33)} \qquad \frac{1}{2\pi} \frac{d}{d\alpha} \int_0^\infty e^{i\phi} e^{-\alpha\phi\Delta_0/2\pi} d\phi = -\frac{\Delta_0}{(\alpha\Delta_0 - 2\pi i)^2},
$$

and so

$$
\text{(4.34)} \qquad\qquad\qquad H(\psi) = A \sin \psi - B \cos \psi,
$$

where

$$
\text{(4.35)} \qquad A = [(\alpha\Delta_0)^2 - (2\pi)^2]K, \quad B = 4\pi\alpha\Delta_0 K, \quad K = \frac{\alpha^2 \Delta_0}{[(2\pi)^2 + (\alpha\Delta_0)^2]^2}.
$$

The odd part is then

$$
\text{(4.36)} \qquad\qquad H^-(\psi) = \frac{2\alpha^2 \Delta_0 [4\pi^2 - \alpha^2 \Delta_0^2] \sin \psi}{\Delta_0 [\alpha^2 \Delta_0^2 + 4\pi^2]^2}.
$$

As long as $2\pi/\alpha\Delta_0 \neq 1$ there are phase-locked states at $\psi = 0, \pi$ as expected. The synchronous solution is stable if $\varepsilon H^{-'}(0) < 0$. This implies that synchronization will occur for excitatory coupling if $\alpha > 2\pi/\Delta_0$ and for inhibitory coupling if $\alpha < 2\pi/\Delta_0$. Thus, *inhibition* rather than excitation synchronizes the neurons when the synapses have sufficiently slow kinetics. The reverse is true for the anti-phase solution $\psi = \pi$. If higher-order terms in the Fourier series expansion of H are included, $H(\psi) = \sum_n h_n e^{in\psi}$, then the transition from synchronous to antisynchronous behavior is smoother, that is, the system no longer makes a sudden jump from one to the other at a critical value of α.

Example: Integrate-and-fire model. Substituting into equation (4.14) the PRC of an IF neuron given by equation (1.43), the α-dependence of phase-locked solutions in the case of a symmetric pair of excitatory or inhibitory IF neurons can be determined [**141**]. The results are summarized in Figure 3(a). For excitatory coupling

($\epsilon > 0$) the synchronous state is unstable for all $0 < \alpha < \infty$. On the other hand, the anti-synchronous solution is stable for $\alpha < \alpha_c$ but loses stability when $\alpha > \alpha_c$ with the creation of two stable partially synchronized or asynchronous states. The emergence of these two additional states can be understood in terms of the behavior of the odd part of the interaction function $H^-(\psi)$ as shown in Figure 3(b). In the limit $\alpha \to \infty$ the two asynchronous states asymptotically approach the synchronous state so that the neurons are almost perfectly synchronized. This is consistent with the analysis of Mirollo and Strogatz [143] who proved rigorously that globally coupled IF oscillators almost always synchronize in the presence of instantaneous excitatory interactions. The stability properties of all solutions are reversed in the case of inhibitory coupling ($\epsilon < 0$) so that, in particular, the synchronous state is now stable for all α. Introduction of a discrete axonal delay τ_a produces a checkerboard pattern of alternating stable/unstable solution branches that can overlap to produce multistable solutions [144].
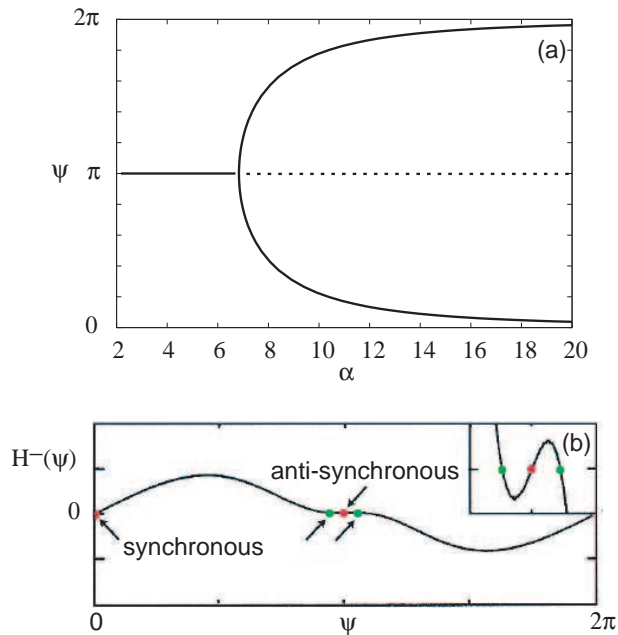

FIGURE 3. (a) Relative phase $\psi = \psi_2 - \psi_1$ for a pair of IF oscillators with symmetric excitatory coupling as a function of α with $I_0 = 2$. In each case the anti-phase state undergoes a bifurcation at a critical value of $\alpha = \alpha_c$ where it becomes unstable and two additional stable solutions ψ, $2\pi - \psi$ are created. The synchronous state remains unstable for all α. (b) Odd part of the phase interaction function for α just above the critical value α_c showing two new phase-locked solutions.

Traveling oscillatory waves on a chain

Both vertebrates and invertebrates have dedicated networks of cells that contain the information necessary to activate different motor neurons in the appropriate sequence and intensity to generate a variety of motor patterns. Such networks

are known as central pattern generators (CPGs). The simplest CPGs control reflex actions, swallowing and coughing. At the next level are those that control rhythmic movements such as breathing and locomotion. A well studied example of the latter is swimming locomotion in vertebrates such as the lamprey [**145, 146, 147**]. The basic mechanism for such coordinated movement is alternating left-right activity within each segment of the spinal cord, combined with a phase lag between the activation of consecutive segments along the body (see Figure 4). This generates an undulatory wave that propagates along the body and pushes the animal forwards through the water. An analogous mechanism also occurs in invertebrates such as the leech [**148**].
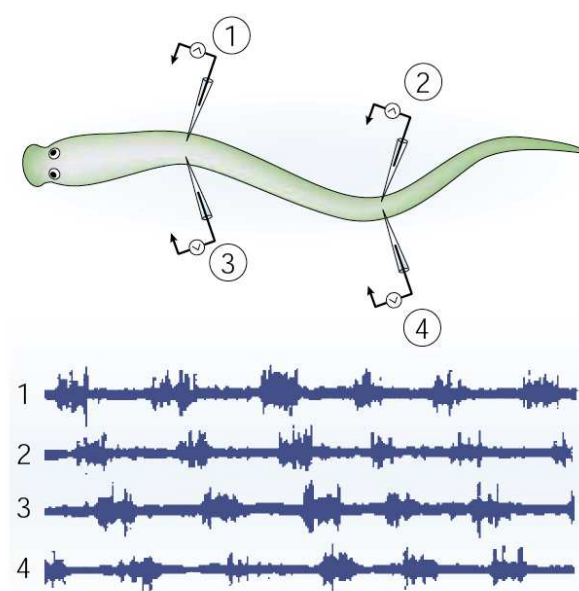
FIGURE 4. Neural activity recorded from four locations on the body of a lamprey during swimming locomotion. The body can be segmented into a bilateral chain of alternating left/right oscillators such as the pairs 1,3 and 2,4. There is also an intersegmental phase-lag between the activity of the pair 1,3 and 2,4.

At the simplest level, the spinal cord may be modeled as a chain N phase oscillators with nearest-neighbor coupling as shown in Figure 5. A traveling wave of activity along the chain then corresponds to a phase-locked solution in which ϕ_n

FIGURE 5. A chain of N phase oscillators.

is a monotonically increasing or decreasing function of n. At least two mechanisms have been identified for generating such a phase gradient along the chain [**149, 150**]: a) Heterogeneity in the form of a gradient in intrinsic frequencies of the individual neurons, that is, $\omega_n = \omega_0 + n\omega_1$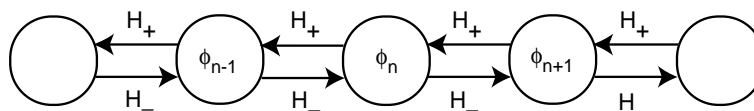 where $\omega_{0,1}$ are constants, will induce a gradient in the relative phases of the coupled system. Such a frequency gradient has been found in the leech CPG for swimming [**148**]. The resulting plane wave propagates opposite to the direction of the gradient, that is, from high to low frequencies. Interestingly, a spatial gradient of frequencies has been observed experimentally in slices of molluscan olfactory lobe, with the wave propagating from high to low frequencies as predicted by the theory [**151**].

b) In the lamprey CPG for swimming, there is no evidence for a gradient in frequency. Moreover, unlike the observed wave in the lamprey, waves produced by frequency gradients do not have constant phase lags along the chain, that is, the wave is not of constant speed. However, it is possible to produce approximately constant speed waves in the bulk of an oscillator chain by having anisotropic interactions, $H_+ \neq H_-$, together with the so-called edge property that $H_+(\theta)$ or $H-(\theta)$ vanishes at a non-zero value of θ.

We briefly illustrate the above results using a simple model of a chain with $H_\pm(\phi) = W_\pm H(\phi)$. Such a network is described by the following system of coupled phase equations:

$$
\begin{aligned}
\dot{\phi}_1 &= \omega_1 + W_+ H(\phi_2 - \phi_1) \\
\dot{\phi}_i &= \omega_i + W_+ H(\phi_{i+1} - \phi_i) + W_- H(\phi_{i-1} - \phi_i), \quad i = 2, \ldots, N-1 \\
(4.37)\ \dot{\phi}_N &= \omega_N + W_- H(\phi_{N-1} - \phi_N).
\end{aligned}
$$

Introducing the intersegmental phase differences $\theta_i = \phi_{i+1} - \phi_i$ leads to the $N-1$-dimensional system of equations

(4.38)
$$
\dot{\theta}_i = \Delta\omega_i + W_+[H(\theta_{i+1}) - H(\theta_i)] + W_-[H(-\theta_i) - H(-\theta_{i-1})], \quad i = 1, \ldots, N-1,
$$

with boundary conditions

$$
(4.39) \qquad\qquad\qquad H(-\theta_0) = 0 = H(\theta_N)
$$

and $\Delta\omega_i = \omega_{i+1} - \omega_i$.

Suppose that there is a gradient of frequencies along the chain, that is, $\Delta\omega_i$ has the same sign for all i. Also take an isotropic, odd interaction function, $W_\pm = 1$ and $H(\theta) = -H(-\theta)$. Then

$$
(4.40) \qquad \dot{\theta}_i = \Delta\omega_i + H(\theta_{i+1}) + H(\theta_{i-1}) - 2H(\theta_i), \quad i = 1, \ldots, N-1.
$$

The phase-locked solutions $\Theta = (\theta_1, \ldots, \theta_{N-1})$ then satisfy the matrix equation

$$
(4.41) \qquad\qquad\qquad \mathbf{H}(\Theta) = -\mathbf{A}^{-1}\mathbf{D},
$$

where $\mathbf{H}(\Theta) = (H(\theta_1), \ldots, H(\theta_{N-1}))^T$, $\mathbf{D} = (\Delta\omega_1, \ldots \Delta\omega_{N-1})$ and $\mathbf{A}$ is a tridiagonal matrix with elements $A_{ii} = -2$, $A_{i,i+1} = 1 = A_{i+1,i}$. Suppose, for concreteness, that $H(\theta) = \sin\theta$, Then a solution Θ will exist only if every component of $\mathbf{A}^{-1}\mathbf{D}$ lies between ± 1. Let $a_0 = \max\{|\mathbf{A}^{-1}\mathbf{D}_i|\}$. If $a_0 < 1$ then for each $i = 1, \ldots, N-1$ there are two distinct solutions $\theta_i^\pm$ in the interval $[0, 2\pi)$ with $H'(\theta_i^-) > 0$ and $H'(\theta_i^+) < 0$. In other words, there are 2^N phase-locked solutions. Linearizing about each phase-locked solution and exploiting the structure of the matrix $\mathbf{A}$, it

can be proven that only the solution $\Theta^- = (\theta_1^-, \dots \theta_{N-1}^-)$ is stable ([**149**]. Assuming that the frequency gradient is monotonic, this solution corresponds to a stable traveling wave. When the frequency gradient becomes too steep to allow phase-locking, that is $a_0 > 1$, two or more pools of oscillators (frequency plateaus) tend to form and oscillate at different frequencies. Waves produced by a frequency gradient do not have a constant speed or, equivalently, constant phase lags along the chain.

Constant speed waves can be generated from equations (4.38) by considering phase-locked solutions defined by $\theta_i = \theta$ for all i with a collective period of oscillation determined using $\dot{\theta}_i = \Omega$ such that

$$(4.42) \qquad\qquad \Omega = \omega_1 + W_+ H(\theta),$$

such that speed of the wave is Ω/θ. The steady state solutions are then

$$
\begin{aligned}
\Delta\omega_1 + W_- H(-\theta) &= 0 \\
\Delta\omega_i &= 0, \quad i = 2, \dots, N-2 \\
\Delta\omega_{N-1} - W_+ H(\theta) &= 0.
\end{aligned}
$$

$$(4.43)$$

This implies that all internal oscillators $(i = 2, \dots, N-2)$ have the same intrinsic frequency. If we further assume that $\Delta w_1 = 0 = \Delta\omega_{N-1}$ then a constant speed wave will exist provided that (i) the interactions are unidirectional with $W_- = 0$ say, and (ii) H satisfies the edge property $H(\theta) = 0$ for some $\theta \neq 0$. For example, if $H(\theta) = \sin(\theta + \sigma)$ for a fixed phase-shift σ, then the steady-state phase solution is $\theta = -\sigma$. It also follows that although the speed of the wave can change by changing the intrinsic frequency ω_1, the phase lag θ remains the same. This is consistent with the swimming motion of invertebrates. Finally, note that if coupling is in both directions, as in the lamprey CPG, one finds that for sufficiently long chains and $H^+ \neq H^-$, the system typically behaves like the unidirectional case except that there is a small *boundary layer* close to one end [**150**].

Phase–locking in strongly coupled IF networks

One of the useful features of the IF model is that one can go beyond the weak coupling regime by studying the existence and stability of phase–locked states directly in terms of the firing time map [**152, 153**]. This generalizes the analysis of the firing time map for a single periodically forced IF neuron (see §1.3) to the network level. It can be shown that increasing the strength of the synaptic coupling can lead to new dynamical instabilities not found in the phase–reduced models. Such instabilities generate non–phase–locked states, characterized by periodic or quasiperiodic variations of the inter-spike intervals (ISIs) on closed orbits. The corresponding mean firing rates exhibit complex spatio-temporal patterns including network–induced bursting.

Consider a network of identical leaky IF neurons labeled by the indices $i = 1, \dots, N$ such that neuron i makes synapses with neuron j:

$$(4.44) \qquad \frac{\mathrm{d}u_i}{\mathrm{d}t} = -u_i + I_0 + \epsilon \sum_{j=1}^{M} w_{ij} \sum_{m \in \mathbf{Z}} g_{\mathrm{syn}}(t - T_j^m)$$

where T_j^m is the mth firing time of the jth neuron, ϵw_{ij} is the strength of the synapse between neuron i and j and the function $g_{\mathrm{syn}}(t)$ represents the effects of synaptic filtering. Equation (4.44) is supplemented by the reset condition $\lim_{\delta \to 0^+} u_i(T_i^m +$

$\delta) = 0$. Suppose that an IF neuron operates as an oscillator such that the inter-spike interval $T_j^{m+1} - T_j^m = \Delta$ for all j, m in the absence of synaptic inputs. Conditions for phase-locking can be derived for arbitrary coupling strength ε by solving equation (4.44) under the ansatz that the firing times are of the form $T_j^n = (n - \psi_j/2\pi)\Delta$ for some self-consistent period Δ and constant phases ψ_j [**141, 140**]. Integrating over the interval $t \in (-\Delta\psi_i/2\pi, \Delta - \Delta\psi_i/2\pi)$ and incorporating the reset condition leads to the result

$$(4.45) \qquad 1 = (1 - \mathrm{e}^{-\Delta})I_0 + \varepsilon \sum_{j=1}^{N} w_{ij} H(\psi_j - \psi_i)$$

with

$$(4.46) \qquad H(\phi) = \mathrm{e}^{-\Delta} \int_0^{\Delta} dt \; \mathrm{e}^t \sum_{k \in \mathbf{Z}} g_{\mathrm{syn}}(t + (k + \phi/2\pi)\Delta)$$

Note that up to a positive constant factor, $H(\phi)$ reduces to the weak coupling phase interaction function of equation (4.13) for $\Delta \to \Delta_0$ and $\widehat{R}$ taken to be the PRC (1.43). It can be seen that equation (4.45) has an identical structure to that of equation (4.26). However, the former is exact whereas the latter is only strictly valid to $\mathcal{O}(\varepsilon)$, since it is derived under the assumption of weak coupling. Moreover, the collective period of oscillations Δ must be determined self-consistently in equation (4.45), since H depends on Δ rather than the natural period Δ_0. The stability of the phase–locked solutions can be determined by considering perturbations of the firing times, as detailed elsewhere [**152, 153**].

4.3. Oscillations in large homogeneous networks

In §2 we pointed out that neurons often form large homogeneous stochastic networks. This suggests that rather than considering individual neurons as deterministic oscillators, it might be more appropriate to consider collective oscillations at the population level. In this section we show how a fully connected network of IF neurons can exhibit collective oscillations through destabilization of an asynchronous state [**19**]. Consider the following synaptically coupled network of nonlinear IF neurons

$$(4.47) \qquad \frac{du_i}{dt} = F(u_i) + \frac{\varepsilon}{N} \sum_{j=1}^{N} \int_{-\infty}^{\infty} g_{\mathrm{syn}}(t' - \tau_a) \sum_m \delta(t - t' - T_j^m) dt',$$

with g_{syn} given by the alpha function (2.3), τ_a a discrete axonal delay and ε determines the strength of coupling. We take a threshold $u_\kappa = 1$ and a reset $u_r = 0$. In the case of a large network, we can replace the sum over delta functions by the population activity $\nu(t)$ so that

$$(4.48) \qquad \frac{du_i}{dt} = F(u_i) + \varepsilon\widehat{\nu}(t),$$

where $\widehat{\nu}(t) = \int_{-\infty}^{\infty} g_{\mathrm{syn}}(t' - \tau_a)\nu(t - t')dt'$. Suppose that there exists an asynchronous state $\nu(t) = \nu_0$. Since the α function is normalized to unity it follows that $\widehat{\nu}(t) = \nu_0$ as well. An implicit equation for ν_0 is then obtained by integrating equation (4.48)

between successive firing times:

$$(4.49) \qquad \frac{1}{\nu_0} = \int_0^1 \frac{du}{F(u) + \varepsilon \nu_0}.$$

We will assume that there exists a unique solution to this equation for given F and ε.

In order to study the stability of the asynchronous state, it is convenient to carry out the change of variables

$$(4.50) \qquad y_i = \nu_0 \int_0^{u_i} \frac{du}{F(u) + \varepsilon \nu_0},$$

with $0 < y_i < 1$ such that equation (4.48) becomes

$$(4.51) \qquad \frac{dy_i}{dt} = \nu_0 + \Gamma(y_i)[\widehat{\nu}(t) - \nu_0]$$

and

$$(4.52) \qquad \Gamma(y) = \frac{\nu_0 \varepsilon}{F(u) + \nu_0 \varepsilon}.$$

In order to incorporate the effects of noise, we include an additive white noise term $\xi_i(t)$,

$$(4.53) \qquad \frac{dy_i}{dt} = \nu_0 + \Gamma(y_i)[\widehat{\nu}(t) - \nu_0] + \xi_i(t),$$

with

$$(4.54) \qquad \langle \xi_i(t) \rangle = 0, \quad \langle \xi_i(t) \xi_j(t') \rangle = \sigma^2 \delta_{ij} \delta(t - t').$$

(Note that diffusive fluctuations of the membrane potential due to stochastic background activity would lead to an additive white noise term in equation (4.48) rather than in equation (4.54). The corresponding stochastic equation for y_i would then involve multiplicative noise, which is much harder to analyze). In the presence of noise the variable y_i can become negative so $-\infty < y_i < 1$. The Langevin equation (4.54) has an associated Fokker–Planck equation

$$(4.55) \qquad \frac{\partial}{\partial t} p(y, t) = -\frac{\partial}{\partial y} J(y, t),$$

where $J(y, t)$ is the probability flux

$$(4.56) \qquad J(y, t) = [\nu_0 + \Gamma(y)[\widehat{\nu}(t) - \nu_0]] \, p(y, t) - \frac{\sigma^2}{2} \frac{\partial}{\partial y} p(y, t).$$

This is supplemented by the boundary conditions arising from reset (see §3)

$$(4.57) \qquad p(1, t) = 0, \quad J(1, t) = \nu(t),$$

$$(4.58) \qquad p(0^+, t) = p(0^-, t), \quad J(0^+, t) - J(0^-, t) = \nu(t),$$

We also require $p(-\infty, t) = 0$ and $J(-\infty, t) = 0$. The steady-state solution of the Fokker–Planck equation is $J(y, t) = \nu_0$ and $p(y, t) = p_0(y)$ with

$$(4.59) \qquad p_0(y) = \begin{cases} e^{2\nu_0 y/\sigma^2} - e^{2\nu_0(y-1)/\sigma^2}, & y < 0 \\ 1 - e^{2\nu_0(y-1)/\sigma^2}, & 0 < y < 1 \end{cases}.$$

The stability of the steady–state can be determined by setting

$$(4.60) \qquad p(y, t) = p_0(y) + \rho(y) e^{\lambda t}, \quad \nu(t) = \nu_0 + \nu_1 e^{\lambda t}$$

and expanding to first order in ρ, ν_1. This gives the eigenvalue equation

$$(4.61) \qquad \lambda\rho(y) = \frac{\sigma2}{2}\frac{\partial2}{\partial y2}\rho(y) - \nu_0\frac{\partial}{\partial y}\rho(y) - \nu_1\widetilde{g}_{\mathrm{syn}}(\lambda)\frac{\partial}{\partial y}[\Gamma(y)p_0(y)],$$

where $\widetilde{g}_{\mathrm{syn}}(\lambda)$ is the Laplace transform

$$(4.62) \qquad \widetilde{g}_{\mathrm{syn}}(\lambda) = \int_0^\infty g_{\mathrm{syn}}(t-\tau_a)\mathrm{e}^{-\lambda t} = \frac{\alpha2}{(\lambda+\alpha)2}\mathrm{e}^{\tau_a\lambda}.$$

Defining the function

$$(4.63) \qquad h(y) = \nu_1\widetilde{g}_{\mathrm{syn}}(\lambda)\frac{\partial}{\partial y}[\Gamma(y)p_0(y)],$$

we can write equation (4.61) as the inhomogeneous equation

$$(4.64) \qquad [\mathcal{L}-\lambda\mathbf{1}]\rho(y) = h(y;\lambda),$$

where

$$(4.65) \qquad \mathcal{L} = \frac{\sigma2}{2}\frac{\partial2}{\partial y2} - \nu_0\frac{\partial}{\partial y}.$$

This inhomogeneous equation can be solved in terms of the associated one–dimensional Green's function satisfying $[\mathcal{L}-\lambda\mathbf{1}]G(y,y';\lambda) = \delta(y-y')$ and $G(1,y',\lambda) = 0$:

$$(4.66) \qquad \rho(y) = \int_{-\infty}^1 G(y,y';\lambda)h(y';\lambda)dy' - \nu_1 G(y,0;\lambda)$$

with

$$(4.67) \quad G(y,y';\lambda) = \begin{cases} A\left(\mathrm{e}^{\mu_+(\lambda)[y-1]} - \mathrm{e}^{-\mu_-(\lambda)[y-1]}\right)\mathrm{e}^{\mu_-(\lambda)[y'-1]}, & y' < y < 1 \\ A\left(\mathrm{e}^{\mu_-(\lambda)[y'-1]} - \mathrm{e}^{-\mu_+(\lambda)[y'-1]}\right)\mathrm{e}^{\mu_+(\lambda)[y-1]}, & y < y', \end{cases}$$

where

$$(4.68) \qquad A = \frac{2}{\sigma2}\frac{1}{\mu_+ + \mu_-},$$

$$(4.69) \qquad \mu_\pm(\lambda) = \frac{1}{\sigma2}\left[\sqrt{\nu_02 + 2\lambda\sigma2} \pm \nu_0\right].$$

Note that the term $\nu_1 G(y,0;\lambda)$ ensures that the flux discontinuity at $y = 0$ is satisfied. Finally, an implicit equation for the eigenvalues λ can be obtained by substituting equation (4.63) into (4.66) and imposing the boundary condition $J(1,t) = \nu(t)$, which corresponds to the following first–order condition

$$(4.70) \qquad -\frac{\sigma2}{2}\frac{\partial}{\partial y}\rho(y,t)|_{y=1} = \nu_1.$$

The resulting characteristic equation is [19]

$$(4.71) \qquad \left(\mathrm{e}^{\mu_-(\lambda)} - 1\right) = \mu_-(\lambda)\widetilde{g}_{\mathrm{syn}}(\lambda)\int_{-\infty}^1 p_0(y)\Gamma(y)\mathrm{e}^{\mu_-(\lambda)y}dy.$$

In the zero noise limit $\sigma \to 0$, we have $\mu_-(\lambda) \to \lambda/\nu_0$ and $p_0(y) \to 1$ for $0 < y < 1$ and is zero otherwise. Thus, equation (4.71) becomes

$$(4.72) \qquad \left(\mathrm{e}^{\lambda/\nu_0} - 1\right) = \frac{\lambda}{\nu_0}\widetilde{g}_{\mathrm{syn}}(\lambda)\int_0^1 \Gamma(y)\mathrm{e}^{\lambda y/\nu_0}dy.$$

In the weak coupling regime, solutions of equation (4.72) are of the form $\lambda = 2\pi i n\nu_0 + \Lambda_n$ for integer n with $\Lambda_n = \mathcal{O}(\epsilon)$. The term Λ_n can be calculated by

performing a perturbation expansion in the coupling ϵ. The lowest order contribution is simply determined by setting $\lambda = 2\pi in\nu_0$ on the right-hand side of equation (4.72). In the case of a linear IF model with $F(u) = I_0 - u$, we have $\Gamma(y) = \mathrm{e}^{y/\nu_0}$ so that

$$(4.73) \qquad \Lambda_n = \epsilon \left(\frac{2\pi in\nu_0}{1 + 2\pi in\nu_0} \right) \widetilde{g}_{\mathrm{syn}}(2\pi in\nu_0) + \mathcal{O}(\epsilon^2).$$

We then have the following stability results in the absence of noise [**19, 125**]:

(i) For zero axonal delays ($\tau_a = 0$) and excitatory coupling ($\epsilon > 0$), the asynchronous state is stable with respect to excitation of the nth mode if and only if $\alpha < \alpha_n$ where

$$(4.74) \qquad \alpha_n = -1 + \sqrt{1 + 4n^2\pi^2\nu_0^2}.$$

Hence, it is stable for sufficiently slow synapses, that is, $\alpha < \alpha_1$. The asynchronous state is always unstable in the case of inhibitory coupling since the condition for stability with respect to the nth harmonic is now $\alpha > \alpha_n$, which cannot be satisfied for all n.

(ii) The asynchronous state is almost always unstable for non-zero delays (in the noise-free case).

(iii) For large n, $|\Lambda_n| \sim 1/n^2$ so that higher harmonics grow or decay slowly.

Note that although the zero delay case is a singular limit in the absence of noise, it becomes non-singular for arbitrarily small amounts of noise, where instabilities with respect to higher harmonics are suppressed [**19, 125**]. One finds that for sufficiently high noise levels the asynchronous state is always stable. Reducing the noise for fixed delay induces an instability due to excitation of one of the harmonic modes with frequency $\omega \approx \omega_n = 2\pi n\nu_0$. A bifurcation at $\omega \approx \omega_1$ implies that the period of the resulting collective oscillation is identical to the period of the individual oscillators. Higher harmonics correspond to instabilities of the asynchronous state that lead to the formation of cluster states [**125, 154**]: each neuron fires with mean rate ν_0, but the population of neurons splits up into several groups that fire in sequence so that the overall activity exhibits faster oscillations. In Figure 6 we show the stability diagram for the asynchronous state of an IF network calculated within the context of the spike response model [**17**]. In this version of the model, the source of noise is now reset noise rather than membrane fluctuations; each time the neuron fires the membrane potential is reset to a random value u_r generated from a Gaussian distribution of width σ. Nevertheless, the qualitative behavior is very similar. Finally, note that fast oscillations are also found in sparsely connected random networks [**124**].
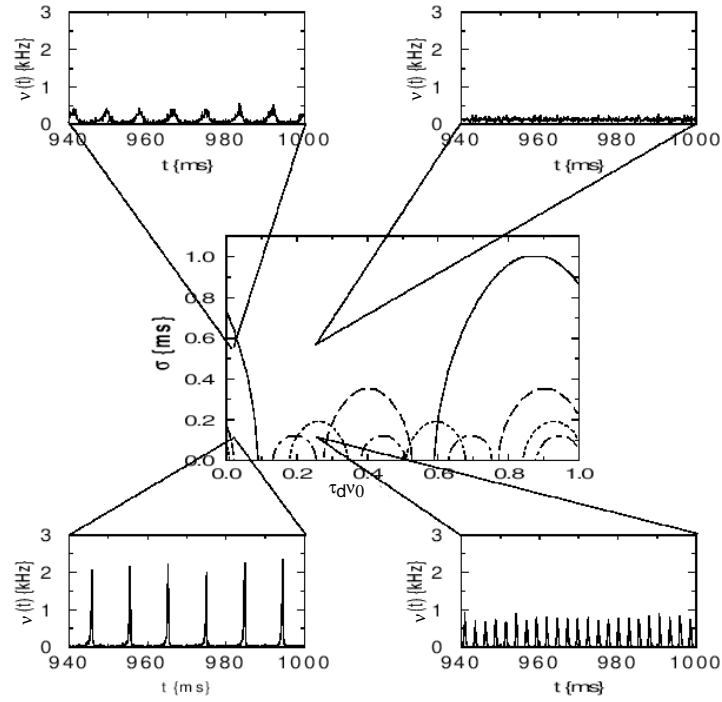
FIGURE 6. Stability diagram (center) for asynchronous state in an IF network as a function of noise amplitude σ and delay τ_a for fixed synaptic time constant $\alpha^{-1} = 4ms$ and membrane time constant $\tau = 10ms$. The input I_0 was chosen so that the population activity of the asynchronous state was $\nu_0 = 0.5\alpha$. The diagram shows the borders of the stability region with respect to the harmonic frequencies ω_1 (solid lines), ω_2 (long–dashed lines), ω_3 (short–dashed lines) and ω_4 (long–short dashed lines). Insets show typical patterns of activity from a simulation of $N = 1000$ neurons. [Reprinted from [**7**], with permission of Cambridge University Press.]

Neural Pattern Formation

Wilson and Cowan [**155, 156**] introduced a rate–based population model of cortical tissue based on the idea that the identity of individual presynaptic neurons is not important, but only the distribution of their level of activity. This leads to a statistical description of cortical activity in which the proportion of active neurons is chosen as a model variable. A justification for a statistical approach can be given in terms of the spatial clustering of neurons with similar response properties in cortex. These cells form vertical columns within the thin convoluted sheet of neural tissue that constitutes the cerebral cortex. For example, Hubel and Wiesel [**157**] reported a columnar-like arrangement of neurons in primary visual cortex that prefer stimuli of similar orientation. Neurons within a cortical column share many inputs and are tightly interconnected, so that it is reasonable to consider the mean activity $\nu(t)$ of the given neural population, rather than keeping track of the spiking of individual cells. However, in order to construct a closed set of equations for population activity, it is necessary that the total input into a population is slowly varying relative to the time-scale of action potential generation. Hence, an implicit assumption in rate–based population models is that neurons within a population have spike trains that are temporally incoherent (see also §3). In this final lecture, we derive integrodifferential equations describing the dynamics of synaptically coupled neuronal populations in spatially structured cortical networks. We then use these equations to investigate a variety of problems regarding large–scale cortical dynamics. First, we consider a Turing–like mechanism for spontaneous pattern formation in visual cortex, and show how this provides a neural mechanism for geometric visual hallucinations. We then show how cortical networks can support persistent spatially coherent states that could provide a basis for working memory. Finally, we study traveling waves in disinhibited cortical slices.

5.1. Reduction to rate models

Suppose that there exist M populations each consisting of N neurons labeled by $i \in \mathcal{I}_p$, $p = 1, \ldots, M$ and $|\mathcal{I}_p| = N$, see Figure 1. Assume that all neurons of a given population are equivalent in the sense that the interaction between neuron $i \in \mathcal{I}_p$ and neuron $j \in \mathcal{I}_q$ only depends on p and q. Each neuron i in population p receives input from all neurons j in population q with strength $w_{ij} = W_{pq}/N$. The total synaptic current to neuron $i \in \mathcal{I}_p$ from the various populations is thus

$$(5.1) \qquad X_p(t) = \sum_{q=1}^{M} W_{pq} \int_0^\infty g_{\text{syn}}(\tau)\nu_q^{(N)}(t - \tau)\mathrm{d}\tau,$$
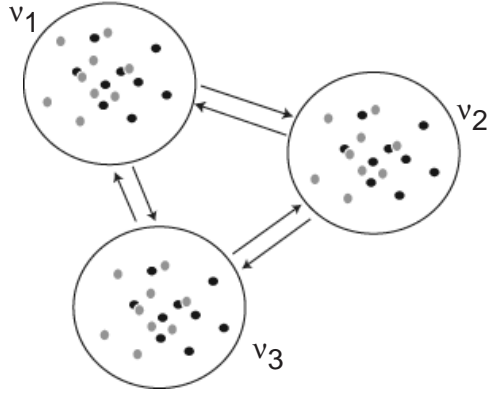
FIGURE 1. Interacting populations of spiking neurons each with its own population activity ν_p, $p = 1, 2, 3$.

where

$$(5.2) \qquad \nu_q^{(N)}(t) = \frac{1}{N} \sum_{j \in \mathcal{I}_q} \sum_{m \in \mathbf{Z}} \delta(t - T_j^m).$$

Now take the thermodynamic limit $N \to \infty$ with $\nu_q(t) = \lim_{N \to \infty} \nu_q^{(N)}$. The macroscopic variable $\nu_q(t)$ represents the total activity of the qth population, that is, the fraction of neurons firing at time t. An asynchronous state may then be defined as one with constant activity $\nu_q(t) = \nu_q^{(0)}$ for all $q = 1, \dots, M$. It follows that the total synaptic current is also time-independent with

$$(5.3) \qquad X_p(t) = X_p^{(0)} = \sum_q W_{pq} \nu_q^{(0)}.$$

From our previous analysis, we have seen that each homogeneous population's activity is related to the synaptic input (assuming zero external inputs) according to some effective gain function which we denote by f, $\nu_q^{(0)} = f(X_q^{(0)})$. This then yields the steady-state equation

$$(5.4) \qquad X_p^{(0)} = \sum_q W_{pq} f(X_q^{(0)}).$$

This analysis can now be extended to the case of time-varying activities provided that each population remains in a state of incoherent firing so that the synaptic input is slowly varying in time. We can then make the approximation $\nu_q(t) \approx f(X_q(t))$ to obtain the closed integral equation

$$(5.5) \qquad X_p(t) = \sum_q W_{pq} \int_0^\infty g_{\text{syn}}(\tau) f(X_q(t - \tau)) \mathrm{d}\tau.$$

In the case of exponential synapses this reduces to the well–known form

$$(5.6) \qquad \tau_s \frac{dX_p}{dt} = -X_p(t) + \sum_q W_{pq} f(X_q(t)).$$

The reduction to a rate equation breaks down, however, when the population activity changes rapidly during one period due to fast transients or the existence of

a coherent state exhibiting collective oscillations, such as when the asynchronous state becomes unstable.

Spatial continuum limit

The physical location of a column of neurons in a region of cortex often reflects the task of that population of neurons. For example, in the auditory system, neurons are organized along an axis that reflects the cell's preferred frequency. As one moves along the axis the preferred frequency changes gradually from high to low frequency tones. Thus there is a one–dimensional frequency or tonotopic map in auditory cortex. Similarly, in primary visual cortex (V1) there is an orderly retinotopic mapping of the visual field onto its surface, with left and right halves of the visual field mapped onto right and left V1 respectively. Superimposed upon this are additional two–dimensional maps reflecting the fact that neurons respond preferentially to stimuli with particular features such as orientation [**158**]. This suggests labeling neurons according to their cortical position. We now give a heuristic argument for how such labeling leads to a continuum model of cortex.

Consider a population of neurons distributed along a one–dimensional axis. Suppose that we partition space into segments of length d such that the number of neurons in segment $[nd, (n+1)d]$ is $N = \rho d$ where ρ is the cell density. We treat neurons in that interval as a homogeneous population of cells (cortical column) labeled by the integer n, and assume that synaptic interactions between the nth and mth populations only depend on the discrete locations of the populations on the line. Writing $W_{nm} = \rho d w(nd, md)$ and $X_n(t) = a(nd, t)$, equation (5.5) becomes

$$(5.7) \qquad a(nd, t) = \rho d \sum_m w(nd, md) \int_0^\infty g_{\text{syn}}(\tau) f(a(md, t - \tau)) \mathrm{d}\tau.$$

Taking the limit $d \to 0$, the summation on the right–hand side can be replaced by an integral to give

$$(5.8) \qquad a(x, t) = \rho \int w(x, y) \int_0^\infty g_{\text{syn}}(\tau) f(a(y, t - \tau)) \mathrm{d}\tau dy.$$

In the case of exponential synapses this reduces to the integro–differential equation

$$(5.9) \qquad \tau \frac{\partial}{\partial t} a(x, t) = -a(x, t) + \rho \int w(x, y) f(a(y, t)) dy.$$

Equation (5.9) is an example of a neural field equation [**156, 159, 101, 102**], which is widely used to study large–scale spatio–temporal dynamics of cortical tissue. It can easily be extended to higher spatial dimensions as well as to separate populations of excitatory and inhibitory neurons, see below.

5.2. Turing mechanism for cortical pattern formation

Let $a_E(\mathbf{r}, t)$ be the activity of excitatory neurons in a given volume element of a slab of neural tissue located at $\mathbf{r} \in \mathbf{R}^2$, and $a_I(\mathbf{r}, t)$ be the corresponding activity of inhibitory neurons. Assuming for concreteness a rate-based model with exponential synapses, we have an evolution equation of the form

$$(5.10) \qquad \tau_l \frac{\partial a_l(\mathbf{r}, t)}{\partial t} = -a_l(\mathbf{r}, t) + \sum_{m=E,I} \int_{\mathbf{R}^2} w_{lm}(\mathbf{r}|\mathbf{r}') f_m[a_m(\mathbf{r}', t)] d\mathbf{r}' + h_l(\mathbf{r}, t)$$

for $l = E, I$, where $w_{lm}(\mathbf{r}|\mathbf{r}') = w_{lm}(|\mathbf{r} - \mathbf{r}'|)$ gives the weight per unit volume of all synapses to the lth population from neurons of the mth population a distance $|\mathbf{r} - \mathbf{r}'|$ away, f_E and f_I are taken to be smooth output functions

$$(5.11) \qquad f_l(x) = \frac{1}{1 + e^{-\eta_l(x - \kappa_l)}}, \quad l = E, I,$$

where η_l determines the slope or sensitivity of the input–output characteristics of the population and κ_l is a threshold, h_E and h_I are external stimuli, and $\tau_{E,I}$ are synaptic time constants. From a mathematical viewpoint, it is often convenient to reduce the above two-population model to an effective one-population model. In particular, suppose that $\tau_I \ll \tau_E$, $w_{II} = 0$ and f_I is a linear function. We can then eliminate a_I in terms of a_E such that

$$(5.12) \qquad \tau \frac{\partial a(\mathbf{r}, t)}{\partial t} = -a(\mathbf{r}, t) + \int_{\mathbf{R}^2} w(|\mathbf{r} - \mathbf{r}'|) f[a(\mathbf{r}', t)] d\mathbf{r}' + h(\mathbf{r}, t),$$

where we have dropped the index E and

$$(5.13) \qquad w(|\mathbf{r} - \mathbf{r}'|) = w_{EE}(|\mathbf{r} - \mathbf{r}'|) - \int w_{EI}(|\mathbf{r} - \mathbf{r}''|) w_{IE}(|\mathbf{r} - \mathbf{r}''|) d\mathbf{r}''.$$

In the case of a constant external input, $h_l(\mathbf{r}) = \bar{h}_l$, there exists at least one fixed point solution $a_l(\mathbf{r}) = \bar{a}_l$ of equation (5.10), where

$$(5.14) \qquad \bar{a}_l = \sum_{m = E, I} W_{lm} f(\bar{a}_m) + \bar{h}_l$$

and $W_{lm} = \int_{\mathbf{R}^2} w_{lm}(\mathbf{r}) d\mathbf{r}$. If $\bar{h}_l$ is sufficiently small relative to the threshold κ then this fixed point is unique and stable. Under the change of coordinates $a_l \to a_l - \bar{h}_l$, it can be seen that the effect of $\bar{h}_l$ is to shift the threshold by the amount $-\bar{h}_l$. Thus there are two ways to increase the excitability of the network and thus destabilize the fixed point: either by increasing the external input $\bar{h}_l$ or reducing the threshold κ. The latter can occur through the action of drugs on certain brain stem nuclei which provides a mechanism for generating geometric visual hallucinations [**160, 161**], see below. The local stability of $(\bar{a}_E, \bar{a}_I)$ is found by linearization:

$$(5.15) \qquad \tau_l \frac{\partial b_l(\mathbf{r}, t)}{\partial t} = -b_l(\mathbf{r}, t) + \mu \sum_{m = E, I} \int_{\mathbf{R}^2} w_{lm}(|\mathbf{r} - \mathbf{r}'|) b_m(\mathbf{r}', t) d\mathbf{r}',$$

where $b_l(\mathbf{r}, t) = a_l(\mathbf{r}, t) - \bar{a}_l$ and we have performed a rescaling of the local weights $f'(\bar{a}_l) w_{lm} \to \mu w_{lm}$ with μ a measure of the degree of network excitability. Assuming solutions of the form $b_l(\mathbf{r}, t) = b_l(\mathbf{r}) e^{-\lambda t / \tau_l}$ we are left with the spectral problem:

$$(5.16) \qquad \lambda b_l(\mathbf{k}) = -b_l(\mathbf{k}) + \mu \sum_m W_{lm}(|\mathbf{k}|^2) b_m(\mathbf{k}),$$

where $b_l(\mathbf{k})$ and $W_{lm}(|\mathbf{k}|^2)$ are, respectively, the Fourier coefficients of $b_l(\mathbf{r})$ and $w_{lm}(\mathbf{r})$. This leads to a matrix *dispersion relation* for λ as a function of $k = |\mathbf{k}|$:

$$(5.17) \qquad \det([\lambda + 1]I - \mu \mathbf{W}(k)) = 0,$$

where $\mathbf{W}$ is the matrix of Fourier coefficients of the w_{lm}. Similarly, in the corresponding one–population model (5.12), we obtain the dispersion relation

$$(5.18) \qquad \lambda = -1 + \mu W(k) \equiv \lambda(k),$$

with $W(k)$ the Fourier transform of $w(\mathbf{r})$. One major difference between the one-population and two-population models is that the latter can exhibit time-periodic solutions [**101**]. We will restrict our discussion to static solutions here.

(a) W(r)
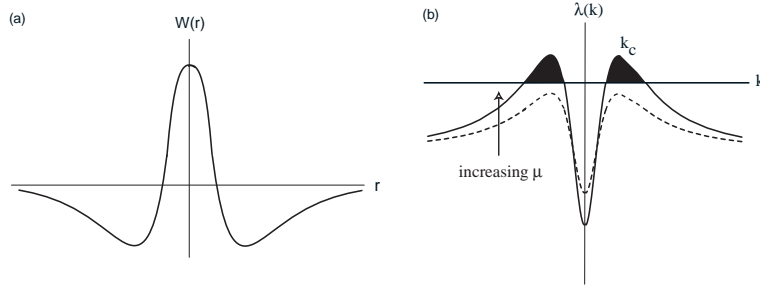
(b) $\lambda(k)$

k_c

k

increasing μ

FIGURE 2. Neural basis of the Turing mechanism. (a) Mexican hat interaction function showing short-range excitation and long-range inhibition. (b) Dispersion curves $\lambda(k)$ for Mexican hat function. If the excitability μ of the cortex is increased, the dispersion curve is shifted upwards leading to a Turing instability at a critical parameter $\mu_c = W(k_c)^{-1}$ where $W(k_c) = [\max_k\{W(k)\}]$. For $\mu_c < \mu < \infty$ the homogeneous fixed point is unstable.

We now determine conditions under which the homogeneous state loses stability leading to the formation of spatially periodic patterns. The standard mechanism for such an instability, which is the neural analog of the Turing instability in reaction-diffusion equations, is a combination of short-range excitation and long-range inhibition. In the case of a one-population model this can be represented by the so-called "Mexican Hat" function (see Figure 2(a)):

$$(5.19) \qquad w(|\mathbf{r}|) = (\frac{A_+}{\sigma_+})e^{-r^2/\sigma_+^2} - (\frac{A_-}{\sigma_-})e^{-r^2/\sigma_-^2},$$

the Fourier transform of which is:

$$(5.20) \qquad W(k) = \frac{1}{2}(A_+ e^{-\frac{1}{4}\sigma_+^2 k^2} - A_- e^{-\frac{1}{4}\sigma_-^2 k^2}).$$

It is simple to establish that λ passes through zero at the critical value μ_c signalling the growth of spatially periodic patterns with wave number k_c, where $W(k_c) = \max_k\{W(k)\}$, see Figure 2(b). Close to the bifurcation point these patterns can be represented as linear combinations of plane waves

$$b(\mathbf{r}) = \sum_n (c_n e^{i\mathbf{k}_n \cdot \mathbf{r}} + c_n^* e^{-i\mathbf{k}_n \cdot \mathbf{r}}),$$

where the sum is over all wave vectors with $|\mathbf{k}_n| = k_c$. Rotation symmetry implies that the space of such modes is infinite-dimensional. That is, all plane-waves with wave vectors on the critical circle $|\mathbf{k}| = k_c$ are allowed (see Figure 3(a)). However, translation symmetry means that we can restrict the space of solutions to that of doubly-periodic functions corresponding to regular tilings of the plane. That is, $b(\mathbf{r} + \boldsymbol{\ell}) = b(\mathbf{r})$ for all $\boldsymbol{\ell} \in L$ where L is a regular square, rhomboid or hexagonal lattice as illustrated in Figure 3(b). The sum over n is now finite with N = 2 (square, rhomboid) or N = 3 (hexagonal) and, depending on the boundary conditions, various patterns of stripes or spots can be obtained as solutions. Amplitude
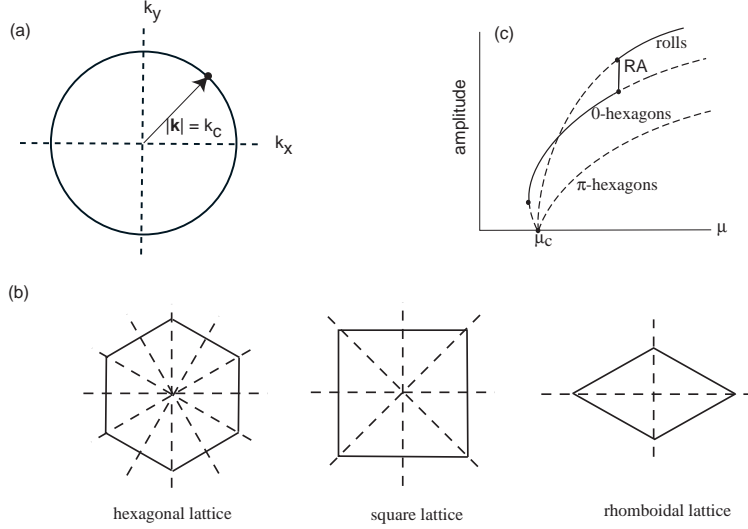
FIGURE 3. (a) Critical circle for Turing instability. (b) Planar lattices: hexagonal, square, rhomboid. (c) Bifurcation diagram showing the variation in amplitude C with parameter μ for patterns on a hexagonal lattice. Solid and dashed curves indicate stable and unstable solutions respectively. The different patterns are distinguished by the coefficients $\mathbf{c} = (c_1, c_2, c_3)$ with $\mathbf{c} = (1, 0, 0)$ for roll or stripe patterns, $\mathbf{c} = (1, 1, 1)$ for 0-hexagons and $\mathbf{c} = (1, 1, -1)$ for π-hexagons. It is also possible for additional patterns to form through secondary bifurcations (such as rectangular (RA) patterns). However, higher-order contributions to the amplitude equation are needed to determine such bifurcations.

equations for the coefficients c_n can then be obtained using perturbation methods [102]. However, their basic structure can be determined from the underlying rotation and translation symmetries of the network model. In the case of a square or rhombic lattice, we can take $\mathbf{k}_1 = k_c(1, 0)$ and $\mathbf{k}_2 = k_c(\cos\varphi, \sin\varphi)$ such that (to cubic order)

$$(5.21) \qquad \frac{dc_n}{dt} = c_n \left[\mu - \mu_c - \Gamma_0 |c_n|^2 - 2\Gamma_\varphi \sum_{m \neq n} |c_m|^2 \right], \quad n = 1, 2,$$

where Γ_φ depends on the angle φ. In the case of a hexagonal lattice we can take $\mathbf{k}_n = k_c(\cos\varphi_n, \sin\varphi_n)$ with $\varphi_1 = 0, \varphi_2 = 2\pi/3, \varphi_3 = 4\pi/3$ such that

$$(5.22) \quad \frac{dc_n}{dt} = c_n \left[\mu - \mu_c - \Gamma_0 |c_n|^2 - -\eta c_{n-1}^* c_{n+1}^* \right] - 2\Gamma_{\varphi_2} c_n \left(|c_{n-1}|^2 + |c_{n+1}^2| \right),$$

where $n = 1, 2, 3 (\mod 3)$. These ordinary differential equations can then be analyzed to determine which particular types of pattern are selected and to calculate their stability [160, 161, 102]. The results can be summarized in a bifurcation diagram as illustrated in Figure 3(c) for the hexagonal lattice with $h > 0$ and $2\Gamma_{\varphi_2} > \Gamma_0$.

Geometric visual hallucinations

The primary visual cortex (V1) is the first cortical area to receive visual information from the retina (see Figure 4). The output from the retina is conveyed by ganglion
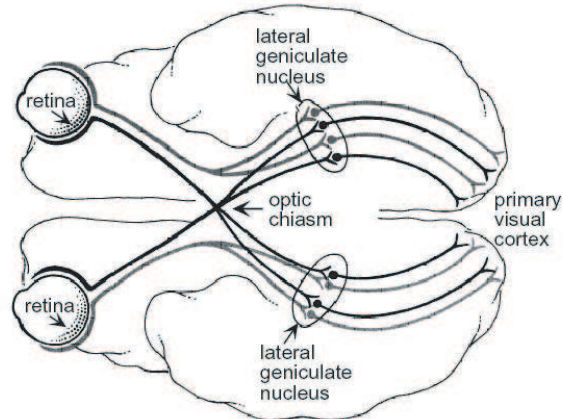

FIGURE 4. Visual pathways from the retina through the lateral geniculate nucleus (LGN) of the thalamus to the primary visual cortex (V1)

cells whose axons form the optic nerve. The optic nerve conducts the output spike trains of the retinal ganglion cells to the lateral geniculate nucleus (LGN) of the thalamus, which acts as a relay station between retina and primary visual cortex (V1). Prior to arriving at the LGN, some ganglion cell axons cross the midline at the optic chiasm. This allows the left and right sides of the visual fields from both eyes to be represented on the right and left sides of the brain, respectively. Note that signals from the left and right eyes are segregated in the LGN and in input layers of V1. This means that the corresponding LGN and cortical neurons are monocular, in the sense that they only respond to stimuli presented to one of the eyes but not the other (ocular dominance).

One of the striking features of the visual system is that the visual world is mapped onto the cortical surface in a topographic manner. This means that neighboring points in a visual image evoke activity in neighboring regions of visual cortex. Moreover, one finds that the central region of the visual field has a larger representation in V1 than the periphery, partly due to a non–uniform distribution of retinal ganglion cells. The retinotopic map is defined as the coordinate transformation from points in the visual world to locations on the cortical surface. In order to describe this map, we first need to specify visual and cortical coordinate systems. Since objects located a fixed distance from one eye lie on a sphere, we can introduce spherical coordinates with the "north pole" of the sphere located at the fixation point, the image point that focuses onto the fovea or center of the retina. In this system of coordinates, the latitude angle is called the eccentricity ϵ and the longitudinal angle measured from the horizontal meridian is called the azimuth φ. In most experiments the image is on a flat screen such that, if we ignore the curvature of the sphere, the pair (ϵ, φ) approximately coincides with polar coordinates on the screen. One can also represent points on the screen using Cartesian coordinates (X, Y). In primary visual cortex the visual world is split in half with the region
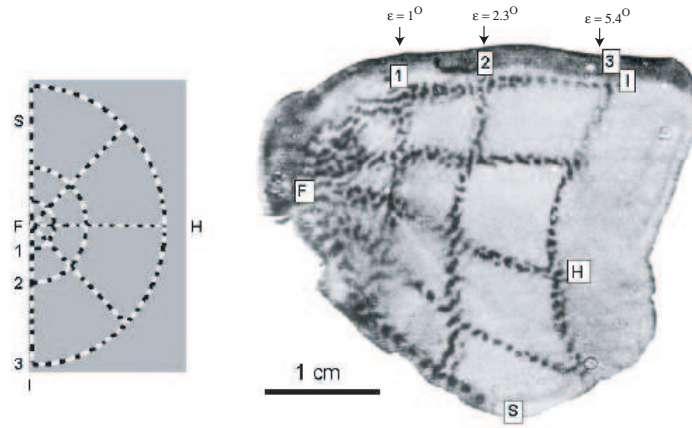
FIGURE 5. An autoradiograph from the primary visual cortex in the left side of a macaque monkey brain. The pattern is a radioactive trace of the activity evoked by the image shown to the left. [Reprinted from [**162**], with permission from J. Neurosci.]

$-90^o \leq \varphi \leq 90^o$ represented on the left side of the brain, and the reflection of this region represented on the right side brain. Note that the eccentricity ϵ and Cartesian coordinates (X, Y) are all based on measuring distance on the screen. However, it is customary to divide these distances by the distance from the eye to the screen so that they are specified in terms of angles. The structure of the retinotopic map in monkey is shown in Figure 5, which was produced by imaging a radioactive tracer that was taken up by active neurons while the monkey viewed a visual image consisting of concentric circles and radial lines. The fovea is represented by the point F on the left hand side of the cortex, and eccentricity increases to the right. Note that concentric circles are approximately mapped to vertical lines and radial lines to horizontal lines.

Motivated by Figure 5, we assume that eccentricity is mapped on to the horizontal coordinate x of the cortical sheet, and φ is mapped on to its y coordinate. An approximate equation for the retinotopic map can then be obtained for eccentricities greater than 1°:

$$(5.23) \qquad x \approx \lambda \ln(\epsilon/\epsilon_0), \quad y \approx -\frac{\lambda \pi \varphi}{180^o}.$$

It follows that the retinotopic map can be approximated by a complex logarithm [**163**]. That is, introducing the complex representations $Z = (\epsilon/\epsilon_0)e^{-i\pi\varphi/180^o}$ and $z = x + iy$ then $z = \lambda \log Z$. Now suppose that a doubly periodic pattern of activity is formed in cortex. If the cortical patterns are mapped back into visual field coordinates using the inverse of the above retinicortical map, then a number of common visual hallucinations are generated [**160**]. This is illustrated in Figures 6 and 7. A more detailed model of visual hallucinations has recently been developed that takes into account the fact that neurons signal the orientation as well as the location of a visual stimulus [**161, 102**]. This model can reproduce a broader range of hallucinations and also has some interesting symmetries arising from the distribution of long-range connections in cortex.

FIGURE 6. Doubly-periodic activity patterns in cortex
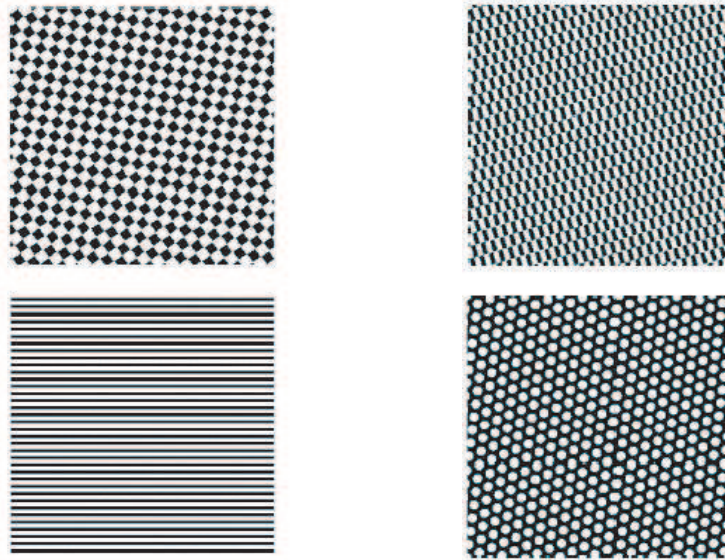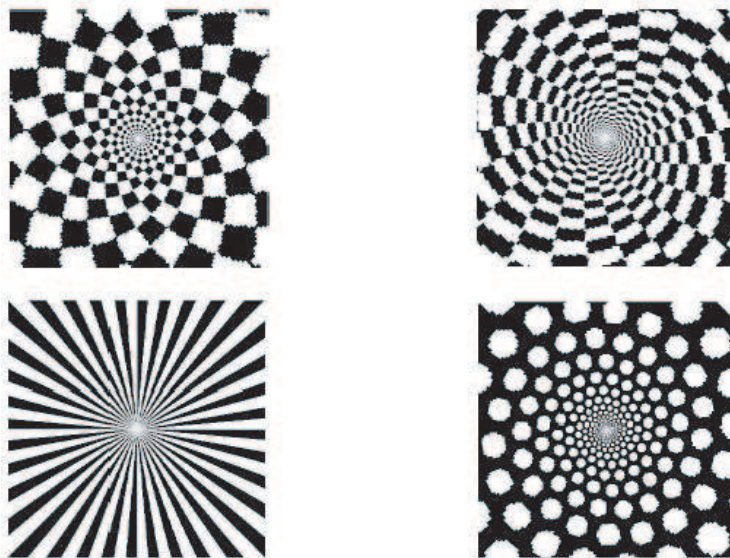

FIGURE 7. Corresponding hallucinatory images generated using the inverse retinocortical map

5.3. Persistent localized states

In addition to spatially periodic patterns, neural networks with Mexican hat interactions also support spatially localized persistent activity states known as bumps. Wilson and Cowan [156] showed numerically how solitary stationary bumps can

arise in a one-dimensional network of excitatory and inhibitory neurons, with short-range excitation keeping the bump active and longer–range inhibition preventing the bump from spreading. Amari [**159**] subsequently obtained analytical solutions for bump states in a simplified one–population model with a step–function nonlinearity. In contrast to the spatially periodic patterns discussed in §4.2, these bump states are highly nonlinear and are far from any spatially and temporally uniform states. We will present the details of Amari's analytical construction.

Consider the neural field equation

$$(5.24) \quad \frac{\partial a(x,t)}{\partial t} = -a(x,t) + \int_{-\infty}^{\infty} w(x-x')H[a(x',t)]dx' + h + s(x,t),$$

where $w(x)$ is a symmetric integrable function, $H(a)$ is the Heaviside step function

$$(5.25) \quad H[a] = \begin{cases} 0 & \text{if } a \leq 0 \\ 1 & \text{if } a > 0 \end{cases}.$$

h is a homogeneous input and $s(x,t)$ is a spatially patterned input. Following Amari [**159**], we restrict w to be a Mexican hat function. Equilibrium solutions of equation (5.24) with $s(x,t) = 0$ satisfy

$$(5.26) \quad A(x) = \int_{-\infty}^{\infty} w(x-x')H[A(x')]dx' + h.$$

Let $R[A] = \{x|A(x) > 0\}$ be the region over which the field is excited. Equation (5.26) can then be rewritten as

$$(5.27) \quad A(x) = \int_{R[A]} w(x-x')dx' + h.$$

Exploiting the fact that any solution can be arbitrarily translated so that it is centered at the origin, we define a stationary pulse solution of width d to be one that is excited over the interval $(-d, d)$. Let

$$(5.28) \quad W(x) = \int_0^x w(y)dy$$

and

$$(5.29) \quad W_m = \max_{x>0} W(x), \quad W_\infty = \lim_{x \to \infty} W(x)$$

such that $W(0) = 0$ and $W(-x) = -W(x)$. For a bump of width d, equation (5.27) reduces to the form

$$(5.30) \quad A(x) = h + W(d+x) - W(x-d).$$

Since $A(d) = 0$ by definition, we obtain the following necessary condition for the existence of a bump:

$$(5.31) \quad W(2d) + h = 0.$$

This condition is also sufficient for the Mexican hat weight distribution [**159**]. It will be shown below that a bump is stable provided the condition $W'(2d) < 0$ is satisfied. The existence and stability of activity bumps for a given h can thus be determined graphically as illustrated in Figure 8(b). For a certain range of values of $h < 0$ one finds bistability between a stable bump and a rest state for which $R[A] = \emptyset$.
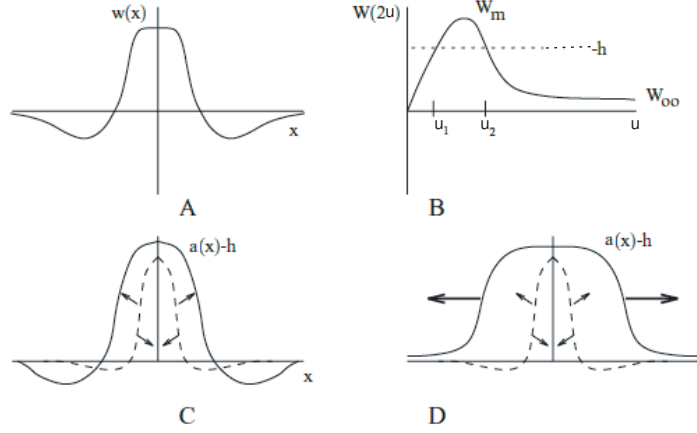
FIGURE 8. Construction of a solitary pulse in the Amari model. (a)
The Mexican hat weight distribution w. (b) Integral $W(x)$ of $w(x)$.
Horizontal line shows the uniform stimulus $-h$ whose intersections with
$W(2d)$ determine the allowed stationary pulse solutions. (c) Unstable
pulse (broken) acts as a separatrix between the stable pulse and the rest
state. (d) Unstable pulse acts as a separatrix between a wavefront and
the rest state.

The linear stability of a stationary pulse can be determined by setting $a(x, t) = A(x) + p(x)e^{\lambda t}$ and expanding to first order in p [**164, 135**]. This leads to the eigenvalue equation

$$(5.32) \qquad (\lambda + 1)p(x) = \int_{-\infty}^{\infty} w(x - x')\delta(A(x'))p(x')dx'.$$

Using the identity

$$(5.33) \qquad \delta(A(x)) = \left(\frac{\delta(x - d)}{|A'(d)|} + \frac{\delta(x - +d)}{|A'(-d)|} \right),$$

and setting $|A'(d)| = |A'(-d)| = \gamma^{-1}$, we have

$$(5.34) \qquad (\lambda + 1)p(x) = \gamma \left(w(x - d)p(d) + w(x + a)p(-d) \right).$$

There are two types of solution to this equation. The first consist of solutions $p(x)$ that vanish at $x = \pm d$ so that $\lambda = -1$. This defines the essential spectrum and does not contribute to any instabilities. The second class of solution, which generates the discrete spectrum, is obtained by setting $x = \pm d$ in the eigenvalue equation,

$$(5.35) \qquad (\lambda + 1)p_+ \;=\; \gamma \left(w(0)p_+ + w(2d)p_- \right)$$
$$(5.36) \qquad (\lambda + 1)p_- \;=\; \gamma \left(w(-2d)p_+ + w(0)p_- \right).$$

This has the solutions $p_- = \pm p_+$ with corresponding eigenvalues

$$(5.37) \qquad \lambda_\pm = -1 + \gamma(w(0) \pm w(2d)).$$

Finally, using the fact that $\gamma^{-1} = w(0) - w(2d)$ we deduce that $\lambda_- = 0$ (reflecting the translation invariance of the system) and $\lambda_+ = \gamma w(2d)$. Thus the bump is stable if $w(2d) = W'(2d) < 0$.

Note that the discrete spectrum is determined completely in terms of the perturbations $p_\pm = p(\pm d)$. This explains why it is also possible to analyze the stability of the bumps by restricting attention to the effects of perturbations at the boundaries of the activity bump as originally formulated by Amari [**159**]. In particular, if $a(x,t) = 0$ at $x = x \pm d + \Delta_\pm(t)$, then

$$0 = A(\pm d + \Delta_\pm(t)) + p(d + \Delta_\pm(t), t)$$
$$= A(\pm d) + A'(\pm d)\Delta_\pm(t) + p(\pm d, t) + \mathcal{O}(\Delta^2),$$

that is,

$$\Delta_\pm(t) = \pm \gamma p(\pm d, t)$$

since $A(\pm d) = 0$ and $A'(\pm d) = \mp \gamma^{-1}$. It follows that $p_- = p_+$ generates a uniform expansion of the bump ($\Delta_- = -\Delta_+$) and $p_- = -p_+$ generates a shift in the center of the bump ($\Delta_- = \Delta_+$).

There have been various extensions of Amari's original analysis described above. Kishimoto and Amari [**165**]) proved the existence of a solitary pulse for a smooth sigmoidal nonlinearity f rather than a hard threshold using a fixed point theorem. More recent extensions include weight distributions that are not of the lateral inhibition type (for which multiple bump states can arise) [**166, 167**], spiking rather than rate-based models [**168**], two-dimensional bumps [**169, 167, 135, 136**], and weakly interacting bumps [**170**]. (For a recent review see [**171**]). Another interesting issue concerns the effect of inhomogeneous inputs. In the homogeneous case, a stationary pulse is only marginally stable, since arbitrarily small fluctuations can shift its center or peak as a consequence of translation symmetry. Amari [**159**] showed that in the presence of small stationary inputs $s(x)$ the peak moves towards a local maximum of $s(x)$. More recently it has been established that if a spatially localized input is presented to a network with some form of slow negative feedback such as spike frequency adaptation (see §5.4), then a stationary pulse can undergo a Hopf instability leading to the formation of a spatially localized oscillation or *breather* [**135, 136**]. This provides an alternative, recurrent network mechanism for generating stimulus–induced oscillations and synchrony, rather than one based on intrinsic single neuron oscillators (see §4).

Working memory and continuous attractors

One of the reasons why persistent activity bumps are of interest is that they are thought to arise in cortical circuits performing certain spatial working memory tasks. Working memory involves cortical "memory neurons" that establish a representation of a stimulus that persists after the stimulus is removed (see Figure 9(a)). A typical experiment is a delayed response task, in which a primate is required to retain information regarding the location of a sensory cue across a delay period between the stimulus and behavioral response. There are three basic kinds of working memory that can be distinguished according to the type of sensory stimulus [**172, 173**]. *Discrete working memory*: in a delayed match-to-sample experiment the behavioral response depends on the memory of one of two items, for example, the stimulus color red or green. Here working memory circuits store information regarding a discrete set of categorical features such as a face, color or word [**128**]. *Spatial working memory*: neurons display persistent activity that is spatially selective. One example is a delayed oculomotor experiment, in which a saccadic eye movement is guided by the memory of the spatial location of a cue stimulus such as

a flashed spot of light. Physiological recordings in prefrontal cortex have shown that spatially localized groups of neurons fire during the recall task and then stop firing once the task has finished [**174**]. The stimulus response of a cell is characterized by a smooth tuning curve that is peaked at a preferred spatial cue and varies from cell to cell. At the network level the memory of cue location is stored as an activity bump. Persistent activity bumps occur in a number of other systems that encode directional or spatial information, including head direction cells in thalamus and basal ganglia [**175**] and place cells in the hippocampus [**103**]. *Parametric working memory*: there is a continuous range of persistent activity that increases mono-tonically with some stimulus parameter. One example is a delayed somatosensory discrimination task, in which a monkey is trained to compare and discriminate the frequencies of two vibrotactile stimuli separated by a delay period [**176**]. Here the stimulus frequency is encoded by the firing rate of persistent activity. A similar monotonic encoding scheme is used by goldfish oculomotor neurons for memory of the current eye position [**177, 178, 179**]. A change in eye position in one direc-tion is preceded by an increase in the activity of certain ON burst neurons. This transient signal is then transformed into elevated persistent activity in the neurons that encode eye position, supplying motorneurons with the tonic drive necessary to maintain the new eye position. Similarly, OFF burst cells initiate movement in the opposite direction by reducing the level of persistent activity (see Figure 9(b)). An interesting aspect of the oculomotor system, which is shared with the head di-rection system, is that some form of *neural integrator* is needed in order determine the change in eye (or head) position based on velocity inputs.
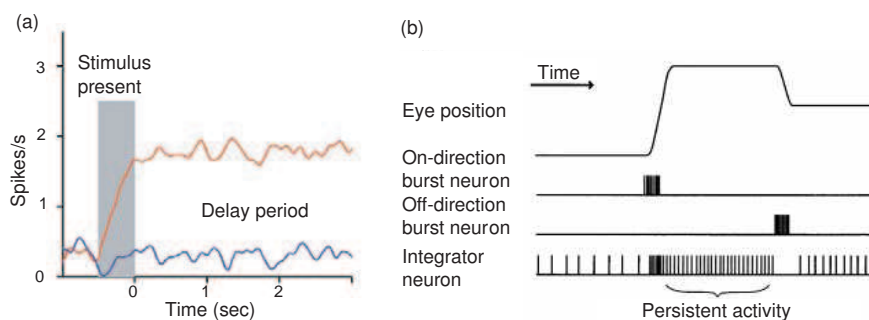

FIGURE 9. (a) An illustration of stimulus–dependent, persistent firing rates in a working memory neuron. (b) Schematic illustration of eye position and neural activity versus time in the oculomotor system. See text for details. [Reprinted from [**179**], Copyright 2000, with permission of Elsevier.]

A characteristic feature of persistent activity in both spatial and parametric working memory is that there exists a continuous manifold of states forming an attractor for the dynamics. Figure 10 shows some examples of such attractors for a simple two–neuron system, in which the firing rates ν_j of the two neurons evolve according to gradient dynamics. That is, there exists a potential function $L(\nu_1, \nu_2)$ such that $\dot{\nu}_j = -\partial L/\partial \nu_j$, $j = 1, 2$. Attracting fixed points of the system then correspond to minima of L. A graded stimulus feature is usually represented

by some form of ring attractor in models of spatial working memory, whereas in models of parametric working memory it is represented by a line attractor. If the stimulus feature is represented by the peak location of an activity bump in a spatially-structured network, then the set of allowed features will form a continuous manifold provided that the network is homogeneous. This manifold will reflect the topology and dimensionality of the network. Thus, a periodic stimulus feature can be encoded by a persistent activity bump in a homogeneous ring network. One of
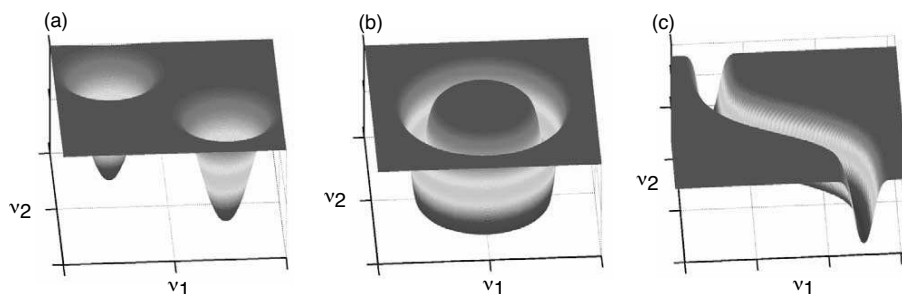

FIGURE 10. Attractor dynamics for a pair of neurons whose firing rates evolve according to a gradient dynamics that minimizes some potential function L. Attracting fixed points correspond to minima of L. (a) A pair of isolated fixed points that could represent discrete categorical features. (b) A ring attractor that could represent head direction or the directional position of some visual cue. (c) A line attractor that could represent eye position or the frequency of a vibrotactile stimulus. [Reprinted from [173], Copyright 2003, with permission of Elsevier.]

the major theoretical challenges is to understand how persistent working memory can be implemented robustly in neural circuits. That is, from a dynamical systems perspective, continuous attractors are structurally unstable so that their existence requires a considerable degree of fine tuning of system parameters. For example, it is necessary to impose strong symmetry constraints on the potential function of the two–neuron system shown in Figure 10 in order to generate a ring or line attractor. Similarly, a continuum of activity bumps only occurs in spatially homogeneous networks. A related issue is that a persistent activity state will be marginally stable with respect to perturbations in directions tangential to the attractor manifold. For example, the peak of an activity bump will tend to drift over time in the presence of arbitrarily small levels of noise. This latter effect may actually have a biological interpretation in terms of the degradation in the memory recall performance of a monkey when the delay in the response is increased. One suggested mechanism for making network models more robust to noise and network inhomogeneities is to introduce some form of bistability at the single neuron level. This idea has been applied to bump formation in spatial working memory [180, 181], and to the formation of line attractors in parametric working memory [182]. Another important issue concerns how to generate persistent states consisting of neurons with low firing rates, given that high levels of recurrent excitation are required in order to maintain persistent activity when a stimulus is removed. (Low firing rates are found in recordings from prefrontal cortex). Large–scale simulations of noisy LIF networks with biophysically realistic synaptic dynamics suggest that robust low

activity persistent states can be generated if a significant fraction of the excitatory connections consist of slow NMDA synapses rather than fast AMPA synapses [183]. The stability of such states can be analyzed using a mean field reduction of the population dynamics along the lines outlined in §3.4, see [184].

5.4. Traveling waves

In the case of excitatory rather than Mexican hat weight functions w, spatially structured rate models can support the propagation of traveling waves of activity. This is consistent with experimental studies that have revealed the propagation of traveling bursts of activity in slices of disinhibited cortical tissue [185, 186, 187, 188]. The underlying mechanism for the propagation of such waves appears to be synaptic in origin rather than diffusive, as in the case of action potentials traveling along the axons of individual neurons. Since there is strong vertical coupling between cortical layers, it is possible to treat a thin vertical cortical slice as an effective one–dimensional medium. Mathematically speaking, one can then distinguish between traveling wavefronts and traveling pulses as illustrated in Figure 11. We will restrict our discussion of analytical methods for studying wave propagation to the simpler case of traveling fronts. However, these methods can be extended to the more realistic case of traveling pulses (see below).
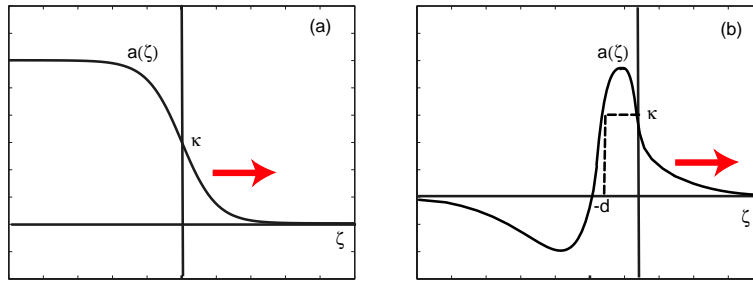

FIGURE 11. (a) Traveling wavefront (b) Traveling pulse of width d as determined by the firing threshold κ

The existence of traveling front solutions in a one–dimensional network has been analyzed by Ermentrout and Mcleod [189] for scalar integro–differential equations of the form

$$(5.38) \qquad \frac{\partial a(x,t)}{\partial t} = -a(x,t) + \int_{-\infty}^{\infty} w(x-x')f(a(x',t))dx',$$

with

$$(5.39) \qquad f(a) = \frac{1}{1 + e^{-\eta(a-\kappa)}}.$$

The weight distribution w is assumed to be a positive, even, continuously differentiable function of x with unit normalization $\int_{-\infty}^{\infty} w(y)dy = 1$. Suppose that the function $F(a) = f(a) - a$ has precisely three zeros at $a = A_{\pm}, A_0$ with $A_- < A_0 < A_+$ and $F'(A_{\pm}) < 0$. It can then be shown that (modulo uniform translations) there exists a unique traveling front solution of equation (5.38) such that $a(x,t) = A(\xi)$,

$\xi = x - ct$, with $A(\xi) \to A_\pm$ as $\xi \to \mp\infty$ [**189**]. Moreover, the speed of the wave satisfies

$$(5.40) \qquad c = \frac{\Gamma}{\int_{-\infty}^{\infty} a'^2 f'(a) d\xi},$$

where

$$(5.41) \qquad \Gamma = \int_{A_-}^{A_+} F(a) da.$$

Since the denominator of equation (5.40) is positive definite, the sign of c is determined by the sign of the coefficient Γ. In particular, if $\kappa = 0.5$ and $\eta > 4$, there exists a pair of stable homogeneous fixed points with $A_- = -A_+$, which in turn implies that $\Gamma = 0$ and the front solution is stationary, see Figure 12.
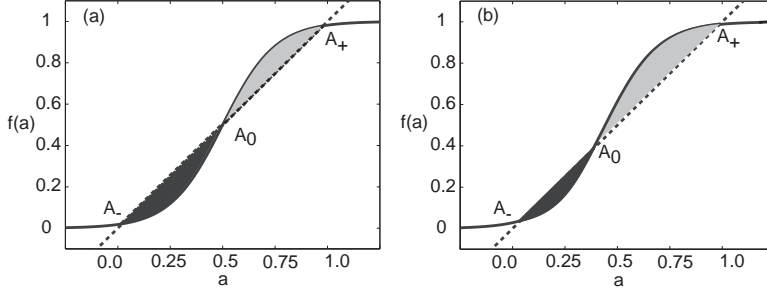

FIGURE 12. Balance condition for the speed of a traveling wave front in a scalar excitatory network with $a(x, t) = A(x - ct)$ such that $A(\mp\infty) = A_\pm$. The solid curve is $f(a) = 1/(1 + e^{-\eta(a-\kappa)})$ with $\eta = 8$ and the dashed line is $g(a) = a$. The wave speed c is positive (negative) if the gray shaded area is larger (smaller) than the black shaded area. (a) $\kappa = 0.5$ such that $c = 0$. (b) $\kappa = 0.4$ such that $c > 0$.

Although the step function $f(a) = H(a - \kappa)$ obtained in the high–gain limit $\eta \to \infty$ is not itself continuously differentiable, the wavefront solution can be calculated explicitly in this case [**189**]. Note that equation (5.38) is then equivalent to equation (5.24). Since equation (5.38) is translation invariant, we are free to impose the condition $A(0) = \kappa$, that is, the wavefront solution passes through threshold at the origin. For concreteness, take $A(\xi)$ to be a monotonically decreasing function of $\xi = x - ct$ such that $A(\xi) < \kappa$ for $\xi > 0$ and $A(\xi) > \kappa$ for $\xi < 0$. Equation (5.38) then reduces to

$$(5.42) \qquad -cA'(\xi) + A(\xi) = \int_{-\infty}^{0} w(\xi - \xi') d\xi' = \int_{\xi}^{\infty} w(x) dx \equiv \widehat{W}(\xi),$$

which has the solution

$$(5.43) \qquad A(\xi) = e^{\xi/c} \left[\kappa - \frac{1}{c} \int_{0}^{\xi} e^{-y/c} \widehat{W}(y) dy \right].$$

Requiring the solution to remain bounded as $\xi \to \infty$ ($\xi \to -\infty$) for $c > 0$ (for $c < 0$) implies that κ must satisfy the condition

$$(5.44) \qquad \kappa = \frac{1}{|c|} \int_0^\infty \mathrm{e}^{-y/|c|} \widehat{W}(\mathrm{sign}(c)y)dy.$$

In the case of an exponential weight distribution $w(x) = (2d)^{-1}\mathrm{e}^{-|x|/d}$, with the length–scale fixed by setting $d = 1$, the relationship between wave speed c and threshold κ is

$$(5.45) \qquad \kappa = \frac{1}{2(1+c)} \text{ (for } c > 0), \quad \kappa = \frac{1+2|c|}{2(1+|c|)} \text{ (for } c < 0)$$

Wave stability

We now indicate how to determine the stability of a traveling wavefront by constructing the so–called Evans function [**190, 191, 192**]. Consider the evolution of small smooth perturbations $\bar{\varphi}$ of a traveling front solution A of equation (5.38) centered about $\xi = 0$. Linearizing about the wave solution, the perturbations evolve according to

$$(5.46) \qquad \frac{\partial \bar{\varphi}}{\partial t} - c\frac{\partial \bar{\varphi}}{\partial \xi} + \bar{\varphi} = \int_{\mathbb{R}} w(\xi - \eta)H'(A(\eta) - \kappa)\bar{\varphi}(\eta)d\eta.$$

Separating variables, $\bar{\varphi}(\xi, t) = \varphi(\xi)e^{\lambda t}$, we find that $\varphi \in \mathcal{C}^1(\mathbb{R}, \mathbb{C})$ satisfies the eigenvalue problem

$$(5.47) \qquad (\mathcal{L} + \mathcal{N}_s)\,\varphi = \lambda\,\varphi$$

where

$$(5.48) \qquad \mathcal{L}\varphi = c\frac{\partial \varphi}{\partial \xi} - \varphi, \qquad \mathcal{N}_s\varphi\,(\xi) = \frac{w(\xi)}{|A'(0)|}\,\varphi(0).$$

We need to characterize the spectrum of the linear operator $\mathcal{L} + \mathcal{N}_s : \mathcal{C}^1(\mathbb{R}, \mathbb{C}) \longrightarrow \mathcal{C}^0(\mathbb{R}, \mathbb{C})$ in order to determine the linear stability of the traveling pulse. The following definitions concern linear operators $\mathcal{T} : \mathcal{D}(\mathcal{T}) \longrightarrow \mathcal{B}$ where $\mathcal{B}$ is a Banach space and the domain $\mathcal{D}(\mathcal{T})$ of $\mathcal{T}$ is dense in $\mathcal{B}$. In our case $\mathcal{D}(\mathcal{L} + \mathcal{N}_s) = \mathcal{C}^1(\mathbb{R}, \mathbb{C})$ which is dense in $\mathcal{C}^0(\mathbb{R}, \mathbb{C})$. λ is in the resolvent set ρ, if $\lambda \in \mathbb{C}$ is such that $\mathcal{T} - \lambda$ has a range dense in $\mathcal{B}$ and a continuous inverse or resolvent operator $R_\lambda(\mathcal{T}) = (\mathcal{T} - \lambda I)^{-1}$, otherwise λ is in the spectrum σ. We decompose the spectrum into the following disjoint sets. λ is an element of the point or discrete spectrum σ_p, if $R_\lambda(\mathcal{T})$ does not exist; λ is an element of the continuous spectrum σ_c if $R_\lambda(\mathcal{T})$ exists, is defined on a dense subset of $\mathcal{B}$, but is not bounded; λ is an element of the residual spectrum σ_r if $R_\lambda(\mathcal{T})$ exists but its domain is not dense in $\mathcal{B}$. We refer to elements of the discrete spectrum as eigenvalues and the union of the continuous and residual spectra as the essential spectrum. It can be shown that the essential spectrum lies in the left–half complex plane so does not contribute to any instabilities [**190**]. Therefore, we will focus on the discrete spectrum.

Resolvent and the discrete spectrum We seek to construct a bounded inverse by solving the inhomogeneous equation

$$(5.49) \qquad (\mathcal{L} + \mathcal{N}_s - \lambda)\varphi = -f,$$

where $f \in \mathcal{C}^0(\mathbb{R}, \mathbb{C})$, using a variation of parameters approach along the lines of Zhang [**190**]. We write equation (5.49) as

$$(5.50) \qquad \frac{\partial}{\partial \xi}\left(e^{-(\frac{1+\lambda}{c})\xi}\,\varphi(\xi)\right) = -\frac{1}{c}\,e^{-(\frac{1+\lambda}{c})\xi}\,\left(\mathcal{N}_s\varphi(\xi) + f(\xi)\right).$$

For $(\mathcal{R}e(\lambda) + 1)/c > 0$, integrating equation (5.50) over $[\xi, \infty)$ yields

$$(5.51) \qquad \varphi(\xi) - \Lambda_+(\lambda; \xi)\,\varphi(0) \;=\; \mathcal{H}_f(\xi).$$

where

$$\Lambda_+(\lambda; \xi) = \frac{1}{c|A'(0)|}\int_\xi^\infty w(\eta)e^{(\frac{1+\lambda}{c})(\xi-\eta)}d\eta,$$

$$\mathcal{H}_f(\xi) = \frac{1}{c}\int_\xi^\infty e^{(\frac{1+\lambda}{c})(\xi-\eta)}f(\eta)d\eta.$$

Using the Hölder inequality, it can be shown that both $\Lambda_+(\lambda; \xi)$ and $\mathcal{H}_f(\xi)$ are bounded for all $\xi \in \mathbb{R}$ and $f \in \mathcal{C}^0(\mathbb{R}, \mathbb{C})$. It is then seen from equation (5.51) that $\varphi(\xi)$ is determined by its restriction $\varphi(0)$, in which case we obtain

$$\left(1 - \Lambda_+(\lambda; 0)\right)\varphi(0) = \frac{1}{c}\int_0^\infty e^{-(\frac{1+\lambda}{c})\eta}f(\eta)d\eta.$$

This can be solved for $\varphi(0)$ and, hence for $\varphi(\xi)$, if and only if $1 - \Lambda_+(\lambda; 0) \neq 0$. This results in a bounded inverse which is defined on all of $\mathcal{C}^0(\mathbb{R}, \mathbb{C})$, and, therefore, all corresponding λ are in the resolvent set. On the other hand, we cannot invert the operator for λ such that $\Lambda_+(\lambda; 0) = 1$. In this case, the equation $(\mathcal{L} + \mathcal{N}_s - \lambda)\varphi = 0$ has nontrivial solutions, indicating that λ is in the discrete spectrum. Hence, if we define the function

$$\mathcal{E}_+(\lambda) = 1 - \Lambda_+(\lambda; 0), \qquad \frac{\mathcal{R}e(\lambda) + 1}{c} > 0,$$

then the eigenvalues correspond to the zeros of $\mathcal{E}_+(\lambda)$. Proceeding along similar lines for $(\mathcal{R}e(\lambda) + 1)/c < 0$ by integrating equation (5.50) over $(-\infty, 0]$ shows that the eigenvalues now correspond to the zeros of the function

$$\mathcal{E}_-(\lambda) = 1 - \Lambda_-(\lambda; 0), , \qquad \frac{\mathcal{R}e(\lambda) + 1}{c} < 0$$

where

$$(5.52) \qquad \Lambda_-(\lambda; \xi) = -\frac{1}{c|A'(0)|}\int_{-\infty}^\xi w(\eta)e^{-(\frac{1+\lambda}{c})\eta}d\eta.$$

The zeros of the Evans function $\mathcal{E}(\lambda)$, which is defined as the composite of the pair of functions $\mathcal{E}_\pm(\lambda)$, then fully determine the discrete spectrum of the operator obtained by linearizing about the wavefront solution.

    Evans function for an exponential weight distribution We now explicitly calculate the zeros of the Evans functions for an exponential weight distribution $w(x) = e^{-|x|}/2$. The region in the complex plane $\mathbf{D} = \{z\ :\ \mathcal{R}e(z) > -1\}$ is the domain of the Evans function $\mathcal{E}_+$, and we need only consider this region to

determine the stability of the wave. For $c > 0$ and $\lambda \in \mathbf{D}$

$$\mathcal{E}_+(\lambda) = 1 - \frac{1}{c|A'(0)|} \int_0^\infty w(\eta) e^{-\left(\frac{1+\lambda}{c}\right)\eta} d\eta,$$

$$= 1 - \frac{1}{2(1+\lambda+c)} \frac{1}{|A'(0)|},$$

and similarly for $c < 0$ and $\lambda \in \mathbf{D}$

$$\mathcal{E}_-(\lambda) = 1 + \frac{1}{c|A'(0)|} \int_{-\infty}^0 w(\eta) e^{\left(-\frac{1+\lambda}{c}\right)\eta} d\eta,$$

$$= 1 + \frac{1}{2(1+\lambda+c)} \frac{1}{|A'(0)|}.$$

From this we can directly solve $\mathcal{E}_\pm(\lambda) = 0$ for λ

$$(5.53) \qquad \lambda = -(1 + |c|) + \frac{1}{2|A'(0)|}, \qquad c \in \mathbb{R},$$

with $A'(0)$ determined from equation (5.43), that is, $A'(0) = c^{-1}(\kappa - 1/2)$. It follows that the eigenvalues are given by

$$(5.54) \qquad \lambda = -(1 + |c|) + \frac{|c|}{2\left|\kappa - \frac{1}{2}\right|}, \qquad c \in \mathbb{R}.$$

Since κ satisfies equation (5.45), we see that the only eigenvalue in $\mathbf{D}$ is the zero eigenvalue $\lambda = 0$. Moreover it can be shown that the eigenvalue is simple [**190**] and, hence, that the natural front is linearly stable modulo uniform translations.

Traveling pulses

Traveling fronts are not particularly realistic representations of waves in cortical slices, since populations of neurons do not stay in the excited state forever. Even in the absence of synaptic inhibition, most neurons posses intrinsic negative feedback mechanisms that slowly bring the cell back to resting voltages after periods of high activity. Hence, rather than a traveling front, propagating activity in the brain is better described as a traveling pulse. We can incorporate a recovery mechanism into the rate equation with the addition of a slow, local negative feedback component q such that equation (5.38) with Heaviside firing rate function becomes [**193**]

$$\frac{\partial a(x,t)}{\partial t} = -a(x,t) + \int_{-\infty}^\infty w(x-x')H(a(x',t)-\kappa)dx' - \beta q(x,t),$$

$$(5.55)\,\frac{1}{\varepsilon}\frac{\partial q(x,t)}{\partial t} = -q(x,t) + a(x,t).$$

This negative feedback could represent spike frequency adaptation or synaptic depression for example. Introducing the traveling wave coordinates (ξ, t), where $\xi = x - ct$, we define a traveling pulse solution of equation (5.55) to be the pair of functions (A, Q), satisfying the conditions

$$A(\xi_i) = \kappa, \qquad i = 1, 2; \qquad\qquad A(\xi) \longrightarrow 0 \qquad \text{as } \xi \longrightarrow \pm\infty;$$

$$A(\xi) > \kappa, \qquad -d < \xi < 0; \qquad\qquad A(\xi) < \kappa, \qquad \text{otherwise},$$

with $\xi = -d, 0$ defining the points at which the activity A crosses threshold, and d is the pulse width. Taking $a(x,t) = A(x-ct)$ and $q(x,t) = Q(x-ct)$, the profile

of the pulse is governed by

$$(5.56) \qquad -c\,A_\xi = -A - \beta Q + \int_{-d}^{0} w(\xi - \eta)d\eta,$$

$$(5.57) \qquad -\frac{c}{\epsilon}\,Q_\xi = -Q \; + \; A.$$

The existence and stability of traveling pulse solutions of equation (5.57) can be analyzed by extending the basic methods used for the scalar equation (5.38) [**190, 191, 192**]. One typically finds two solution branches corresponding to a stable fast wave and an unstable slow wave, see Figure 13.
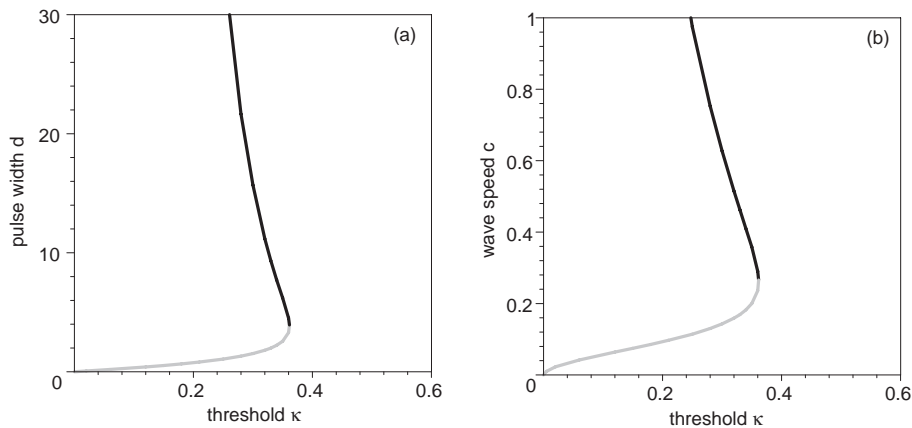

FIGURE 13. Existence of right–moving traveling pulses in the case of the excitatory network (5.55) for an exponential weight distribution with $w(x) = e^{-\sigma|x|}$. Here $\sigma = 1, \varepsilon = 0.01$ and $\beta = 2.5$. (a) Plot of pulse width d against threshold κ. (b) Plot of wave speed c against threshold κ. Stable (unstable) branches indicated by black (gray) curves.

Analysis of the above model provides valuable information regarding how the speed of a traveling wave, which is relatively straightforward to measure experimentally, depends on various features of the underlying neural tissue [**193**]. Indeed, one prediction of the model, concerning how the speed of the wave depends on the firing threshold of the neurons, has recently been confirmed experimentally in disinhibited rat cortical slices [**194**]. External electric fields are used to modulate the threshold and thus control wave propagation, see Figure 14. Finally, note that traveling pulses have also been studied in spiking neuron models, under the simplifying assumption that each neuron only fires once in a propagating sequence [**151, 195**]. This simplification is motivated by simulations of more detailed conductance–models suggesting that the propagation velocity is determined primarily by the response of the postsynaptic neuron to the first one or two presynaptic spikes [**186**].

Thalamic waves

There are significant differences in the mechanisms underlying the spread of activity in cortical and thalamic slices. In computational and experimental studies of disinhibited neocortical slices, one finds that neuronal discharges propagate continuously at a velocity $c \sim 10$ cm/sec [**186**]. On the other hand, in models of thalamic
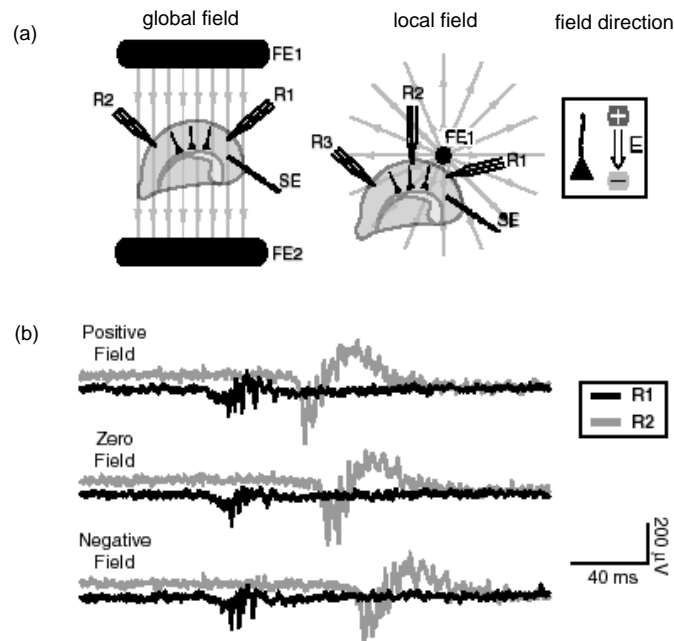
FIGURE 14. (a) Rat cortical slices are bathed in picrotoxin (a GABA$_A$ blocker) and a stimulation electrode (SE) is placed in layers 5-6 to initiate epileptiform bursts. An electric field is applied globally or locally across the slice using Ag/AgCl electrodes (FE1,FE2). Layer 5 neurons have long apical dendrites and are easily polarizable by an electric field, which controls the effective firing threshold of the neuron. (b) The time for an activity pulse to travel between two recording electrodes R1 and R2 depends on the applied electric field, reflecting the dependence of wave speed on the effective firing threshold. [Reprinted from Richardson, Schiff and Gluckman, [194], Copyright 2005, with permission from the American Physical Society.]

slices, composed of excitatory thalamocortical neurons and inhibitory reticular thalamic neurons, waves propagate in a lurching manner at a velocity $c \sim 1$ cm/sec [196]. This is thought to form the basic mechanism for the generation of 7- to 14-Hz spindle oscillations during the onset of sleep [28]. Each recruitment cycle of the lurching waves has two stages (see Figure 15): I. A new group of inhibitory RE cells is excited by synapses from TC cells, and this RE group then inhibits a new group of TC cells. II. The new recruited TC cells rebound from hyperpolarization and fire a burst of spikes, which further recruit more RE cells during next cycle. A detailed analysis of the post inhibitory rebound mechanism underlying the generation of continuous and lurching waves in thalamic networks has recently been carried out using conductance–based [197] and integrate–and–fire–or–burst models [198].
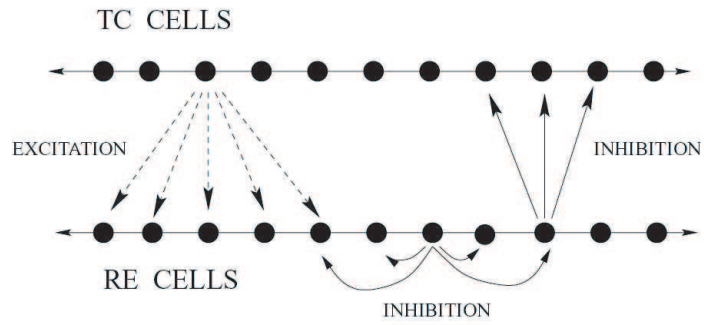
FIGURE 15. Two-layer thalamic model. Inhibitory reticular (RE) cells inhibit excitatory thalamocortical (TC) cells, and TC cells excite RE cells. Mutual inhibition between RE cells has a relatively small effect on discharge propagation.

Bibliography

[1] E Izhikevich. *Dynamical Systems in Neuroscience: The Geometry of Excitability and Bursting*. MIT Press, Cambridge, MA, 2006.

[2] C Koch. *Biophysics of Computation*. Oxford University Press, 1999.

[3] J H Byrne and J L Roberts. *From molecules to networks: an introduction to cellular and molecular neuroscience*. Elsevier, Amsterdam, 2004.

[4] D Terman. An introduction to dynamical systems and neuronal dynamics. In *Tutorials in Mathematical Biosciences I, Lecture Notes in Mathematics, Vol. 1860*, pages 21–68. Springer, Berlin, 2005.

[5] A Borisyuk and J Rinzel. Understanding neuronal dynamics by geometrical dissection of minimal models. In *Methods and Models in Neurophysics, Les Houches Summer School, Session LXXX*, pages 21–68. Elsevier, 2005.

[6] G B Ermentrout. Neural oscillators. In *Tutorials in Mathematical Biosciences I, Lecture Notes in Mathematics, Vol. 1860*, pages 69–106. Springer, Berlin, 2005.

[7] W Gerstner and W Kistler. *Spiking neuron models*. Cambridge University Press, Cambridge, 2002.

[8] A L Hodgkin and A F Huxley. A quantitative description of membrane and its application to conduction and excitation in nerve. *J. Physiol.*, 117:500–544, 1952.

[9] S Coombes and P C Bressloff (eds). *Bursting: The Genesis of Rhythm in the Nervous System.* World Scientific Press, 2005.

[10] A Winfree. *The geometry of biological time*. Springer-Verlag, New York, 1980.

[11] Y Kuramoto. *Chemical Oscillations, Waves and Turbulence*. Springer-Verlag, New-York, 1984.

[12] L Glass and M C Mackey. *From Clocks to Chaos*. Princeton Univ Press, Princeton, 1988.

[13] J Guckenheimer and P J Holmes. *Nonlinear Oscillations, Dynamical Systems and Bifurcations of Vector Fields*. Springer-Verlag, New York, 1983.

[14] C Morris and H Lecar. Voltage oscillations in the barnacle giant muscle fiber. *J. Biophys.*, 35:193–213, 1981.

[15] J P Keener, F C Hoppensteadt, and J Rinzel. Integrate–and–fire models of nerve membrane response to oscillatory input. *SIAM J. Appl. Math.*, 41(3):503–517, 1981.

[16] W Gerstner and J L van Hemmen. Coding and information processing in neural networks. In E Domany, J L van Hemmen, and K Schulten, editors, *Models of Neural Networks II*, pages 1–93. Springer-Verlag, 1994.

[17] W Gerstner and W Kistler. Population dynamics of spiking neurons: fast transients, asynchronous states and locking. *Neural Comput.*, 12:43–89, 2000.

[18] W M Kistler, W Gerstner, and J L van Hemmen. Reduction of the Hodgkin-Huxley equations to a single-variable threshold. *Neural Comput.*, 9:1015–1045, 1997.

[19] L F Abbott and C van Vresswijk. Asynchronous states in networks of pulse–coupled oscillators. *Phys. Rev. E*, 48(2):1483–1490, 1993.

[20] G B Ermentrout and N Kopell. Parabolic bursting in an excitable system coupled with a slow oscillation. *SIAM J. of Appl. Math.*, 46:233–253, 1986.

[21] G B Ermentrout. Type I membranes, phase resetting curves, and synchrony. *Neural Comput.*, 8:979–1001, 1996.

[22] B Gutkin and G B Ermentrout. Dynamics of membrane excitability determine interspike interval variability; a link between spike generation mechanisms and cortical spike train statistics. *Neural Comput.*, 10:1047–1065, 1998.

[23] X-J Wang and J Rinzel. Oscillatory and bursting properties of neurons. In M. Arbib, editor, *Handbook of Brain Theory and Neural Networks*. MIT Press, 1995.

[24] X-J Wang and J Rinzel. Alternating and synchronous rhythms in reciprocally inhibitory model neurons. *Neural Comput.*, 4:84–97, 1992.

[25] G D Smith, C L Cox, S M Sherman, and J Rinzel. Fourier analysis of sinusoidally driven thalamocortical relay neurons and a minimal integrate-and-burst model. *J. Neurophysiol.*, 83:588–610, 2000.

[26] A R R Casti et al. A population study of integrate–and–fire–or burst neurons. *Neural Comput.*, 14:957–986, 2002.

[27] S Coombes, M R Owen, and G D Smith. Mode-locking in a periodically forced integrate-and-fire-or-burst neuron model. *Physical Review E*, 64:041914, 2001.

[28] M Steriade. Coherent oscillations and short-term plasticity in corticothalamic networks. *Trends in Neurosci.*, 2:337–345, 1999.

[29] A Destexhe and T J Sejnowski. *Thalamocortical Assemblies: How Ion Channels, Single Neurons and Large-Scale Networks Organize Sleep Oscillations*. Oxford University Press, Oxford, 2001.

[30] R W Guillery and S M Sherman. Thalamic relay functions and their role in corticocortical communication: generalizations from the visual system. *Neuron*, 33:163–175, 2002.

[31] E F Pace-Schott and J A Hobson. The neurobiology of sleep: genetics, cellular physiology and subcortical networks. *Nature Rev. Neurosci.*, 3:591–605, 2002.

[32] M A Huertas, J R Groff, and G D Smith. Feedback inhibition and throughput properties of an ifb network model of retinogeniculate transmission. *J. Comput. Neurosci.*, 19:147–180, 2005.

[33] B Babadi. Bursting as an effective relay mode in a minimal thalamic model. *J. Comput. Neurosci.*, 18:229–243, 2005.

[34] A Fogelson and R S Zucker. Presynaptic calcium diffusion from various arrays of single channels. implications for transmitter release and synaptic facilitation. *Biophys. J.*, 48:1003–1017, 1985.

[35] R Bertram, G D Smith, and A Sherman. Modeling study of the effects of overlapping calcium microdomains on neurotransmitter release. *Biophys. J.*, 76:735–750, 1999.

[36] E R Kandel and J H Schwartz anf T M Jessel. *Principles of Neural Science*. McGraw Hill, New York, 2000.

[37] A Destexhe, Z F Mainen, and T J Sejnowski. Synthesis of models for excitable membranes synaptic transmission and neuromodulation using a common kinetic formalism. *J. Comput. Neurosci.*, 1:195–231, 1994.

[38] R C Malenka and R A Nicoll. Long-term potentiation–a decade of progress? *Science*, 285:1870–1874, 1999.

[39] H Markram and M Tsodyks. Redistribution of synaptic efficacy between neocortical pyramidal neurons. *Nature*, 382:807–810, 1996.

[40] L F Abbott, J A Varela, K Sen, and S B Nelson. Synaptic depression and cortical gain control. *Science*, 275:220–224, 1997.

[41] L F Abbott and E Marder. Modelling small networks. In C Koch and I Segev, editors, *Methods in Neuronal Modelling*, pages 361–410. MIT Press, 2nd edition, 1998.

[42] R S Zucker. Short term synaptic plasticity. *Ann. Rev. Neurosci.*, 12:13–31, 1989.

[43] G L Millhauser, E E Salpeter, and R E Oswald. Diffusion model of ion–channel gating and the origin of power–law distributions from single–channel recordings. *Proc. Natl. Acad. Sci. USA*, 85:1503–1507, 1988.

[44] S Fusi, P J Drew, and L F Abbott. cascade models of synaptically stored memories. *Neuron*, 45:599–611, 2005.

[45] G Gilboa, R Chen, and N Brenner. History–dependent multiple-time-scale dynamics in a single-neuron model. *J. Neurosci.*, 25:6479–6489, 2005.

[46] W Rall and H A Snir. Cable theory for dendritic neurons. In C Koch and I Segev, editors, *Methods in Neuronal Modelling (2nd ed.)*. MIT Press, Cambridge, 1998.

[47] H C Tuckwell. *Introduction to Theoretical Neurobiology*, volume 1. (Linear cable theory and dendritic structure) of *Cambridge Studies in Mathematical Biology*. Cambridge University Press, 1988.

[48] P C Bressloff and S Coombes. Physics of the extended neuron. *Int. J. Mod. Phys. B*, 11(20):2343–2392, 1997.

[49] G Stuart, N Spruston, and M Hausser. *Dendrites*. Oxford University Press, New York, 1999.

[50] J P Miller, W Rall, and J Rinzel. Synaptic amplification by active membrane in dendritic spines. *Brain Res.*, 325:325–330, 1985.

[51] G M Shepherd, R K Brayton, J P Miller, I Segev, J Rinzel, and W Rall. Signal enhancement in distal cortical dendrites by means of interactions between active dendritic spines. *Proc. Natl. Acad. Sci. USA*, 82:2192–2195, 1985.

[52] G M Shepherd. The dendritic spine: a multifunctional unit. *J. Neurophysiol.*, 75:2197–2210, 1996.

[53] S M Baer and J Rinzel. Propagation of dendritic spikes mediated by excitable spines: a continuum theory. *J. Neurophysiol.*, 65:874–890, 1991.

[54] S Coombes and P C Bressloff. Solitary waves in a model of dendritic cable with active spines. *SIAM J. Appl. Math.*, 61:432–453, 2000.

[55] R Yuste and W Denk. Dendritic spines as a basic functional units of neuronal integration. *Nature*, 375:682–684, 1995.

[56] A Matus. Actin plasticity in dendritic spines. *Science*, 290:754–758, 2000.

[57] R Yuste and T Bonhoeffer. Morphological changes in dendritic spines associated with LTP. *Ann. Rev. Neurosci.*, 24:1071–1089, 2001.

[58] N Mataga, Y Mizuguchi, and T K Hensch. Experience-dependent pruning of dendritic spines in visual cortex by tissue plasminogen activator. *Neuron*, 44:1031–1041, 2004.

[59] S Oray, A Majewska, and M Sur. Dendritic spine dynamics are regulated by monocular deprivation and extracellular matrix degredation. *Neuron*, 44:1021–1030, 2004.

[60] C Koch and A M Zador. The function of dendritic dendritic spines. devices subserving biochemical rather than electrical compartmentalization. *J. Neurosci.*, 13:413–422, 1993.

[61] E A Nimchinsky, B L Sabatini, and K Svoboda. Structure and function of dendritic spines. *Ann. Rev. Physiol.*, 64:313–353, 2002.

[62] K M Franks and T J Sejnowski. Complexity of calcium signaling in synaptic spines. *Bioessays*, 24:1130–1144, 2002.

[63] D Holcman, Z Schuss, and E Korkotian. Calcium dynamics in dendritic spines and spine motility. *Biophys. J.*, 87:81–91, 2004.

[64] D O Hebb. *The organization of behavior*. Wiley, New York, 1949.

[65] T V P Bliss and T Lomo. Long–lasting potentiation of synaptic transmission in the dentate area of unanaeasthetized rabbbit following stimulation of the perforant path. *J. Physiol. (London)*, 232:331–356, 1973.

[66] S M Dudek and M F Bear. Homosynaptic long–term depression in area ca1 of hippocampus and effects of NMDA receptor blockade. *Proc. natl. Acad. Sci.*, 89:4363–4367, 1992.

[67] T V P Bliss and G L Collingridge. A synaptic model of memory: long–term potentiation in the hippocampus. *Nature*, 361:31–39, 1993.

[68] J E Lisman. Long-term potentiation: outstanding questions and attempted synthesis. *Phi. Trans. R. Soc. Lond. B*, 358:829–842, 2003.

[69] R C Malenka and M F Bear. LTP and LTD: an embarrassment of riches. *Neuron*, 44:5–21, 2004.

[70] J C Magee and D Johnston. A synaptically contriolled associative signal for hebbian plasticity in hippocampal neurons. *Science*, 275:209–213, 1997.

[71] H Markram, J Lubke, M Frotscher, and B Sakmann. Regulation of synaptic efficacy by conincidence of postsynaptic aps and epsps. *Science*, 275:213–215, 1997.

[72] G Bi and M Poo. Synaptic modification of correlated activity: Hebb's postulate revisited. *Ann. Rev. Neurosci.*, 24:139–166, 2001.

[73] G Bi and M Poo. Synaptic modification in cultured hippocampal neurons: dependence on spike timing, synaptic strength and postsynaptic cell type. *J. Neurosci.*, 18:10464–10472, 1998.

[74] J E Lisman. Amechanism for the hebb and the anti–hebb processes underlying learning and memory. *Proc. Natl. Acad. Sci*, 86:9574–9578, 1989.

[75] R C Malenka, J A Kauer, R S Zucker, and R A Nicoll. Postsynaptic calcium is sufficient for potentiation of hippocampal synaptic transmission. *Science*, 242:81–84, 1988.

[76] S N Yang, Y G Tang, and R A Nicoll. Selective induction of LTP and LTD by postsynaptic calcium elevation. *J. Neurophysiol.*, 81:781–787, 1999.

[77] H Shouval, M F Bear, and L N Cooper. A unified model of NMDA receptor–dependent bidirectional synaptic plasticity. *Proc. Natl. Acad. Sci.*, 99:10831–10836, 2002.

[78] C Jahr and C Stevens. A quantitative description of NMDA receptor-channel kinetic behavior. *J. Neurosci.*, 10:1830–1837, 1990.

[79] J E Lisman and N Spruston. Postsynaptic depolarization requirements for LTP and LTD: a critique of spike timing–dependent plasticity. *Nat. Neurosci.*, 8:839–841, 2005.

[80] J Rubin, R C Gherkin, G Q Bi, and C C Chow. Calcium time course as a signal for spike–timing–synaptic–plasticity. *J. Neurophsyiol.*, 93:2600–2613, 2005.

[81] G L Collingridge, J T R Isaac, and Y T Wang. Receptor trafficking and synaptic plasticity. *Nature Rev. Neurosci.*, 5:952–962, 2004.

[82] D Choquet and A Trillier. The role of receptor diffusion in the organization of the postsynaptic membrane. *Nat. Rev. Neurosci.*, 4:251–265, 2003.

[83] A Triller and D Choquet. Surface trafficking of receptors between synaptic and extrasynaptic membranes. *Trends Neurosci.*, 28:133–139, 2005.

[84] B Earnshaw and P C Bressloff. A biophysical model of AMPA receptor trafficking and its regulation during ltp/ltd. *J. Neurosci.*, 26:12362–12373, 2006.

[85] J E Lisman and H Schulman anf H Cline. The molecular basis of camkii function in synaptic and behavioral memory. *Nat. Rev. Neurosci.*, 3:175–190, 2002.

[86] A M Zhabotinsky. Bistability in the Ca^{2+}/calmodulin–dependent protein kinase–phosphotase system. *Biophys. J.*, 79:2211–2221, 2000.

[87] J E Lisman and A M Zhabotinsky. A model of synaptic memory: A camkii/pp1 switch that potentiates transmission by organizing an AMPA receptor anchoring system. *Neuron*, 31:191–201, 2001.

[88] P Miller, A M Zhaobotinsky, J E lisman, and X-J Wang. The stability of a stochastic CaMKII switch: dependence on the number of enzyme molecules and protein turnover. *PLoS Biology*, 3:705–717, 2005.

[89] J D Petersen, X Chen, L Vinade, A Dosemeci, and J E Lisman. Distribution of (PSD)–95 and CaMKII to the postsynaptic density. *J. Neurosci.*, 23:11270–11278, 2003.

[90] P N R Rao and T J Sejnowski. Self-organizing neural systems based on predictive learning. *Phil. Trans. R. Soc. Lond.*, 361:1149–1175, 2003.

[91] M R Mehta, M Quirk, and M Wilson. Experience–dependent asymmetric shape of hippocampal receptive fields. *Neuron*, 25:707–715, 2000.

[92] W Schultz. Getting formal with dopamine and reward. *Neuron*, 36:241–263, 2002.

[93] P R Montague, S E Hyman, and J D Cohen. Computational roles for dopamine in behavioural control. *Nature*, 431:760–767, 2004.

[94] F Rieke, D Warland, R van Steveninck, and W Bialek. *Spikes – exploring the neural code.* MIT Press, Cambridge, MA, 1997.

[95] P Dayan and L F Abbott. *Theoretical neuroscience.* MIT, Cambridge, MA, 2001.

[96] R Baddeley, L F Abbott, M J A Booth, F Sengpiel, T Freeman, E A Wakeman, and E T Rolls. Responses of neurons in primary and interior temporal visual cortices to natural scenes. *Proc. Royal Society Lond.*, B264:1775–1783, 1997.

[97] M N Shadlen and W T Newsome. Noise, neural codes and cortical organization. *Curr. Opin. Neurobiology*, 4:569–579, 1994.

[98] S Thorpe, D Fize, and C Marlot. Speed of processing in the human visual system. *Nature*, 381:520–522, 1996.

[99] M Rossumn, G G Turrigiano, and S B Nelson. Fast propagation of firing rates through layered networks of noisy neurons. *J. Neurosci.*, 22:1956–1966, 2002.

[100] M Tsodyks and T J Sejnowski. Rapid switching in balanced cortical network models. *Network Comput. Neural Syst.*, 6:111–124, 1995.

[101] G B Ermentrout. Neural networks as spatio-temporal pattern-forming systems. *Rep. Prog. Phy.*, 61:353–430, 1998.

[102] P C Bressloff. Pattern formation in visual cortex. In C C Chow, B Gutkin, D Hansel, C Meunier, and J Dalibard, editors, *Les Houches 2003: methods and models in neurophysics*, pages 477–574. Elsevier, 2005.

[103] J O'Keefe and M L Recce. Phase relationship between hippocampal place units and the EEG theta rhythm. *Hippocampus*, 3:317–330, 1993.

[104] J E Lisman. Relating hippocampal circuitry to function: recall of memory sequences by reciprocal dentate-ca3 interactions. *Neuron*, 22:233–242, 1999.

[105] G Laurent. Odor encoding as an active, dynamical process: experiments, computation and theory. *Ann. Rev. Neurosci.*, 24:263–297, 2001.

[106] K R Delaney, A Galperin, M S Fee, J A Flores, R Gervais, D W Tank, and D Kleinfeld. Waves and stimulus-modulated dynamics in an oscillating olfactory network. *Proc. Natl. Acad. Sci. USA*, 91:669–673, 1994.

[107] C M Gray. Synchronous oscillations in neuronal systems: mechanisms and functions. *J. Comput. Neurosci.*, 1:11–38, 1994.

[108] Y Dan, J M Alonso snd W M Usrey, and R C Reid. Coding of visual information by precisely correlated spikes in the lateral geniculate nucleus. *Nature Neurosci.*, 1:501–507, 1998.

[109] R C DeCharms and M Merzenich. Primary cortical representation of sounds by the coordination of action potential timing. *Nature*, 381:610–613, 1995.

[110] W Singer and C M Gray. Visual feature integration and the temporal correlation hypothesis. *Ann. Rev. Neurosci.*, 18:555–586, 1995.

[111] M N Shadlen and J A Movshon. Synchrony unbound: a critical evaluation of the temporal binding hypothesis. *Neuron*, 24:67–77, 1999.

[112] C M Gray. The temporal correlation hypothesis of visual feature integration: still alive and well. *Neuron*, 24:31–47, 1999.

[113] E Salinas and T J Sejnowski. Correlated neuronal activity and the flow of neural information. *Nature Rev. Neurosci.*, 4:539–550, 2001.

[114] W Bair, C Koch, W T Newsome, and K H Britten. Power spectrum analysis of bursting cells in area mt in the behaving monkey. *J. Neurosci.*, 14:2870–2893, 1994.

[115] W R Softky and C Koch. Cortical cell should spike regularly but do not. *Neural Comput*, 4:643–646, 1992.

[116] H C Tuckwell. *Introduction to theoretical neurobiology*, volume 2. (Nonlinear and stochastic theories) of *Cambridge studies in Mathematical Biology*. Cambridge University Press, 1988.

[117] van Kampen. *Stochastic processes in physics and chemistry*. North-Holland, Amsterdam, 1992.

[118] C W Gardiner. *Handbook of stochastic methods, 2nd edition*. Springer, Berlin, 1997.

[119] M J E Richardson. Effects of synaptic conductance on the voltage distribution and firing rate of spiking neurons. *Phys. Rev. E*, 69:051918, 2004.

[120] P Konig, A K Engel, and W Singer. Integrator or coincidence detector? the role of the cortical neuron revisited. *Trends Neurosci.*, 19:130–137, 1996.

[121] L Gammaitoni, P Hanggi, P Jung, and F Marchesoni. Stochastic resonance. *Rep. Prog. Phys.*, 70:223–287, 1998.

[122] A Longtin. Stochastic resonance in neuron models. *J. Stat. Phys.*, 70:309–327, 1993.

[123] B Linder, J Garcia-Ojalvo, A Neiman, and L Schimansky-Geier. Effects of noise in excitable systems. *Phys. Rep.*, 392:321–424, 2004.

[124] N Brunel and V Hakim. Fast global oscillations in networks of integrate–and–fire neurons with low firing rates. *Neural Comput.*, 11:1621–1671, 1999.

[125] W Gerstner and J L Van Hemmen. Coherence and incoherence in a globally coupled ensemble of pulse–emitting units. *Phys. Rev. Lett.*, 71(3):312–315, 1993.

[126] C van Vreeswijk and L F Abbott. Self–sustained firing in populations of integrate–and–fire neurons. *SIAM J. Appl. Maths*, 53(1):253–264, 1993.

[127] C van Vreeswijk and H Sompolinsky. Chaotic balanced state in a model of cortical circuits. *Neural Comput.*, 10:1321–1371, 1998.

[128] D J Amit and N Brunel. Model of global spontaneous activity and local structured activity during delay periods in the cerebral cortex. *Cereb Cortex*, 7:237–252, 1997.

[129] N Brunel. Dynamics of sparsely connected networks of excitatory and inhibitory spiking neurons. *J Comput. Neurosci*, 8:183–208, 2000.

[130] A Omurtag, B W Knight, and L Sirovich. On the simulation of large populations of neurons. *J. Comput. Neurosci.*, 8:51–63, 2000.

[131] L Sirovich. Dynamics of neuronal populations: eigenfunction theory; some solvable cases. *Network: Comput. Neural Syst.*, 14:249–272, 2003.

[132] D Cai, L Tao, M Shelley, and D W McLaughlin. An effective kinetic representation of fluctuation–driven neuronal networks with application to simple and complex celss in visual cortex. *Proc. Natl. Acad. Sci. USA*, 101:7757–7562, 2004.

[133] H G Schuster and P Wagner. A model for neuronal oscillations in visual cortex. *Biol. Cybern.*, 64:77–82, 1990.

[134] E R Grannan, D Kleinfeld, and H Sompolinsky. Stimulus dependent synchronization of neuronal assemblies. *Neural Comput.*, 5:550–569, 1993.

[135] S E Folias and P C Bressloff. Breathing pulses in an excitatory neural network. *SIAM J. Appl. Dyn. Syst.*, 3:378–407, 2004.

[136] S E Folias and P C Bressloff. Breathers in two–dimensional neural media. *Phys. Rev. Lett.*, 95:208107, 2005.

[137] G B Ermentrout and N Kopell. Multiple pulse interactions and averaging in systems of coupled neural oscillators. *J. Math Biol.*, 29:195–217, 1991.

[138] F C Hoppensteadt and E Izhekevich. *Weakly Connected Neural Nets*. Springer-Verlag, New York, 1997.

[139] G B Ermentrout. The behaviour of rings of coupled oscillators. *Journal of Mathematical Biology*, 23:55–74, 1985.

[140] P C Bressloff and S Coombes. Symmetry and phase-locking in a ring of pulse-coupled oscillators with distributed delays. *Physica D*, 126:99–122, 1999.

[141] C van Vreeswijk, G B Ermentrout, and L F Abbott. When inhibition not excitation synchronizes neural firing. *J. Comput. Neurosci.*, 1:313–321, 1994.

[142] D Hansel, G Mato, and C Meunier. Synchrony in excitatory neural networks. *Neural Comput.*, 7:2307–2337, 1995.

[143] R E Mirollo and S H Strogatz. Synchronisation of pulse–coupled biological oscillators. *SIAM J. Appl. Math.*, 50(6):1645–1662, 1990.

[144] S Coombes and G J Lord. Desynchronisation of pulse–coupled integrate–and–fire neurons. *Phys. Rev. E*, 55(3):R2104–R2107, 1997.

[145] A H Cohen, G B Ermentrout, T Kiermel, N Kopell, K A Sigvardt, and T L Williams. Modeling of intersegmental coordination in the lamprey central pattern generator for motion. *Trends in Neurosci.*, 15:434–438, 1992.

[146] E Marder and R L Calabrese. Principles of rhythmic motor pattern generation. *Physiol. Rev.*, 76:687–717, 1996.

[147] S Grillner. The motor infrastructure: from ion channels to neuronal networks. *Nat. Rev. Neurosci.*, 4:573–586, 2003.

[148] W O Friesen and R A Pearce. Mechanism of intersegmental coordination in leech locomotion. *Semin. Neurosci.*, 4:41–47, 1993.

[149] G B Ermentrout and N Kopell. Frequency plateaus in a chain of weakly coupled oscillators. *SIAM J. Appl. Math.*, 15:215–237, 1984.

[150] N Kopell and G B Ermentrout. Symmetry and phase-locking in chains of weakly coupled oscillators. *Comm. Pure Appl. Math.*, 39:623–660, 1986.

[151] G B Ermentrout. The analysis of synaptically generated travelling waves. *J. Comput. Neurosc.*, 5:191–208, 1998.

[152] P C Bressloff and S Coombes. Dynamics of strongly coupled spiking neurons. *Neural Comput.*, 12:91–129, 2000.

[153] P C Bressloff and S Coombes. Dynamical theory of spike train dynamics in networks of integrate-and-fire oscillators. *SIAM J. Appl. Math*, 60:828–841, 2000.

[154] D Golomb and J Rinzel. Clustering in globally coupled inhibitory neurons. *Physica D*, 72:259–282, 1994.

[155] H R Wilson and J D Cowan. Excitatory and inhibitory interactions in localized populations of model neurons. *Biophys. J.*, 12:1–23, 1972.

[156] H R Wilson and J D Cowan. A mathematical theory of the functional dynamics of cortical and thalamic nervous tissue. *Kybernetik*, 13:55–80, 1973.

[157] D H Hubel and T N Wiesel. Receptive fields, binocular interaction and functional architecture in the cat's visual cortex. *J. Neurosci.*, 3:1116–1133, 1962.

[158] N V Swindale. The development of topography in the visual–cortex: A review of models. *Network*, 7(2):161–274, 1996.

[159] S Amari. Dynamics of pattern formation in lateral inhibition type neural fields. *Biol. Cybern.*, 27:77–87, 1977.

[160] G B Ermentrout and J Cowan. A mathematical theory of visual hallucination patterns. *Bio. Cybern.*, 34:137–150, 1979.

[161] P C Bressloff J D Cowan, M Golubitsky, P J Thomas, and M Wiener. Geometric Visual Hallucinations, Euclidean Symmetry and the Functional Architecture of Striate Cortex. *Phil. Trans. Roy. Soc. Lond. B*, 356:299–330, 2001.

[162] R. B. H. Tootell, E Switkes, M. S. Silverman, and S.L. Hamilton. Functional anatomy of macaque striate cortex. II. Retinoptic organization. *J. Neurosci.*, 8:1531–1568, 1988.

[163] E Schwartz. Spatial mapping in the primate sensory projection: analytic structure and relevance to projection. *Biol. Cybern.*, 25:181–194, 1977.

[164] D Pinto and G B Ermentrout. Spatially structured activity in synaptically coupled neuronal networks: Ii. lateral inhibition and standing pulses. *SIAM J. Appl. Math*, 62:226–243, 2001.

[165] K Kishimoto and S Amari. Existence and stability of local excitations in homogeneous neural fields. *J. Math. Biol.*, 7:303–318, 1979.

[166] C R Laing, W C Troy, B Gutkin, and G B Ermentrout. Multiple bumps in a neuronal model of working memory. *SIAM J. Appl. Math*, 63:62–97, 2002.

[167] C R Laing and W C Troy. Pde methods for nonlocal models. *SIAM J. Appl. Dyn. Syst.*, 2:487–516, 2003.

[168] C R Laing and C C Chow. Stationary bumps in networks of spiking neurons. *Neural Comput.*, 13:14731494, 2001.

[169] H Werner and T Richter. Circular stationary solutions in two-dimensional neural fields. *Biol. Cybern.*, 85:211–217, 2001.

[170] P C Bressloff. Weakly interacting pulses in synaptically coupled excitable neural media. *SIAM J. Appl. Math.*, 66:57–81, 2005.

[171] S Coombes. Waves, bumps and patterns in neural field theories. *Biol. Cybern.*, 93:91–108, 2005.

[172] X-J Wang. Synaptic reverberation underlying mnemonic persistent activity. *Trends Neurosci.*, 24:455–463, 2001.

[173] C D Brody, R Romo, and A Kepecs. Basic mechanisms for graded persistent activity: discrete attractors, continuous attractors, and dynamic representations. *Curr. Opin. Neuro.*, 13:204–211, 2003.

[174] J M Fuster and G Alexander. Neuron activity related to short-term memory. *Science*, 173:652, 1971.

[175] J S Taube and J P Bassett. Persistent neural activity in head direction cells. *Cereb. Cortex*, 13:1162–1172, 2003.

[176] T Ritz and T J Sejnowski. Neuronal correlates of parametric working memory in the prefrontal cortex. *Nature*, 399:470–473, 1999.

[177] H S Seung. How the brain keeps the eyes still. *Proc. Natl. Acad. Sci. USA*, 93:13339–13344, 1996.

[178] E Aksay, R Baker, H S Seung, and D W Tank. Anatomy and discharge properties of premotor neurons in the goldsh medulla that have eye-position signals during xations. *J. Neurophysiol.*, 84:1035–1049, 2000.

[179] H S Seung, D D Lee, B Y Reis, and D W Tank. Stability of the memory of eye position in a recurrent network of conductance-based model neurons. *Neuron*, 26:1259–271, 2000.

[180] M Camperi and X-J Wang. A model of visuospatial short-term memory in prefrontal cortex: recurrent network and cellular bistability. *J. Comp. Neurosci.*, 5:383–405, 1998.

[181] C P Fall, T J Lewis, and J Rinzel. Background–activity–dependent properties of a network model for working memory that incorporates cellular bistability. *Biol. Cybern.*, 93:109–18, 2004.

[182] A A Koulakov, S Raghavachari, A Kepecs, and J E Lisman. Model for a robust neural integrator. *Nat. Neurosci.*, 5:775–782, 2002.

[183] X-J Wang. Synaptic basis of cortical persistent activity: the importance of nmda receptors to working memory. *J. Neurosci.*, 19:9587–9603, 1999.

[184] A Renart, N Brunel, and X-J Wang. Mean–field theory of irregularly spiking neuronal populations and working memory in recurrent cortical networks. In J Feng, editor, *Computational Neuroscience: a comprehensive approach*, pages 431–490. CRC Press, Boca Raton, Fl, 2004.

[185] R D Chervin, P A Pierce, and B W Connors. Periodicity and directionality in the propagation of epileptiform discharges across neocortex. *J. Neurophysiol.*, 60:1695–1713, 1988.

[186] D Golomb and Y Amitai. Propagating neuronal discharges in neocortical slices: Computational and experimental study. *J. Neurophysiol.*, 78:1199–1211, 1997.

[187] J-Y Wu, L Guan, and Y Tsau. Propagating activation during oscillations and evoked responses in neocortical slices. *J. Neurosci.*, 19:5005–5015, 1999.

[188] D Pinto, S L patrick, W C Huang, and B W Connors. Initiation, propagation, and termination of epileptiform activity in rodent neocortex in vitro involve distinct mechanisms. *J. Neurosci.*, 25:8131–8140, 2005.

[189] G B Ermentrout and J B Mcleod. Existence and uniqueness of travelling waves for a neural network. *Proc. Roy. Soc. Edin. A*, 123:461–478, 1993.

[190] L Zhang. On the stability of traveling wave solutions in synaptically coupled neuronal networks. *Diff. Int. Eq.*, 16:513–536, 2003.

[191] S Coombes and M R Owen. Evans functions for integral neural field equations with heaviside firing rate function. *SIAM J. Appl. Dyn. Syst.*, 4:574–600, 2004.

[192] S E Folias and P C Bressloff. Stimulus–locked traveling pulses and breathers in an excitatory neural network. *SIAM J. Appl. Math.*, 65:2067–2092, 2005.

[193] D Pinto and G B Ermentrout. Spatially structured activity in synaptically coupled neuronal networks: I. traveling fronts and pulses. *SIAM J. Appl. Math*, 62:206–225, 2001.

[194] K A Richardson, S J Schiff, and B J Gluckman. Control of traveling waves in the mammalian cortex. *Phys. Rev. Lett.*, 028103, 2005.

[195] P C Bressloff. Synaptically generated wave propagation in excitable neural media. *Phys. Rev. Lett.*, 82:2979–2982, 1999.

[196] D Golomb, X-J Wang, and J Rinzel. Propagation of spindle waves in a thalamic slice model. *J. Neurophysiol.*, 75:750–769, 1996.

[197] D H Terman, G B Ermentrout, and A C Yew. Propgating activity patterns in thalamic neuronal networks. *SIAM J. Appl. Math*, 61:1578–1604, 2003.

[198] S Coombes. Dynamics of synaptically coupled integrate–and–fire–or–burst neurons. *Phys. Rev. E*, 67:041910, 2003.